

University of Louisville

## ThinkIR: The University of Louisville's Institutional Repository

---

Electronic Theses and Dissertations

---

12-2010

# Signal processing in the tectothalamic pathway.

Haiyang Wei  
*University of Louisville*

Follow this and additional works at: <https://ir.library.louisville.edu/etd>

---

### Recommended Citation

Wei, Haiyang, "Signal processing in the tectothalamic pathway." (2010). *Electronic Theses and Dissertations*. Paper 1543.  
<https://doi.org/10.18297/etd/1543>

This Doctoral Dissertation is brought to you for free and open access by ThinkIR: The University of Louisville's Institutional Repository. It has been accepted for inclusion in Electronic Theses and Dissertations by an authorized administrator of ThinkIR: The University of Louisville's Institutional Repository. This title appears here courtesy of the author, who has retained all other copyrights. For more information, please contact [thinkir@louisville.edu](mailto:thinkir@louisville.edu).

SIGNAL PROCESSING IN THE TECTOTHALAMIC PATHWAY

By

Haiyang Wei

B.S., University of Science & Technology of China, 2003

M.S., University of Louisville, 2007

A Dissertation

Submitted to the Faculty of the  
Graduate School of the University of Louisville  
In Partial Fulfillment of the Requirements  
For the Degree of

Doctor of Philosophy

Department of Anatomical Sciences and Neurobiology  
University of Louisville, School of Medicine  
Louisville, Kentucky

December 2010



SIGNAL PROCESSING IN THE TECTOTHALAMIC PATHWAY

By

Haiyang Wei

B.S., University of Science & Technology of China, 2003

M.S, University of Louisville, 2007

A Dissertation Approved on

December 1, 2010

by the following Dissertation Committee:

---

Dissertation Director

## ACKNOWLEDGMENTS

This thesis would not have been possible without the support, patience and guidance of my committee members, my family and my friends.

I owe my deepest gratitude to my advisor, Dr. Martha Bickford, for her guidance, caring, patience, and support. I am indebted to my other committee members Drs. Charles Hubscher, David Magnuson, George Mower and Peter Rowell, for their guidance, suggestions and help. I am grateful to Drs. Woody Petry, Robin Krimm, Robert Lundy, Nigel Cooper and Nobuyuki Kuwabara, for the wonderful research environment they provided to me. Additional thanks to Drs. Terry Sejnowski, Meixia Zhang and Chris Whitaker, Mr. Arkadiusz Slusarczyk, Mr. Michael Eisenback, Ms. Cathie Caple, and Mr. Max Bonjean, for their help on my research projects.

Many thanks to my friends in the lab, Jianli Li, Ranida Chomsung, Sean Masterson, Jon Day-Brown, Dmitry Familtsev and Donna Dillihay, and many others outside the lab and department, for their support and friendship.

Finally, my heartfelt gratitude to my wife Lu Yang, for her unconditional love and support, to my daughter Sophia Wei, for the joy and happiness she brings to me, and to my parents and family for their love.

## **ABSTRACT**

### **SIGNAL PROCESSING IN THE TECTOTHALAMIC PATHWAY**

Haiyang Wei

December 1, 2010

The pulvinar is the largest nucleus of the human dorsal thalamus and is affected in a variety of brain disorders, such as schizophrenia. The experiments described in this dissertation elucidate key features of tecto-pulvino-cortical pathways as a first step toward understanding their role in coding visual stimuli and coordinating appropriate responsive actions. The tree shrew is used as the animal model because the visual structures of the tree shrew brain display many of the features of the primate brain, and the tectopulvinar pathways are particularly enhanced in this species.

The connections formed between the tectorecipient pulvinar nucleus and cortex were explored using tract tracing, immunohistochemistry, light, confocal, and electron microscopy. It was found that the pulvinar nucleus is reciprocally connected to two regions of the temporal cortex. Pulvinocortical terminals were found to contact dendritic spines of pyramidal cells, potentially influencing corticocortical projections to the striate cortex. Corticopulvinar synapses were found to be formed distal to tectopulvinar synapses on the dendrites of pulvinar neurons, suggesting that pulvinar neurons integrate inputs from the SC and temporal cortex.

The membrane properties of neurons in the tectorecipient pulvinar were compared to those of neurons of the tree shrew dorsal lateral geniculate nucleus (dLGN), using whole cell recordings in slices maintained in vitro, western blotting, stereology, and neuron modeling techniques. These studies revealed that, compared to the dLGN, pulvinar neurons express a higher density of low threshold transient (T-type) calcium channels resulting in a greater propensity to fire with bursts of action potentials. These bursts may serve to increase the influence of pulvinocortical connections and/or synchronize the activity patterns of the multiple targets of the pulvinar nucleus.

Finally, the properties of tectopulvinar synapses were explored using in vitro whole cell recordings in brain slices, immunohistochemistry and confocal microscopy. The results of these experiments suggest that the tectopulvinar terminals form convergent connections on pulvinar neurons and contain the vesicle-tethering proteins synapsin I and synapsin II. We suggest that these features allow pulvinar neurons to relay a dynamic range of visual signals from the SC in order to initiate and guide the appropriate responsive actions.

## TABLE OF CONTENTS

	PAGE
ACKNOWLEDGMENTS.....	iii
ABSTRACT.....	iv
LIST OF FIGURES.....	viii
CHAPTER	
I. INTRODUCTION.....	1
Relay nuclei and intralaminar nuclei.....	2
Types of thalamic cells.....	2
Intinsic properties of thalamic cells.....	4
Drivers and modulators.....	8
Circuitries and synaptic properties.....	9
Lateral posterior and pulvinar nuclei.....	11
II. SYNAPTIC ORGANIZATION OF CONNECTIONS BETWEEN THE TEMPORAL CORTEX AND PULVINAR NUCLEUS OF THE TREE SHREW	
Outline.....	15
Introduction.....	16
Methods.....	17
Results.....	23
Discussion.....	30



III. THALAMIC BURST FIRING PROPENSITY: A COMPARISON OF THE DORSAL LATERAL GENICULATE AND PULVINAR NUCLEI IN THE TREE SHREW	
Outline.....	65
Introduction.....	66
Methods.....	67
Results.....	75
Discussion.....	82
IV. DIFFUSE AND SPECIFIC TECTOPULVINAR EPSPS IN THE TREE SHREW: RELATION TO SYNAPSINS AND SYNAPTIC CLUSTERS	
Outline.....	109
Introduction.....	110
Methods.....	113
Results.....	117
Discussion.....	122
V. SUMMARY AND FUTURE DIRECTIONS.....	146
REFERENCES.....	151
CURRICULUM VITAE.....	168

## LIST OF FIGURES

FIGURE	PAGE
Chapter II	
1. The biotinylated dextran amine (BDA) injection sites in the pulvinar nucleus.....	42
2. Micrographs illustrate the laminar distribution of pulvinocortical terminals in the temporal cortex.....	44
3. Micrographs illustrate the distribution of pulvinocortical terminals in 2 cortical areas of the temporal cortex.....	46
4. Iontophoretic injections of biotinylated dextran amine in the pulvinar nucleus label 2 foci of terminals in the temporal cortex.....	48
5. Three-dimensional reconstructions of single BDA injections in pulvinar nucleus label 2 terminal foci in the temporal cortex.....	50
6. Corticopulvinar and pulvinocortical projections are topographically organized.....	52
7. Most pulvinocortical terminals contact non-GABAergic spines with asymmetric synapses. ....	54
8. Corticopulvinar cells are labeled in layer VI of 2 zones .....	56
9. The pulvinar nucleus and temporal cortex are reciprocally connected.....	58
10. The micrographs illustrate the morphology of axons and terminals labeled by an injection of BDA in the temporal cortex.....	60

11. Examples of the corticothalamic terminals in Pc labeled by the anterograde transport of BDA from T2.....	62
12. A summary of the results of the current study and those of our previous study of tectopulvinar projections .....	64

Chapter III

1. <i>In vitro</i> recording methods.....	87
2. Three types of neurons are distinguished by their responses to hyperpolarizing current steps.....	90
3. Three types of neurons are distinguished by their responses to hyperpolarizing current ramps. ....	92
4. Current ramps reveal distinct firing characteristics of single LTS and multi LTS neurons.....	94
5. Current ramps reveal further features of burst firing in multi LTS neurons .....	96
6. The pulvinar nucleus contains more T-type calcium channels than the dLGN....	98
7. The pulvinar nucleus contains fewer neurons than the dLGN.....	100
8. Space-plot representation of the different burst regimes in function of the T-current distribution. ....	102
9. Single-LTS require different, slower, channel kinetics.....	105
10. Voltage-trace responses to depolarized current ramps of various durations in three different cell models reproducing the protocol and results of Figure 3.....	108

Chapter IV

1. <i>In vitro</i> recording methods.....	127
2. Two types of EPSPs.....	129

3.	Two types of EPSPs display distinct frequency-dependent short-term plasticity.....	131
4.	Two types of EPSPs display distinct short-term plasticity by paired-pulse stimulation.....	133
5.	“Mixed” EPSP show characteristics of two types of EPSPs.....	135
6.	Convergence of tectopulvinar terminals.....	137
7.	Confocal images of dLGN tissue labeled with antibodies against synapsin I or II (purple), and vGLUT1 or 2 (green).....	139
8.	Confocal images of Pd tissue labeled with antibodies against synapsin I or II (purple), and vGLUT1 or 2 (green).....	141
9.	Confocal images of Pc tissue labeled with antibodies against synapsin I or II (purple), and vGLUT1 or 2 (green).....	143

# CHAPTER I

## INTRODUCTION

The thalamus is a symmetrical structure joined at the midline in the brains of vertebrates, and can be divided into several subdivisions: the dorsal thalamus (which is the largest division and often referred to simply as the “thalamus”), the ventral thalamus, the epithalamus and the hypothalamus (Herrick, 1918). The dorsal thalamus is the largest part of the diencephalon and expands with the development of the cerebral cortex. It serves as the most important relay to the cerebral cortex. Almost all the information we receive from the outside world flows through dorsal thalamus, the main exception being the relay of olfactory information. Thus, the dorsal thalamus plays a critical role in gating and modulating the flow of information from peripheral sensory receptors to the cerebral cortex.

Based on classical neuroanatomical and neurophysiological methods, the dorsal thalamus can be divided into several distinct cell groups termed nuclei that differ in both function and structure. Each of the nuclei receives specific types of afferent signals (e.g. visual, auditory, somatosensory, etc.) (Walker, 1938). However, the original structural and functional definitions of thalamic nuclei have been modified after decades of technical advances and the acquisition of new information. Almost all of the classic thalamic nuclei have been found to contain distinct sub-regions based on function,

connections, or cell morphology. There are also cell groups that cross the borders of classical nuclei, and each classical thalamic nucleus can contain several functionally-distinct parallel pathways (Sherman and Guillery, 2006).

### ***Relay nuclei and intralaminar nuclei***

The majority of the thalamic nuclei project either to the striatum (caudate nucleus, nucleus accumbens, “ventral striatum” and putamen) and/or the cerebral cortex (neocortex, palaeocortex and hippocampal formation). Major groups of relay nuclei that provide output to the cerebral cortex are the anterior, medial, lateral/pulvinar, ventral, dorsal lateral geniculate (dLGN) and medial geniculate nuclei. Intralaminar nuclei and the pulvinar nucleus additionally project to the striatum (Day-Brown et al., 2010)

### ***Types of thalamic cells***

It's widely accepted that the morphology of a neuron relates to its functional properties and that one may expect distinct cell types to play different roles in information processing. Two major dorsal thalamic cell groups are classified based on their axon projection targets: relay cells have axons that project to the telencephalon and interneurons have local axons located very close to their cell body in most cases. These two cell groups also differ in their dendritic patterns and the neurotransmitters they produce. Relay cells use glutamate as a neurotransmitter while interneurons use gamma amino butyric acid (GABA). The ratio of interneurons to relay cells can be quite different depending on the species and nuclei. For example, in the cat dLGN, interneurons make up 20%-25% of the overall cell population (LeVay and Ferster, 1979), while in the rats, this ratio is 20%-30% in the dLGN, or less than 1% in the somatosensory thalamus (Guillery and Sherman, 2002).

The thalamic relay cells have similar morphology and membrane properties; slight variation can be found in somal size, dendritic branching and dendritic appendages (Steriade et al., 1997). The visual thalamus, especially the primary visual pathway from the retina, through the dLGN, to the primary visual cortex or V1, has been most thoroughly investigated. We probably know more about the dLGN than any other thalamic nucleus. In many species (primates, carnivores and tree shrews) the dLGN contains several laminae, and the retinal inputs are topographically organized. This is referred to as a retinotopic map. In cats, two major types of relay cells, X cells and Y cells have been studied in detail. The functional X/Y difference is established in the retina; X cells receive retinal inputs from  $\beta$  cells, and Y cells from  $\alpha$  cells. Y cells have larger receptive fields and better responses to lower spatial and higher temporal frequencies of visual stimuli compared to X cells, while X cells have better linear summation to stimuli (Sherman and Spear, 1982). There is also morphological variance between X and Y cells. X cells tend to have elongated tufts of dendrites that are orientated perpendicular to the laminar borders. These cells have clusters of dendritic appendages near proximal dendritic branch points (Sherman and Friedlander, 1988). Y cell dendrites tend to have a more stellate distribution (Sherman and Friedlander, 1988). A third and relatively small group of cells, W cells, have been identified mostly based on their laminar localization in the dLGN or their cortical arborizations of axons (Casagrande and Xu, 2004). The classification based on cell morphology is still ambiguous because often intermediate cell types are found, and no strict criteria are set for this class of cells.

Interneurons have the smallest cell bodies among thalamic neurons. They have long, thin and sinuous dendrites and clusters of dendritic appendages that connect to stem

dendrites by long, thin process. This conformation looks like the terminal arbor of an axon, thus has been referred to as axoniform (Guillery, 1969). Actually these dendritic appendages synapse on relay cells and this is the main output of interneurons (Montero, 1987). Interneurons also have conventional axons that arborize within the extent of the dendritic arbor (Montero, 1987). In the cat's dLGN, interneurons were thought to be mostly associated with the X pathway (Sherman and Friedlander, 1988). However, subsequent studies showed that nearly half of the synaptic targets of Y retinogeniculate terminals are interneurons, and interneurons contact the dendrites of Y relay cells (Datskovskaia et al., 2001; Dankowski and Bickford, 2003). All interneurons are GABAergic, and their outputs inhibit postsynaptic targets (Montero, 1987; Guillery et al., 2001).

All the cells in the thalamic reticular nucleus (and perigeniculate nucleus) of the ventral thalamus are GABAergic and provide inhibitory innervations to the relay cells of the thalamus (Houser et al., 1980; Jones and Yang, 1985; Sanchez-Vives et al., 1997; Pinault and Deschenes, 1998). The nucleus forms a sheet surrounds the dorsal and lateral part of the dorsal thalamus; any axons that pass between cortex and thalamus must go through the nucleus and the thalamocortical and corticothalamic fiber bundles usually innervate the reticular cells (Ohara and Lieberman, 1985; Williamson et al., 1993).

### ***Intrinsic properties of thalamic cells***

The morphological properties of neurons may provide insight into how neurons process and relay information to their axonal projection targets. Another important aspect of a neuron is its electrical properties. The conventional view of neuronal transmission is that the soma and axon hillock make a more or less linear summation of all the excitatory



and inhibitory postsynaptic potentials (EPSPs and IPSPs) they receive from their dendrites and somata, and if their summation causes enough of increase in the membrane potential, they generate action potentials (APs). However, this concept is oversimplified because the membrane potential can change in a highly nonlinear, voltage-dependent manner, depending on the ion channels expressed by individual neurons. The cable properties of dendrites make the situation even more complicated in that the dendrites can conduct the synaptic potentials in all directions and shunting can occur at any branch point. Furthermore, some regions of dendrites have special electrical characteristics which electrically isolate them from other dendritic regions.

Thalamocortical relay cells are electrically compact, and synaptic potentials generated at the most distal dendrites can significantly influence the soma and axon without much attenuation (Bloomfield et al., 1987). Interneurons, in contrast to relay cells, are not electrically compact. The main reason for this is that they have longer and thinner dendrites. Also, many of the distal dendrites of interneurons, including their dendritic synaptic terminals are thought to be electrically and functionally isolated from the soma and axon of interneurons (Bloomfield and Sherman, 1989).

The neuron membrane displays nonlinearities due to several membrane conductances which are usually voltage-dependent or ligand-gated, or controlled by the concentration of certain ions. Some of the major and best-understood conductances in the thalamus include  $\text{Ca}^{2+}$ ,  $\text{Na}^+$ , and  $\text{K}^+$  conductances. Two major voltage-dependent  $\text{Na}^+$  conductances have been described in the thalamus. One  $\text{Na}^+$  conductance is the transient and rapidly activating and inactivating  $I_{\text{Na,t}}$  involved in the generation of action potentials. The other  $\text{Na}^+$  conductance is the persistent and non-inactivating  $I_{\text{Na,p}}$  which helps

maintain steady firing. Several voltage- and/or  $\text{Ca}^{2+}$ -dependent  $\text{K}^+$  conductances also exist in the thalamus.  $I_{\text{K}}$  is activated by strong depolarization and its function is to repolarize the action potential.  $I_{\text{C}}$  is activated by increases in  $\text{Ca}^{2+}$  and its function is action potential repolarization and modulation of interspike interval.  $I_{\text{AHP}}$  is a slow afterhyperpolarization that generates action potential adaptation; this conductance is sensitive to increases in  $\text{Ca}^{2+}$ .  $I_{\text{A}}$  is a transient inactivating current that delays the onset of firing, and modulates interspike interval.  $I_{\text{A}}$  and its relationship with  $I_{\text{T}}$ , a low threshold  $\text{Ca}^{2+}$  conductance, is of particular interest because both of these two conductances share some similar properties and can modulate the output of thalamic cells. Other  $\text{K}^+$  conductances including  $I_{\text{K,leak}}$  which contributes to the neuronal resting membrane potential, and  $I_{\text{h}}$ , which is a hyperpolarization-activated mixed cation conductance, that generates a depolarizing current (McCormick and Huguenard, 1992; Rhodes and Llinas, 2005).

$\text{Ca}^{2+}$  conductances are of special importance to thalamic relay cells. At least two voltage-dependent  $\text{Ca}^{2+}$  conductances are found in the thalamus, high threshold  $\text{Ca}^{2+}$  conductances, and the low threshold  $\text{Ca}^{2+}$  conductance  $I_{\text{T}}$ . The high threshold  $\text{Ca}^{2+}$  conductances can be further divided into L and N types; other types also exist (Johnson et al., 1996; Wu et al., 1998). Very little is known about these high threshold  $\text{Ca}^{2+}$  conductances, but they are known to be important for neurotransmitter release from synaptic terminals (Tytgat et al., 1991).

Thalamic relay cells have two distinct firing modes, burst firing mode and tonic firing mode, and these are controlled by the low threshold  $\text{Ca}^{2+}$  conductance (Deschenes et al., 1984; Jahnsen and Llinas, 1984a, b). During tonic firing mode, the low threshold

$\text{Ca}^{2+}$  conductance and other related conductances are inactivated, and when synaptic inputs bring the cell to firing threshold, the cell produces a steady stream of action potentials; the duration and frequency of these action potentials increases linearly in relation to the increase in strength and duration of the synaptic inputs. During burst firing mode, the low threshold  $\text{Ca}^{2+}$  conductance is de-inactivated. In this mode, in response to membrane depolarizations, the low threshold  $\text{Ca}^{2+}$  conductance can be activated which can subsequently trigger a brief burst of action potentials. The burst mode allows thalamic neurons to respond to synaptic inputs even when they are relatively hyperpolarized.

Several characteristics of low threshold calcium spikes (LTS) need to be mentioned here. The LTS can only be activated by depolarization from a relatively hyperpolarized mode, and this depends on the nature of the low threshold  $\text{Ca}^{2+}$  conductance activation-inactivation curve. The activation-inactivation of the LTS is a slow process compared to other conductances. The recovery time for LTSs is over 100 ms, and the membrane potential has to be maintained in a hyperpolarized state for a length of time for de-inactivation of this conductance to occur. Because of the overlapping windows of activation and inactivation of this conductance, thalamic neurons may experience spontaneous membrane potential fluctuations when the membrane potential drops within a certain range, and in combination with other conductances, this can generate rhythmic bursting (Sherman, 2001).

Another notable characteristic of the low threshold  $\text{Ca}^{2+}$  conductance is that it mediates a nonlinear response to stimuli. There are two aspects to this nonlinearity; in contrast to the tonic firing mode, the burst firing mode will not follow the time course of

a stimulus, nor will it follow the intensity of the stimulus. That is, the response will saturate rapidly once a stimulus reaches a certain threshold and will not increase in relation to the stimulus intensity (McCormick and Huguenard, 1992; Guido et al., 1995; Lu et al., 1995).

The binding of neurotransmitters may change thalamic conductance dynamically. For example, activation of nicotinic acetylcholine receptors can increase  $I_{Na}$ ,  $I_K$ , and  $I_{Ca}$ , while binding of muscarinic receptors can reduce  $I_{AHP}$  and  $I_{K,leak}$  (McCormick, 1993). The distribution of different ion channels on relay cells and interneurons is still unclear. In the dLGN, the low threshold calcium channels are distributed on soma and dendrites of thalamic cells and there is no evidence of their distribution on axons (Kovacs et al., 2010). Finally, the voltage-dependent activation of  $I_A$  is very similar to that of  $I_T$ , but usually occurs at more depolarized levels in relay cells and interneurons (Pape et al., 1994). This provides the possibility that when a LTS is evoked by synaptic input,  $I_A$  can be activated at the same time to interact with  $I_T$  to reduce the amplitude and slope of the LTS.

### ***Drivers and modulators***

Although a single thalamic nucleus may receive input from multiple regions of the brain, it is thought that in all nuclei one input has a higher weight compared to other inputs. These inputs are referred to as “drivers” and the other inputs “modulators”. This idea has been tested most thoroughly in the dLGN, where the response properties of geniculate cells are similar to their retinal inputs (Sherman and Guillery, 1998). Thus the retina is considered to drive the dLGN, while other inputs, such as the cholinergic inputs from the brainstem modulate the retinogeniculate response. It is still unclear what inputs

“drive” many of the nuclei of the dorsal thalamus, or if this concept will apply to all nuclei.

### *Circuitries and synaptic properties*

Retinal ganglion cells provide the driving input to the dLGN, but make up a small proportion of the synaptic junctions in the dLGN. In other nuclei, presumed drivers may provide as little as 2% of the input (Wang et al., 2002a). The retinal inputs are glutamatergic and when observed using an electron microscope, they form large terminal boutons which have a complex synaptic organization. They are referred to as RLP profiles because they contain round vesicles and are large and they contain pale mitochondria. RLP profiles form complex synaptic connections with adjacent profiles in an area free of glial cytoplasm; this region is called a glomerulus (Szentagothai, 1963). For other nuclei, identification of the driving afferents is more difficult to access. It has been proposed that some nuclei receive their driving input from layer V corticothalamic cells. These nuclei have been referred to as higher order nuclei, while nuclei that are driven by ascending sensory inputs (e.g. the dLGN) are referred to as first order nuclei (Sherman and Guillery, 2006). Based on this definition, the rostral part of the rat LPN can be considered higher order because it is innervated by layer V corticothalamic pyramidal cells (Bourassa and Deschenes, 1995). These cells provide input to the LPN in the form of large terminals with round vesicles (RL profiles) that are structurally similar to retinogeniculate terminals (Li et al., 2003a). In addition, stimulation of layer V inputs to the rostral LPN elicits a frequency dependent depression in relay cells (Li et al., 2003b) which is similar to the response of dLGN neurons to stimulation of retinogeniculate axons (Chen et al., 2002).

Modulatory inputs can be further divided into at least three groups: intrinsic inhibitory inputs, cortical inputs, and brainstem inputs. The intrinsic inhibitory inputs arise from the thalamic reticular nucleus (TRN) and intranuclear interneurons. All thalamic nuclei receive GABAergic inputs from the TRN (Ohara and Lieberman, 1985). TRN terminals have flattened synaptic vesicles and form symmetrical synapses. They are referred to as F1 profiles and usually contact thalamocortical cells outside of glomeruli (Wang et al., 2002b). Based on the synaptic relationships between the TRN, dorsal thalamic nuclei, and the cortex, the TRN can provide feedback or feedforward inhibition of relay cells (Wang et al., 2007).

Intranuclear interneurons have two outputs to relay cells, conventional axon output, which is morphologically similar to TRN terminals (F1 profiles), and axoniform dendritic terminals which are referred to as F2 profiles. F2 profiles can be distinguished morphologically from F1 profiles based on the density of vesicles. F2 profiles contain sparsely distributed vesicles and F1 profiles contain densely packed vesicles. In addition, F1 profiles are only presynaptic profiles, while F2 profiles are both pre- and post-synaptic. F2 profiles are often located within glomeruli and are post-synaptic to RL profiles as well as pre-synaptic to dendrites that are post-synaptic to the same RL profile; this formation is called a triad (Datskovskaia et al., 2001).

Cortical modulatory inputs arise from layer VI corticothalamic pyramidal cells which form synaptic terminals that contain round vesicles and are of relatively small size (RS profiles). They usually make a single synapse with an adjacent dendritic process. Cells in the rat LPN respond to stimulation of the cortical layer VI axons with a frequency- dependent facilitation, a response that is similar to the cortical input to the

LGN (Li et al., 2003b). Other major difference between layer V and layer VI cortical inputs is that layer V does not innervate the TRN while layer VI does (Murphy and Sillito, 1996).

Brainstem inputs to the thalamus can vary with species and specific thalamic nuclei. These inputs including cholinergic input from parabrachial region (also known as the pedunclopontine tegmentum or PPT), noradrenergic inputs from the locus coeruleus, serotonergic inputs from dorsal raphe nucleus (Fitzpatrick, Diamond et al. 1989), and GABAergic inputs from the pretectum (Wang et al., 2002b). In the dLGN, cholinergic inputs can also arise from the parabigeminal nucleus (De Lima and Singer, 1987). Cholinergic terminals from the PPT are densely distributed in the dLGN and pulvinar nucleus and form synaptic terminals that are similar to layer VI corticothalamic RS profiles, but are of slightly larger size. PPT inputs also are distinct from cortical inputs in that they can form triads or pseudo triads (Erisir et al., 1997; Patel and Bickford, 1997).

#### ***Lateral posterior and pulvinar nuclei***

In rodents, the homologue of the primate pulvinar nucleus is the lateral posterior nucleus, and this nucleus makes up a relatively small part of their thalamus. In contrast, the pulvinar is the largest nucleus in the primate thalamus. The expansion of the pulvinar nucleus in species with more complex visual capabilities parallels the overall expansion of the cerebral cortex, and in particular the expansion of cortical regions devoted to visual signal processing. In primates, the cortical connections of the pulvinar nucleus include the striate cortex (V1) as well as multiple extrastriate regions in both the parietal and temporal cortex (Cavada and Goldman-Rakic, 1993; Cusick et al., 1993; Stepniewska et al., 1999; Matsuzaki et al., 2004).

The pulvinar nucleus is thought to be involved in indicating the salience of visual images and events and coordinating appropriate responsive actions (Robinson and Petersen, 1992), but its detailed function is still ambiguous. The morphology of pulvinar relay cells and interneurons do not appear to be remarkably different from those in other thalamic nuclei (Campos-Ortega and Hayhow, 1972; Mathers, 1972). However, some regions of the pulvinar nucleus receive input from both cortical layers V and VI (RS and RL profiles; (Mathers, 1972; Robson and Hall, 1977), and thus can be defined as higher order nuclei. It has been proposed that the function of higher order nuclei is to relay information from one cortical area to another, rather than to relay sensory signals from the periphery to the cortex (Guillery and Sherman, 2002). However, there is still much to be elucidated concerning the connections formed between the pulvinar nucleus and the cortex and the function of these connections.

Some regions of the pulvinar nucleus receive input from the pretectum or superior colliculus (Harting et al., 1973; Benevento and Fallon, 1975). Since both of these areas receive direct input from the retina (Perry and Cowey, 1984; Leventhal et al., 1985), the pulvinar nucleus may also function to relay subcortical visual signals to the cortex. Humans with lesions of V1 do not perceive visual stimuli, but they can still navigate using visual cues, a phenomenon referred to as “blindsight”. Blindsight is thought to be mediated by projections from the superior colliculus and/or pretectum to the pulvinar nucleus. This is supported by the fact that in species with expanded tectopulvinar pathways, such as the tree shrew, animals maintain a large degree of visual capacity after complete lesion of V1 and subsequent degeneration of the dLGN (Diamond and Hall, 1969; Killackey and Diamond, 1971). These studies, as well as studies of human



blindsight, suggest that a substantial amount of visual information passes through structures other than the primary visual pathway through the dLGN to V1, and that this information can be utilized to evaluate visual signals and initiate appropriate responsive actions.

It is important to elucidate the detailed circuitry of the pulvinar nucleus not only to understand human vision and the mechanisms underlying phenomena such as blindsight, but also because the pulvinar nucleus is thought to be affected in several brain disorders. For example, in schizophrenics, the pulvinar nucleus is smaller and contains fewer neurons when compared to the pulvinar nucleus of control subjects (Byne et al., 2009). In particular, abnormal tectopulvinar pathways may account for the disturbances of visual motion processing experienced by schizophrenic patients (Chen et al., 2005; O'Donnell et al., 2006; Brittain et al., 2010). Tectopulvinar pathways have also recently been found to be affected in autism (Kleinhans et al., 2011).

The experiments described in the following chapters elucidate key features of tecto-pulvino-cortical pathways. The tree shrew is used as the animal model because the visual structures of the tree shrew brain display many of the features of the primate brain, and the tectopulvinar pathways are particularly enhanced in this species. Chapter 2 describes the connections formed between the tectorecipient regions of the pulvinar nucleus and the cortex, which were explored using anatomical techniques including tract tracing, immunohistochemistry, light, confocal, and electron microscopy. Chapter 3 compares the membrane properties of neurons in the tectorecipient regions of the tree shrew pulvinar to those of neurons of the tree shrew dLGN. These experiments utilized whole cell recordings in slices of the pulvinar maintained in vitro, western blotting,

stereology, and neuron modeling techniques. Chapter 4 describes the properties of tectopulvinar synapses explored using in vitro whole cell recordings in brain slices, immunohistochemistry and confocal microscopy. Chapter 5 summarizes the 3 data chapters and describes future research necessary to fully elucidate the function of the tecto-pulvino-cortical pathways.

## CHAPTER II

### SYNAPTIC ORGANIZATION OF CONNECTIONS BETWEEN THE TEMPORAL CORTEX AND PULVINAR NUCLEUS OF THE TREE SHREW

#### Outline

We examined the synaptic organization of reciprocal connections between the temporal cortex and the dorsal (Pd) and central (Pc) subdivisions of the tree shrew pulvinar nucleus, regions innervated by the medial and lateral superior colliculus, respectively. Both Pd and Pc subdivisions project topographically to 2 separate regions of the temporal cortex; small injections of anterograde tracers placed in either Pd or Pc labeled 2 foci of terminals in the temporal cortex. Pulvinocortical pathways innervated layers I–IV, with beaded axons oriented perpendicular to the cortical surface, where they synapsed with spines that did not contain gamma amino butyric acid (GABA), likely located on the apical dendrites of pyramidal cells. Projections from the temporal cortex to the Pd and Pc originate from layer VI cells, and form small terminals that contact small caliber non-GABAergic dendrites. These results suggest that cortical terminals are located distal to tectopulvinar terminals on the dendritic arbors of Pd and Pc projection cells, which subsequently contact pyramidal cells in the temporal cortex. This circuitry could provide a mechanism for the pulvinar nucleus to activate subcortical visuomotor circuits and modulate the activity of other visual cortical areas. The potential relation to primate tecto-pulvino-cortical pathways is discussed.

## Introduction

In primates and other species with significant visually guided behavior, a large proportion of the dorsal thalamus generates visuosensory- and eye-movement-related signals. Although the visual pathways from the retina through the lateral geniculate nucleus (dLGN) to the striate cortex (V1) have been studied in detail, relatively little is known regarding the synaptic organization of pathways connecting the extrageniculate visual thalamus with the cortex. The purpose of this study was to examine the synaptic organization of thalamocortical terminals and corticothalamic terminals connecting the cortex to well-defined subdivisions of the pulvinar nucleus that receive visual input from the superficial layers of the superior colliculus (SC).

Tree shrews (*Tupaia*) are small, fast moving animals with excellent motion vision and visually guided behavior. Particularly striking features of the tree shrew brain are the greatly enlarged SC, and a correspondingly large pulvinar nucleus. The fact that the tree shrew brain possesses many primate characteristics (Kaas and Preuss 1993; Kaas 2002), led at one time to their classification in the primate order (LeGros Clark 1934; Campbell 1980). Although now classified in the order *Scandentia*, tree shrews still are considered to represent a prototype of early prosimian primates. Therefore, studies of the connections between the cortex and pulvinar nucleus in the tree shrew should shed light on the organization of these connections in primates.

The tree shrew pulvinar contains 2 tectorecipient subdivisions: the dorsal (Pd) and central (Pc) pulvinar (Lyon et al. 2003a, 2003b). The tectal projections to these 2 subdivisions are organized differently; those to Pd terminate diffusely, whereas those to Pc terminate in a more spatially precise manner (Luppino et al. 1988). In subsequent

studies using anterograde and retrograde tracing techniques, as well as electron microscopy, we concluded further that although both Pd and Pc receive topographically organized projections from the SC, the Pd receives additional diffuse projections, which possibly arise from wide-ranging axon collaterals of tectopulvinar cells (Chomsung et al. 2008). We also identified differences in the synaptic arrangements of tectal terminals in the Pd and Pc. These results support the argument that the tectorecipient part of the tree shrew pulvinar nucleus comprises 2 distinct zones.

The aims of the current study were 4-fold. First, we tested whether the Pd and Pc target distinct cortical areas to determine whether these pulvinar subdivisions comprise parallel pathways from the SC to the cortex. Second, we examined the laminar distribution and ultrastructure of pulvinocortical terminals in an effort to determine the cortical cell types targeted by the tectorecipient pulvinar nucleus. Third, we examined the laminar origin and reciprocity of corticopulvinar connections to determine how the organization of the tectorecipient pulvinar nucleus compares to that of other dorsal thalamic nuclei. Finally, we measured the size of corticopulvinar terminals and their postsynaptic targets (to compare to our previous measurements of tectal terminals and their postsynaptic targets, Chomsung et al. 2008) in order to understand how cortical and tectal inputs are distributed on the dendritic arbors of Pd and Pc neurons. Our results define the unique circuitry of the tectorecipient zones of the pulvinar nucleus, and provide the first characterization of the synaptic organization of pulvinocortical projections in any species.

## **Methods**

A total of 27 adult (average weight 175 g) tree shrews (*Tupaia belangeri*); 17 males and 10 females, were used for these experiments. Fourteen tree shrews were used to examine the distribution, morphology and synaptic targets of pulvinocortical terminals labeled by unilateral (10 animals) or bilateral (4 animals) injections of the anterograde tracer biotinylated dextran amine (BDA) in the pulvinar nucleus (6 of these animals were also used for a previous study, Chomsung et al. 2008). Six tree shrews were used to examine the distribution of pulvinocortical cells labeled by injecting the retrograde tracers rhodamine dextran amine (RDA, 3 animals) rhodamine labeled microspheres (“red beads,” 1 animal), cholera toxin subunit B (CTB, 1 animal), or fluorogold (FG, 1 animal) in the temporal cortex. Three tree shrews were used to examine the distribution of corticopulvinar cells labeled by injecting the retrograde tracer FG in the pulvinar nucleus. Corticopulvinar cells were also labeled in one animal that received dual injections of BDA and FG in the pulvinar nucleus. Four animals were used to examine the distribution, morphology, and synaptic targets of corticopulvinar terminals labeled by injecting BDA in the cortex. In addition, corticopulvinar terminals were also labeled in one animal that received dual injections of BDA and CTB in the temporal cortex. Selected sections from BDA-injected tree shrews were stained for acetylcholinesterase (AChE) to distinguish the dorsal (Pd) and central (Pc) regions of the pulvinar nucleus (Lyon et al. 2003a). All methods were approved by the University of Louisville Animal Care and Use Committee and conform to the National Institutes of Health guidelines.

### ***Tracer Injections***

Tree shrews that received RDA (10K; Molecular Probes, Eugene, OR), BDA (3000 MW; Molecular Probes), FG (Fluorochrome LLC, Denver, CO), CTB (List

Biological Laboratories, Inc., Cambell, CA; catalogue #105), or red bead (Lumafluor, Naples FL) injections were initially anesthetized with intramuscular injections of ketamine (100 mg/kg) and xylazine (6.7 mg/kg). Additional supplements of ketamine and xylazine were administered approximately every 45 min to maintain deep anesthesia through completion of the tracer injections. The heart rate was continuously monitored with a MouseOx pulse oximeter (STARR Life Sciences Corp., Pittsburgh, PA). Prior to injection, the tree shrews were placed in a stereotaxic apparatus and prepared for sterile surgery. A small area of the skull overlying the dorsal pulvinar nucleus, central pulvinar nucleus, dorsal temporal cortex, or posterior temporal cortex was removed and the dura reflected.

For all of the pulvinar injections, and 6 of the temporal cortex injections, a glass pipette containing BDA (5% in saline, tip diameter 2  $\mu\text{m}$ ), FG (2% in saline, tip diameter 2–10  $\mu\text{m}$ ), BDA + FG (5% BDA and 2% FG in saline; tip diameter 2  $\mu\text{m}$ ), or BDA + CTB (5% BDA + 1% desalted CTB in 0.1 M phosphate buffer, pH 6.0; tip diameter 2  $\mu\text{m}$ ) was lowered vertically and the tracer was ejected iontophoretically (2  $\mu\text{A}$  positive current for 15–30 min). For the remaining injections, a 1- $\mu\text{L}$  Hamilton syringe containing 0.1–0.3  $\mu\text{L}$  of RDA (10% in saline), or 0.5- $\mu\text{L}$  red beads (undiluted solution), was lowered vertically into the temporal cortex and the tracers were ejected via pressure. After a 7-day survival period, the tree shrews were given an overdose of sodium pentobarbital (250 mg/kg) and were perfused through the heart with Tyrode solution, followed by a fixative solution of 2% paraformaldehyde and 2% glutaraldehyde (RDA or BDA injections) or 4% paraformaldehyde (BDA, FG, or CTB injections) in 0.1 M phosphate buffer, pH 7.4 (PB).

The brain was removed from the skull, sectioned into 50- $\mu$ m-thick slices using a vibratome (Leica VT100E, Leica Microsystems, Bannockburn, IL) and collected in a solution of 0.1 M PB. In some cases, sections were preincubated in 10% methanol in PB with 3% hydrogen peroxide (to react with the endogenous peroxidase activity of red blood cells not removed during the perfusion). The BDA was revealed by incubating sections in a 1:100 dilution of avidin and biotinylated horseradish peroxidase (ABC; Vector Laboratories, Burlingame, CA) in phosphate-buffered saline (0.01 M PB with 0.9% NaCl, pH 7.4) overnight at 4 °C. The sections were subsequently rinsed, reacted with nickel-intensified 3,3'-diaminobenzidine (DAB) for 5 min, and washed in PB. RDA and FG were revealed with green or ultraviolet light, or by incubating with a rabbit anti-rhodamine antibody (Chemicon International, Temecula, CA) diluted 1:10 000, or a rabbit anti-FG antibody (Fluorochrome) diluted 1:50 000, followed by a biotinylated goat-anti-rabbit antibody, ABC, and DAB reaction. CTB was revealed using a rabbit-anti-cholera toxin antibody (Sigma, catalogue # C3062) diluted 1:10 000, followed by a biotinylated goat-anti-rabbit antibody (Vector, catalogue # BA-1000), ABC, and DAB reaction. Red beads were revealed under green light illumination. To reveal the distribution of BDA and FG, or BDA and CTB, for confocal microscopy, the BDA was revealed by incubating sections in a 1:100 dilution of streptavidin conjugated to Alexa Fluor 546 (Molecular Probes, Eugene, OR) and the FG or CTB were revealed with the rabbit antibodies listed above followed by a 1:100 dilution of a goat-anti-rabbit antibody conjugated to Alexa Fluor 488 (Molecular Probes). Sections were mounted on slides for light microscopic examination (BDA, RDA, FG, CTB, and red bead injections) or were prepared for electron microscopy (BDA injections).



### ***AChE Staining***

Alternate sections from 13 cases were stained for AChE to distinguish the Pd and Pc (Lyon et al. 2003a). We used a protocol modified from Geneser-Jensen and Blackstad (1971). Briefly, the tissue was rinsed in deionized water, placed in a solution of AChE for 3 h, and then rinsed in saline, followed by deionized water, before reacting with a 1.25% sodium sulfite solution for 1 min. Following deionized water rinses, the tissue was then incubated in a 1% silver nitrate solution for 5 min, rinsed with deionized water and placed in a 5% sodium thiosulfite solution to adjust the contrast of the tissue staining (approximately 5 min). Finally, the tissue was rinsed in saline, and mounted on slides for light microscope examination.

### ***Light Microscopic Data Analysis***

A Neurolucida system and tracing software (MicroBrightField, Inc., Williston, VT) was used to plot the distribution of FG-labeled corticopulvinar cells, BDA-labeled corticopulvinar terminals, RDA-labeled and red bead-labeled pulvinocortical cells, BDA-labeled pulvinocortical terminals, and CTB-labeled corticotectal cells. In some cases, adjacent sections stained for AChE were used to distinguish the borders of the Pd. The Neurolucida system was also used to create a 3-dimensional (3D) reconstruction of cortical sections and thalamus sections. The distributions of labeled pulvinocortical terminals and pulvinar injection sites were then added to these reconstructions.

### ***Electron Microscopy***

Temporal cortex or pulvinar sections that contained BDA-labeled pulvinocortical terminals or corticopulvinar terminals were postfixed in 2% osmium tetroxide, dehydrated in an ethyl alcohol series, and flat embedded in Durcupan resin between 2

sheets of Aclar plastic (Ladd Research, Williston, VT). Durcupan-embedded sections were first examined with a light microscope to select areas for electron microscopic analysis. Selected areas were mounted on blocks, ultrathin sections (70–80 nm, silver-gray interference color) were cut using a diamond knife, and sections were collected on Formvar-coated nickel slot grids. Selected sections were stained for the presence of gamma amino butyric acid (GABA) using previously reported postembedding immunocytochemical techniques (Patel and Bickford 1997; Kelly et al. 2003; Li et al. 2003; Baldauf et al. 2005; Huppé-Gourgues et al. 2006; Chomsung et al. 2008). The GABA antibody (Sigma, catalogue # A2052, used at a dilution of 1:1000–1:2000) and was tagged with a goat-anti-rabbit antibody conjugated to 15-nm gold particles (Amersham, Arlington Heights, IL). The GABA stained sections were air dried and stained with a 10% solution of uranyl acetate in methanol for 30 min before examination with an electron microscope.

### ***Ultrastructural Analysis***

Ultrathin sections were examined using an electron microscope. All labeled terminals involved in a synapse were photographed within each examined section. The pre- and postsynaptic profiles were characterized on the basis of size, (shortest width and area measured using a digitizing tablet and Sigma Scan Software; SPSS, Inc., Chicago, IL), the presence or absence of vesicles, and the overlying gold particle density. The ultrastructural features of adjacent terminals were also noted. In the cortex, profiles were considered to be GABAergic if the gold particle density was higher than that found overlying 95% of the BDA-labeled pulvinocortical terminals. In the pulvinar nucleus,

profiles were considered to be GABAergic if the gold particle density was higher than that found overlying 95% of the BDA-labeled corticopulvinar terminals.

### ***Computer Generated Figures***

Light level photographs were taken using a digitizing camera (Spot RT; Diagnostic Instruments, Inc., Sterling Heights, MI). Confocal images were taken using an Olympus Fluoview laser scanning microscope (BX61W1). Electron microscopic images were taken using a digitizing camera (SIA-7C; SIA, Duluth, GA) or negatives, which were subsequently scanned and digitized (SprintScan 45i; Polaroid, Waltham, MA). Using Photoshop software (Adobe Systems, Inc., San Jose, CA), the brightness and contrast were adjusted to optimize the images. Plots and 3D reconstructions of cell and terminal distributions were generated using a NeuroLucida system (MicroBrightField, Inc., Williston, VT).

## **Results**

### ***Topography of Pulvinocortical Projections***

To determine the distribution of pulvinocortical projections, we injected the pulvinar nucleus with BDA (Fig. 1) to label terminals by anterograde transport. We placed injections within the Pd and Pc, both of which receive input from the SC. As previously described (Chomsung et al. 2008), these injections resulted in the retrograde labeling of cells in the lower stratum griseum superficiale (SGS) and stratum opticum (SO) of the SC. Injections that invaded the external medullary lamina (LME; Fig. 1A,B) also labeled cells in the temporal cortex (Fig. 2B), likely due to uptake by corticothalamic and/or corticotectal axons that travel in the LME. The smaller injections, which were confined to the pulvinar nucleus and did not involve the LME, labeled terminals, but not

cells, in the temporal cortex (Figs 2*A* and 3). In addition, pulvinar injections labeled terminals in the caudate nucleus, putamen, and amygdala (data not shown).

Injections restricted to the Pd or Pc labeled terminals in restricted regions of the temporal cortex (Figs 3 and 4). A consistent finding was that small injection sites labeled 2 discrete foci of pulvinocortical terminals. To determine the topography of these projections, we used a NeuroLucida system to reconstruct the patches of labeled terminals in 3 dimensions. As illustrated in Figure 5, the labeled pulvinocortical axons terminated topographically within an area of the posterior temporal cortex, and additionally in an area of the more rostral/dorsal temporal cortex, which we will hereafter refer to as T1 and T2, respectively. As injections in the pulvinar nucleus shifted from rostral to caudal, the patches of labeled terminals shifted from caudal to rostral. Figure 5 also demonstrates that dual topographic projections were labeled by either Pd or Pc injections.

Because each injection site also labeled tectopulvinar cells in restricted regions of the medio-lateral dimension of the SC (described in detail in Chomsung et al. 2008), which has been mapped using physiological recording techniques (Lane et al. 1971), we approximated the representations of the visual field that would presumably be transferred from the SC, through the pulvinar nucleus, to the temporal cortex. These results suggest that the upper visual field is represented in the caudal regions of the temporal cortex, whereas the lower visual field is represented in more rostral regions (summarized in Fig. 12*A*). Approximation of peripheral or central visual field representations was not possible because the pulvinar injections labeled tectopulvinar cells in bands that spanned the rostro-caudal dimension of the SC (Fig. 9*A*; Chomsung et al. 2008).

The distribution of pulvinocortical cells labeled following retrograde tracer injections into the temporal cortex confirmed the general topography of pulvinocortical projections. Injections in caudal regions of the temporal cortex labeled cells in more rostral/dorsal regions of the pulvinar nucleus (Fig. 6C,D), whereas injections in the rostral temporal cortex labeled cells in the caudal/ventral pulvinar nucleus (Fig. 6E,F).

#### ***Laminar Distribution and Synaptic Targets of Pulvinocortical Terminals***

The terminals labeled following both large and small pulvinar injections were most densely distributed in layer IV, but extended through layers III and II to layer I (Figs 2A, 3). Compared with the striate cortex, cortical layers are difficult to discern in the temporal cortex. However, the retrograde labeling of layer V cells following a large pulvinar injection (which invaded the LME, Fig. 1A) served to confirm that the majority of pulvinocortical terminals were distributed above layer V (Fig. 2B). The laminar distribution and morphology of terminals was similar in T1 and T2. However, terminals in T1 tended to be more densely distributed in layer IV than in more superficial layers (Fig. 3A), whereas pulvinocortical terminals in T2 tended to be more evenly distributed through layers IV–I (Fig. 3B), forming discrete columns of terminals. This slight difference in the laminar distribution of pulvinocortical terminals was accentuated in the most rostral regions of the T2, where the cortex is thicker than that of the T1 projection zone.

In both the T1 and T2, the pulvinocortical axons gave rise to boutons which were distributed along the axon in a “beads on a string” pattern (Fig. 2B). The axons were generally oriented perpendicular to the cortical surface, and single axons could be followed from layer IV to layer I. We examined the synaptic targets of a total of 387

labeled pulvinocortical terminals within the 2 projection zones of 4 tree shrews. All blocks analyzed at the ultrastructural level contained terminals in lamina I–IV. The labeled terminals made a total of 442 synaptic contacts (226 synapses in T1 and 216 synapses in T2). Examples of synaptic contacts in the 2 projection zones are illustrated in Figure 7. Similar synaptic contacts were observed in all cases.

The size of pulvinocortical terminals was similar in T1 and T2 (shortest width  $0.62 \pm 0.15 \mu\text{m}$  in T1 and  $0.68 \pm 0.16 \mu\text{m}$  in T2). In both areas we found that pulvinocortical terminals form asymmetric contacts with spines and small dendrites (shortest width  $0.40 \pm 0.13 \mu\text{m}$  in T1 and  $0.44 \pm 0.12 \mu\text{m}$  in T2). Most pulvinocortical terminals formed single synapses (53.54% in T1 and 48.68% in T2; Fig. 7D,F), whereas other contacts could be classified as perforated (32.82% in T1 and 37.03% in T2; Fig. 7A, B, E, and H). Pulvinocortical terminals were also observed to form multiple synapses (13.64% in T1 and 14.29% in T2; Fig. 7C,G).

Each examined section was also stained for GABA using postembedding immunocytochemical techniques to determine whether pulvinocortical terminals contact GABAergic or non-GABAergic cells. With the assumption that pulvinocortical terminals are non-GABAergic, the gold particle density overlying the labeled terminals was used as a measure of background staining, which is fixation dependent and varies from case to case (T1 animal 1 mean density =  $14.06 \pm 11.59$  gold particles/ $\mu\text{m}^2$ ,  $n = 103$ ; T1 animal 2 mean density =  $4.44 \pm 4.38$  gold particles/ $\mu\text{m}^2$ ,  $n = 95$ ; T2 animal 1 mean density =  $10.69 \pm 7.98$  gold particles/ $\mu\text{m}^2$ ,  $n = 100$ ; T2 animal 3 mean density =  $14.34 \pm 10.44$  gold particles/ $\mu\text{m}^2$ ,  $n = 89$ ). Using this criteria, all postsynaptic targets of pulvinocortical terminals were found to be non-GABAergic (T1 animal 1 mean density =

$8.79 \pm 9.02$ ,  $n = 119$ ; T1 animal 2 mean density =  $5.64 \pm 7.49$ ,  $n = 107$ ; T2 animal 1 mean density =  $5.02 \pm 6.08$ ,  $n = 119$ ; T2 animal 3 mean density =  $8.44 \pm 7.12$ ,  $n = 97$ ).

### ***Laminar Origin and Reciprocity of Corticopulvinar Connections***

Injections of FG that were confined to the Pd and/or Pc (and did not involve the LME) labeled cells exclusively in layer VI of the temporal cortex (Figs 6A, B, and 9A). Small injections labeled 2 clusters of cells in T1 and T2 (Fig. 8), whereas larger injections labeled a continuous band of cells in the temporal cortex (Fig. 9D,E).

Injections of FG that included, but were not confined to the pulvinar nucleus, labeled cells in both layers V and VI of the cortex. These results suggest that all corticothalamic projections to the Pd and Pc originate from layer VI of the temporal cortex, whereas projections to adjacent nuclei (ventral pulvinar and lateral intermediate nucleus) may originate from cells in both layers V and VI (although the involvement of the LME complicates interpretation).

To test whether corticopulvinar and pulvinocortical connections are reciprocal, we injected both BDA and FG from the same pipette into a single site in the pulvinar nucleus (Fig. 9C). This resulted in closely overlapping distributions of cells and terminals in the temporal cortex (Fig. 9A,D,E). Similarly, when we injected both BDA and CTB from the same pipette into the temporal cortex (Fig. 9F), we found that pulvinocortical cells and corticopulvinar terminals overlapped extensively within the pulvinar nucleus (Fig. 9B,G,H).

### ***Morphology and Synaptic Targets of Corticopulvinar Terminals***

Figure 10A illustrates the morphology of terminals in the Pc labeled by anterograde transport from an injection in T2. The labeled axons were of small caliber and gave rise to small diffusely distributed boutons that emanate from short stalks. For comparison, Figure 10B illustrates the morphology of axons in the pretectum (PT) labeled from the same injection site. These corticopretectal axons (which are shown at the same magnification as the corticopulvular axons in Fig. 10A), are thicker and give rise to larger boutons. All terminals in the Pd and Pc labeled following BDA injections in either T1 or T2 exhibited a morphology that was similar to that illustrated in Figure 10A.

We examined the synaptic targets of a total of 417 labeled corticothalamic terminals in the pulvular nucleus of 3 tree shrews. Each labeled terminal made a single synaptic contact in the sections examined. Examples of synaptic contacts are illustrated in Figure 11.

In both Pd and Pc, we found that terminals labeled from the temporal cortex were small profiles that contained round vesicles (RS profiles; mean terminal width in Pd =  $0.46 \pm 0.10 \mu\text{m}$ ; mean terminal width in Pc =  $0.48 \pm 0.13 \mu\text{m}$ ) that contacted relatively small caliber dendrites (shortest widths of postsynaptic dendrites:  $0.73 \pm 0.29 \mu\text{m}$  in Pd and  $0.79 \pm 0.33 \mu\text{m}$  in Pc) with thick postsynaptic densities. There was no significant difference in the sizes of corticopulvular terminals or their postsynaptic dendrites in the Pd and Pc (Student's *t*-test). However, the sizes of corticopulvular terminals and their postsynaptic dendrites were both found to be significantly smaller (Student's *t*-test,  $P < 0.001$ ) than our previous measurements (Chomsung et al. 2008) of tectopulvular terminals (Pd,  $0.62 \pm 0.22$ ; Pc  $0.62 \pm 0.21$ ) and their postsynaptic dendrites (Pd,  $1.07 \pm 0.67$ , Pc,  $0.97 \pm 0.46$ ).



Each examined section was also stained for GABA using postembedding immunocytochemical techniques to determine whether pulvinocortical terminals contact GABAergic interneurons or non-GABAergic projection cells. With the assumption that corticopulvinar terminals are non-GABAergic, the gold particle density overlying the labeled terminals was used as a measure of background staining, which is fixation dependent and varies from case to case (Pd animal 1 mean density =  $2.58 \pm 2.92$  gold particles/ $\mu\text{m}^2$ ,  $n = 100$ ; Pc animal 2 mean density =  $4.36 \pm 5.26$  gold particles/ $\mu\text{m}^2$ ,  $n = 102$ ; Pc animal 2 mean density =  $7.67 \pm 6.0$  gold particles/ $\mu\text{m}^2$ ,  $n = 101$ ; Pc animal 3 mean density =  $6.68 \pm 7.75$  gold particles/ $\mu\text{m}^2$ ,  $n = 114$ ). Using this criterion, we found that the majority of dendrites postsynaptic to labeled terminals were non-GABAergic (Pd animal 1 mean density =  $2.02 \pm 2.22$  gold particles/ $\mu\text{m}^2$ ,  $n = 89$ ; Pc animal 2 mean density =  $3.23 \pm 2.55$  gold particles/ $\mu\text{m}^2$ ,  $n = 90$ ; Pc animal 2 mean density =  $3.33 \pm 2.96$  gold particles/ $\mu\text{m}^2$ ,  $n = 93$ ; Pc animal 3 mean density =  $3.41 \pm 4.19$  gold particles/ $\mu\text{m}^2$ ,  $n = 108$ ).

The gold density overlying the remaining profiles was significantly higher (Student's *t*-test  $P < 0.001$  in each case) than that overlying the labeled corticopulvinar terminals (Pd animal 1 mean density =  $22.03 \pm 12.26$  gold particles/ $\mu\text{m}^2$ ,  $n = 11$ ; Pc animal 2 mean density =  $36.97 \pm 16.43$  gold particles/ $\mu\text{m}^2$ ,  $n = 12$ ; Pc animal 2 mean density =  $34.10 \pm 12.84$  gold particles/ $\mu\text{m}^2$ ,  $n = 8$ ; Pc animal 3 mean density =  $37.82 \pm 19.20$  gold particles/ $\mu\text{m}^2$ ,  $n = 6$ ). Overall, 11 of 100 or 11% of the postsynaptic profiles in the Pd, and 26 of 317 or 8.2% of the postsynaptic profiles in Pc were GABAergic. Of

these GABAergic postsynaptic profiles, 63.6% (7/11) in Pd and 65.4% or (17/26) in Pc contained vesicles (e.g., Fig. 11A).

## **Discussion**

Figure 12 summarizes the main findings of this study of 859 pulvinocortical and corticopulvinar synapses, and of our previous study of 539 tectopulvinar synapses (Chomsung et al. 2008). We found that the Pd and Pc are reciprocally and topographically connected with 2 regions of the temporal cortex. Projections from the Pd and Pc contact non-GABAergic spines in layers I–IV of the temporal cortex, and projections from cells in layer VI of the temporal cortex primarily contact small caliber non-GABAergic dendrites in the Pd and Pc. Compared with tectopulvinar terminals, corticopulvinar terminals are smaller and contact smaller caliber dendrites in the Pd and Pc. The difference in the size of the dendrites postsynaptic to these 2 terminal types suggests that corticopulvinar terminals are located distal to tectopulvinar terminals on the dendritic arbors of pulvinar projection cells. In the discussion that follows we will relate these results to previous studies of the tree shrew and other species, and consider how the classification of thalamic nuclei into first and higher order applies to the organization of the tectorecipient pulvinar nucleus. Reciprocal Topographic Pulvinocortical Connections Define 2 Temporal Areas

Our results indicate that the tectorecipient pulvinar nucleus is reciprocally connected with the temporal cortex: layer VI cells in the temporal cortex project to the Pd and Pc, and the Pd and Pc project to layers I–IV of the temporal cortex. Our results also indicate that the projections from the Pd and Pc to the temporal cortex are topographic. Small injections in the pulvinar resulted in discrete patches of labeled terminals in the

temporal cortex, and small injections in the temporal cortex labeled discrete groups of cells in the pulvinar nucleus. Both sets of experiments indicate that the caudal pulvinar nucleus is connected with more rostral regions of the temporal cortex, whereas the rostral pulvinar connects to more caudal regions of the temporal cortex. These results corroborate the findings of Luppino et al. (1988), who described the distribution of pulvinar cells labeled by retrograde transport following injections in dorsal (Td) and ventral (Tv) subdivisions of the tree shrew temporal cortex, as well as Diamond et al. (1970) and Harting et al. (1973) who described the distribution of degenerating thalamocortical cells and terminals following cortical or thalamic lesions respectively.

However, although the current and past retrograde tracing studies, and previous anterograde and retrograde degeneration studies suggest that the rostral/dorsal temporal cortex receives input primarily from the Pc, and the posterior/ventral temporal cortex receives input primarily from the Pd, our anterograde tracing studies indicate that the Pc and Pd send dual topographic projections to both areas. We previously found that the Pd receives input from the medial SC (which responds to upper visual field stimuli), whereas the Pc receives input from the lateral SC (which responds to lower visual field stimuli). Thus, we conclude that the Pd and Pc together may respond to the entire visual field (in agreement with Lyon et al. 2003b). With this in mind, our anterograde tracing results suggest that the entire visual field is represented in 2 separate areas of the temporal cortex (summarized in Fig. 12A). This corroborates the original division of the temporal cortex into Td and Tp based on the pattern of corticocortical cells and terminals labeled following tracer injections in V1 (Sesma et al. 1984). The finding that single injections in

V1 labeled patches of cells and terminals in 2 distinct areas supported the view that each area contained a complete map of the visual field.

More recently, the temporal cortex of the tree shrew has been subdivided into multiple smaller areas based on architectonics (Wong and Kaas 2009). Comparison of the cortical areas defined by pulvinar projection patterns to those defined by cytoarchitectural features indicates that the Pd and Pc project most densely to the posterior and inferior temporal cortex, with some extension into the dorsal temporal and parietal cortex. Thus, although our results support the view that projections from the Pd and Pc define 2 topographically organized cortical areas, further studies of these projections in relation to cytoarchitecture, corticocortical projection patterns, and/or physiological response properties may reveal that the cortical targets of the Pd and Pc constitute multiple functional subdivisions. A particularly important question for future studies is whether activity patterns of Pd and Pc pulvinocortical cells differ as a result of the diffuse tectal projection that terminates only in Pd, and whether diffuse tectopulvinar terminals in the Pd differentially contact cells that project to the temporal cortex, striatum or amygdala.

Finally, single cells in the tree shrew pulvinar nucleus might branch to innervate the 2 cortical targets (as suggested in Fig. 12B), although our results do not rule out the possibility that these projections arise from different cell types located adjacent to one another. Evidence for collateral projections was provided by Diamond and Hall (1969) who noted that large lesions of the tree shrew temporal cortex produced widespread degeneration of pulvinar neurons, but little discernable degeneration was observed following small lesions in the temporal cortex. Harting et al (1973) subsequently searched for the presence of sustaining collateral pulvinocortical projections in a large

series of experiments with precisely placed pulvinar lesions. However, a single focus of degenerating pulvinocortical terminals was always observed in the temporal cortex. The difference in our results may be due to the more sensitive anterograde tracing techniques that are now available. In fact, studies in other species indicate that branching pulvinar axons may be quite common. For example, Rockland et al. (1999) examined the morphology and distribution of cortical projections originating in the primate lateral pulvinar. Reconstructions of individual labeled axons revealed widespread terminations in multiple layers, often with several foci. In addition, cells in the pulvinar nucleus or its homologs have been shown to be double-labeled from dual tracer injections placed in distinct cortical areas (Kaufman et al. 1984; Cusick et al. 1985; Tong and Spear 1986; Miceli et al. 1991).

#### ***Pulvinocortical Terminals Contact Spines***

This study is the first to examine the ultrastructure of pulvinocortical terminals in any species. We found that terminals in the temporal cortex labeled via tracer injections in the Pd or Pc formed asymmetrical synapses on the spines of non-GABAergic neurons. These contacts are similar to those observed for geniculostriate terminals of the cat, ferret, and monkey (Einstein *et al.* 1987; Ding and Casagrande 1998; Latawiec et al. 2000; Erisir and Dreusicke 2005; Nahmani and Erisir 2005; Anderson et al. 2009). However, most geniculostriate axons form restricted arbors (in the tree shrew, axons originating from laminae 1, 2, 4, and 5 of the dLGN terminate in layer IVa or IVb of the striate cortex), overlapping the horizontally oriented dendritic fields of spiny stellate cells (Raczkowski and Fitzpatrick 1990; Muly and Fitzpatrick 1992). In the cat, spiny stellate cells were found to be prominent in layer IV of the striate cortex, but were not found in

the temporal (auditory) cortex (Smith and Populin 2001). It is not yet known whether the temporal cortex of the tree shrew contains spiny stellate cells but, in any case, the more widespread distribution of pulvinocortical axons, oriented perpendicular to the cortical surface from layer IV through layer I, suggests that spines on the apical dendrites of pyramidal cells might be a more likely target of pulvinocortical terminals.

Pulvinocortical projections could terminate on spines on the apical dendrites of layer V projection cells. In this case, projections from the pulvinar nucleus to the temporal cortex might activate subcortical visuomotor circuits via contacts on corticotectal cells, corticopretectal cells and/or cortico-striatal cells. Pulvinocortical terminals might also contact spines on the apical dendrites of corticocortical pyramidal cells. Extensive projections from the temporal cortex to the striate cortex have been identified in the tree shrew (Sesma et al. 1984; Lyon et al. 2003b), so it is possible that pulvinocortical projections to the temporal cortex could additionally contribute to the contextual modulation of striate activity patterns by regulating the activity of corticocortical cells. In either case, the density of projections from the Pd and Pc to the temporal cortex suggests that tectopulvinar pathways can significantly impact cortical activity patterns.

### ***Synaptic Organization of the Pd and Pc: “Second Order” Nuclei***

The dLGN is considered a “first order” thalamic nucleus because the activity of geniculocortical neurons is driven by large retinal terminals that innervate proximal dendrites, and modulated by small cortical terminals that innervate distal dendrites (Jones and Powell 1969; Cleland et al. 1971; Hajdu et al. 1982; Hamos et al. 1987; Vidnyanszky and Hamori 1994; Sherman and Guillery 1996, 1998; Sillito et al. 2006). The inputs from

cortical layer V to the dorsal thalamus are similar to retinogeniculate terminals. They are large terminals that participate in complex synaptic arrangements known as glomeruli, and contact proximal dendrites (Vidnyanszky et al. 1996; Erişir et al. 1997; Feig and Harting 1998; Li et al. 2003; Baldauf et al. 2005). Similarities in the excitatory postsynaptic potentials (EPSPs) elicited by stimulation of layer V corticothalamic terminals or retinogeniculate terminals *in vitro* have also been noted (Turner and Salt 1998; Chen et al. 2002; Li et al. 2003; Reichova and Sherman 2004). Thus, it has been suggested that layer V corticothalamic inputs drive thalamic responses in a manner similar to retinogeniculate inputs, and regions of the dorsal thalamus that receive input from cortical layer V are considered “higher order” nuclei because they may transfer layer V cortical information to other cortical areas (Guillery and Sherman 2002).

We found that the tectorecipient pulvinar nucleus cannot be classified as a higher order nucleus because we found that its cortical input arises exclusively from layer VI (confirming a previous report by Kawamura and Diamond 1978), and that corticopulvinar terminals in the Pd and Pc are all small terminals that primarily contact small caliber non-GABAergic dendrites. Furthermore, the Pd and Pc form reciprocal connections with the temporal cortex, whereas higher order nuclei form nonreciprocal connections (Van Horn and Sherman 2004; Llano and Sherman 2008).

On the other hand, several features of the tectorecipient pulvinar nucleus are different from those of first order nuclei. First the tectorecipient pulvinar does not contain the large glomerular terminals that are characteristic of the primary or driving inputs of first order nuclei (such as the retinal input to the dLGN; Hajdu et al. 1982). Although tectal terminals innervate proximal dendrites, they are smaller than retinogeniculate

terminals and do not form glomeruli. Instead they form tubular clusters that surround central dendrites (Robson and Hall 1977; Kelly et al. 2003; Chomsung et al. 2008; Masterson et al. 2009a), and preliminary studies have revealed that the characteristics of tectal EPSPs elicited *in vitro* are different from those of either corticothalamic EPSPs, or retinogeniculate EPSPs (Masterson et al. 2009b). Furthermore, the laminar distribution of pulvinocortical terminals originating from the Pd and Pc is different from that of geniculostriate terminals (Harting et al. 1973).

We therefore conclude that a third category is necessary to describe the organization of the tectorecipient pulvinar nucleus of the tree shrew. Traditionally, the retino-tecto-thalamocortical pathways have been considered secondary visual pathways that relay ascending sensory signals in parallel with the primary retino-geniculocortical pathways (Diamond and Hall 1969; Schneider 1969). Our anatomical results support the idea that the Pd and Pc are “second order” nuclei (Masterson et al. 2009a) that relay visual information from the SC to the temporal cortex, and that the activity of the Pd and Pc is modulated by the temporal cortex directly via layer VI corticothalamic projections, as well as indirectly via layer V corticotectal projections (Fig. 12B).

#### ***Relation to Primate Pulvinocortical Connections***

The main tectorecipient zone of the primate pulvinar nucleus is the inferior subdivision. In the prosimian primate *Galago senegalensis* (lesser bushbaby), tectal terminals fill most of the inferior division of the pulvinar nucleus (Glendenning et al. 1975). In the new and old world simian primates, *Saimiri sciureus* (squirrel monkey), *Callithrix jacchus* (marmoset), and *Macaca mulatta* (macaque or rhesus monkey), tectal



terminals are confined primarily to the posterior and central medial subdivisions of the inferior pulvinar (PIp and PIcm; Stepniewska et al. 2000).

In simian primates, retrograde tracing experiments have shown that the tectorecipient subdivisions PIp and PIcm primarily project to cortical areas surrounding the middle temporal area (MT), which can be identified by dense myelin staining (Cusick et al. 1993; Stepniewska et al. 1999, 2000; Kaas and Lyon 2007). Furthermore, pulvinar neurons which can be orthodromically activated from the SC are intermingled with cells that can be antidromically activated from area MT (Berman and Wurtz 2008). Based on its extensive connections with V1, it has been suggested that the tree shrew area Td is a possible homolog of the primate area MT (Sesma et al. 1984; Lyon et al. 1998). However, the myelin pattern used to identify area MT in primates is much less apparent in tree shrews (Wong and Kaas 2009).

Anterograde tracing studies of the cortical projections of the tectorecipient pulvinar of simian primates have not yet been carried out. However, anterograde degeneration studies of the *Galago* indicate that the projections from the tectorecipient subdivision of the pulvinar nucleus are very similar to those that we have identified in the current study. Lesions confined to the inferior pulvinar nucleus resulted in the degeneration of terminals in the temporal cortex, and many of the lesions resulted in 2 patches of degeneration, with one patch overlapping area MT, and another in the ventral temporal cortex (Glendenning et al. 1975). Although it was concluded that MT is the primary target of the *Galago* tectorecipient pulvinar, the pattern of pulvinocortical projections is strikingly similar to our observations in the tree shrew.

Behavioral studies of *Galago* indicate that lesions of area MT impair the ability of animals to locate an object in space (Wilson et al. 1979), whereas lesions of the ventral temporal cortex impair the ability of animals to learn visual discrimination tasks (Diamond and Hall 1969; Killackey et al. 1971; Atencio et al. 1975). A role for pulvinocortical pathways in pattern discrimination was further demonstrated by the finding that lesions of the inferior (but not the lateral or medial) pulvinar nucleus of macaque monkeys impaired visual pattern discrimination learning (Chalupa et al. 1976). Behavioral studies of tree shrews further indicate that tecto-pulvino-cortical pathways play a major role in pattern discrimination because this ability is impaired after lesions confined to the superficial layers of the SC (where tectopulvinar cells are located), or after lesions of the ventral temporal cortex (Casagrande and Diamond 1974).

However, despite the many similarities in the organization of tecto-pulvino-cortical pathways of tree shrews and primates, the tree shrew is distinguished from primates by the relative lack of visual impairment after ablation of the entire striate cortex. Although *Galagos* and other primates exhibit a profound sensory loss after ablation of V1, deficits in tree shrews are only revealed when the animals attempt to discriminate very complex images (Diamond and Hall 1969; Killackey et al. 1971; Ware et al. 1974; Atencio et al. 1975). It has been proposed that the expanded tectopulvinar pathway of the tree shrew underlies this difference. In fact, it has been estimated that the tree shrew SGS has a volume that is approximately one-half the size of its striate cortex, and 6 times greater than its dLGN. In comparison, the macaque SGS is about one-fifth the volume of its dLGN (Norton 1982).

Another difference between the tree shrew and primate is that the tectorecipient and striate-recipient zones of the pulvinar nucleus are clearly segregated in the tree shrew, but show a considerable degree of overlap in primates. In tree shrews, projections from the striate cortex to the extrageniculate thalamus are limited to the ventral pulvinar nucleus and lateral intermediate nucleus (Huerta et al. 1985; Day-Brown et al. 2007), and, as demonstrated in the current study, only the temporal cortex projects to the Pd and Pc. In contrast, the tectorecipient zones of the primate pulvinar nucleus receive extensive input from both the striate and temporal cortex (Glendenning et al. 1975; Symonds and Kaas 1978; Lin and Kaas 1979; Raczkowski and Diamond 1980, 1981; Wall et al. 1982; Ungerleider et al. 1983). Furthermore, the majority of the striate cortex input to the primate pulvinar nucleus is in the form of large glomerular terminals characteristic of higher order nuclei (Ogren and Hendrickson 1979).

This difference in the organization of the tectorecipient zones of the primate pulvinar nucleus and that of other species could account for the conflicting accounts regarding the effects of SC input on pulvinar response properties. In the macaque, lesions of the SC have little effect on the response properties of neurons in the tectorecipient zone of the pulvinar nucleus, whereas lesions of the striate cortex greatly diminished their visual responsiveness (Bender 1983). In contrast, lidocaine injections in the SC of the rabbit greatly reduce the responsiveness of neurons in the lateral posterior nucleus, and this effect is topographic (Casanova and Molotchnikoff 1990).

An increased dependence on input from the striate cortex may distinguish the tectorecipient regions of the primate pulvinar nucleus from that of the tree shrew, and this organization may be reflected in the more severe sensory deficits following striate cortex

damage. Thus, although studies of the tree shrew suggest that tectopulvinar-cortical pathways play a role in pattern vision, it remains unclear whether this is the case in primates. The current study provides further evidence that the tree shrew offers a model system to investigate the tectopulvinar and striate-pulvinar pathways in relative isolation to help clarify their respective roles in vision.

## **Conclusions**

The main contribution of this study is the characterization of the synaptic organization of pulvinocortical projections. Projections from the tectorecipient zones of the pulvinar nucleus are densely distributed in the temporal cortex, forming 2 topographic maps. In contrast to the horizontal arrangement of geniculocortical terminals, pulvinocortical terminals are arranged in columns; the spines postsynaptic to pulvinocortical terminals likely arise from the apical dendrites of pyramidal cells.

In addition, we have more clearly defined the unique circuitry of the tectorecipient zones of the tree shrew pulvinar nucleus. Although other regions of the pulvinar nucleus can be categorized as higher order based on their direct innervation by cortical layer V, the only direct cortical inputs to the Pd and Pc originate from layer VI cells which form small terminals that innervate small caliber dendrites. Furthermore, all connections with the temporal cortex appear to be reciprocal. Thus, it does not appear that the Pd and Pc receive input from one cortical area and transfer this information to other cortical areas (the proposed function of higher order nuclei, Guillery 1995; Guillery and Sherman 2002). Instead, we hypothesize that the SC drives the responses of Pd and Pc cells, which may subsequently influence behavior by activating subcortical visuomotor circuits.

**Figure 1.**

The micrographs illustrate the biotinylated dextran amine injection sites in the pulvinar nucleus that either covered both Pd and Pc subdivisions (*A, B*) or were confined to either the Pd (*C–G*) or the Pc (*I–L*). Most injections were confined to the pulvinar nucleus, but in some cases invaded the underlying external medullary lamina (LME, panels *A* and *B*) or PT (panel *E*, right). Scale bar in *A* = 500  $\mu\text{m}$  and applies to (*A–D*), (*F*), (*H*), (*J*), and (*K*). Scale bar in (*E*) = 1 mm. Scale bar in (*G*) = 500  $\mu\text{m}$ . Scale bar in (*L*) = 100  $\mu\text{m}$  and applies to (*J*).

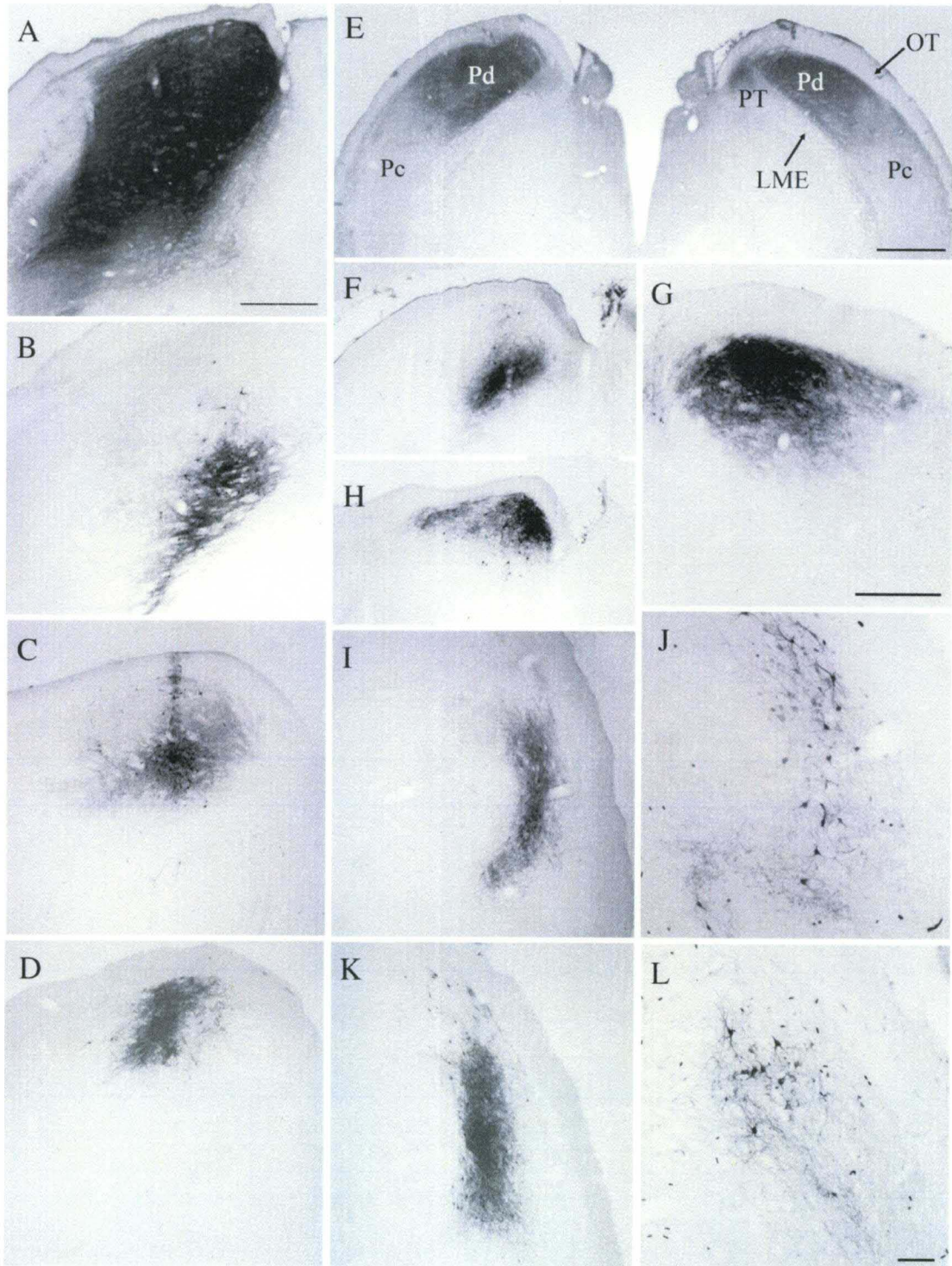


**Figure 2.**

Micrographs illustrate the laminar distribution of pulvinocortical terminals in the temporal cortex. Injections confined to the Pd and/or Pc label terminals that are most densely distributed in layer IV, but extend through layer I (A). Injections that involved the external medullary lamina labeled terminals in layers I–IV, as well as cells in layers V and VI. (B) Shown are pulvinocortical terminals overlapping the apical dendrites of layer V projection cells.

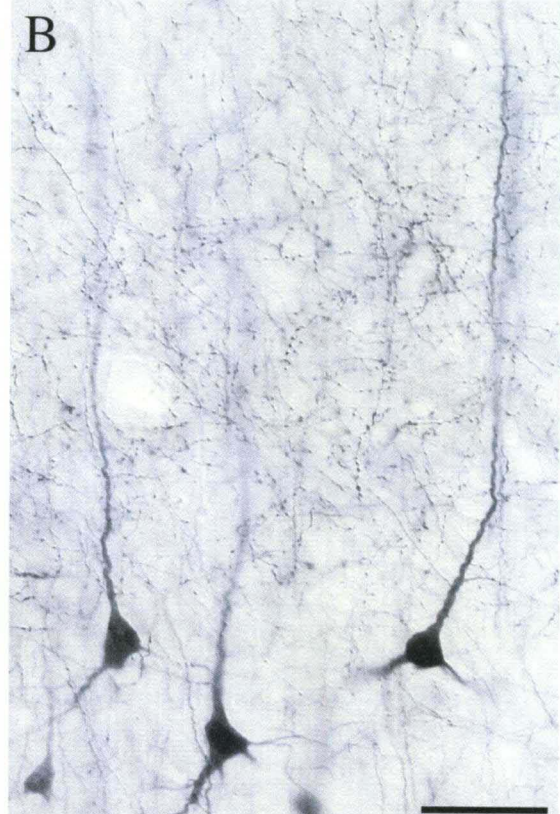
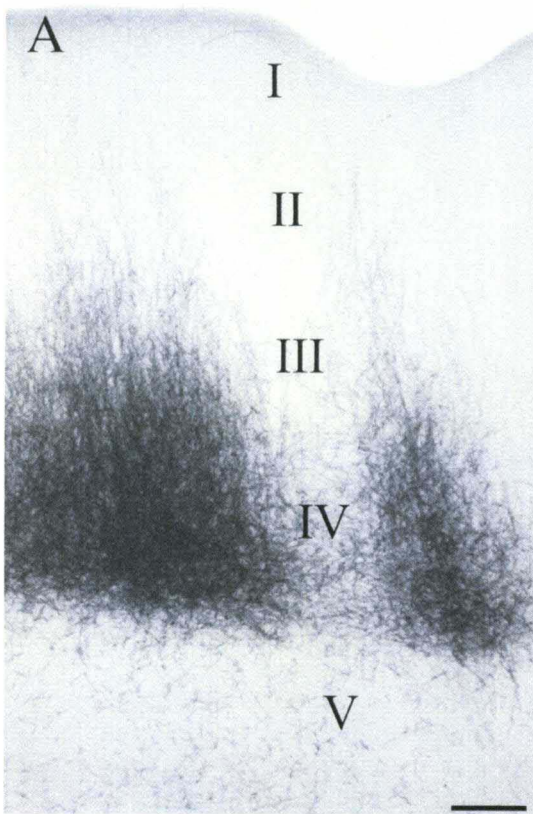




**Figure 3.**

Micrographs illustrate the distribution of pulvinocortical terminals in 2 cortical areas of the temporal cortex resulting from a single injection of biotinylated dextran amine in the pulvinar nucleus. (A and B) Illustrate patches of terminals labeled in area T1 and T2, respectively (locations of these areas are shown in Fig. 5). The approximate laminar boundaries are indicated. Scale=100  $\mu\text{m}$ .

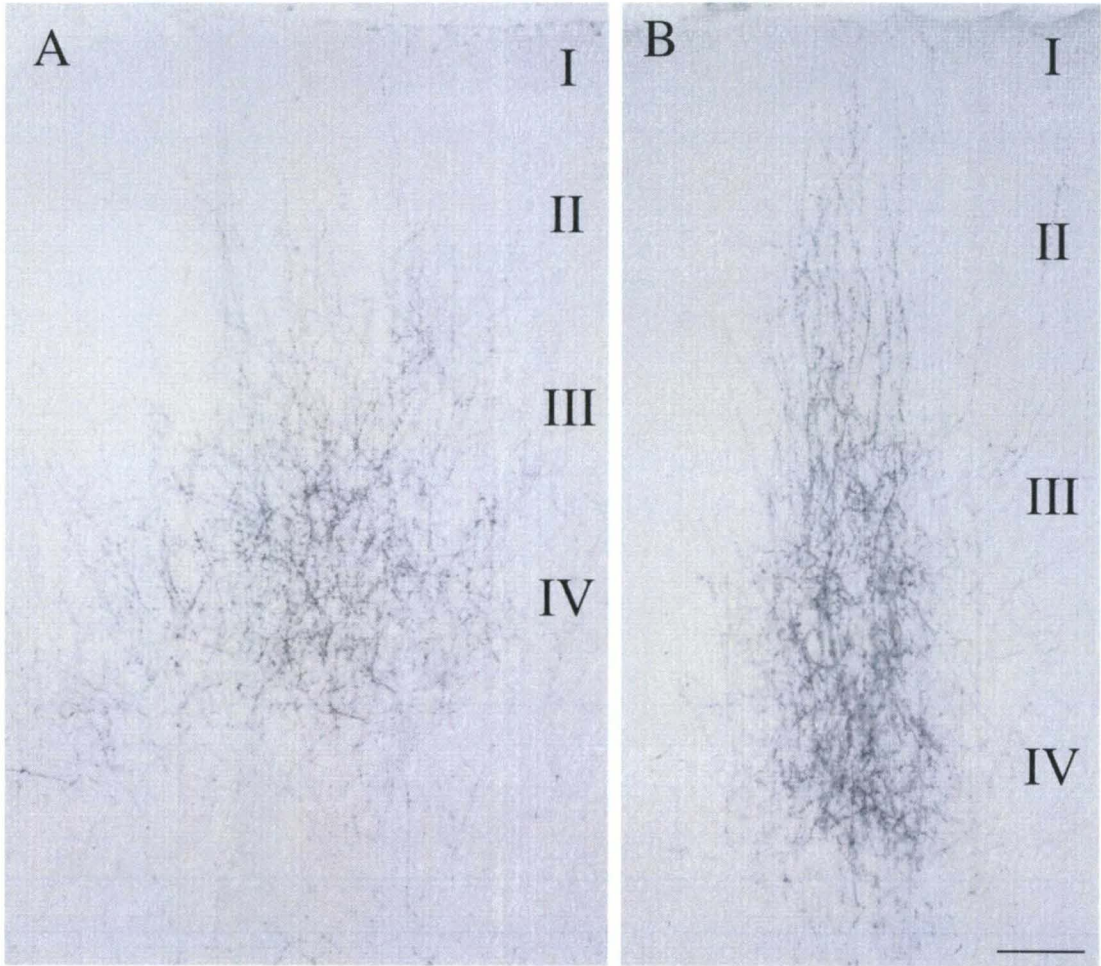


**Figure 4.**

Iontophoretic injections of biotinylated dextran amine in the pulvinar nucleus label 2 foci of terminals in the temporal cortex. Injection sites in the caudal Pc (A) and rostral Pd (D) are shown in black, and the resulting dual terminal distributions (T1 and T2) are shown in gray (B, C, E, F).

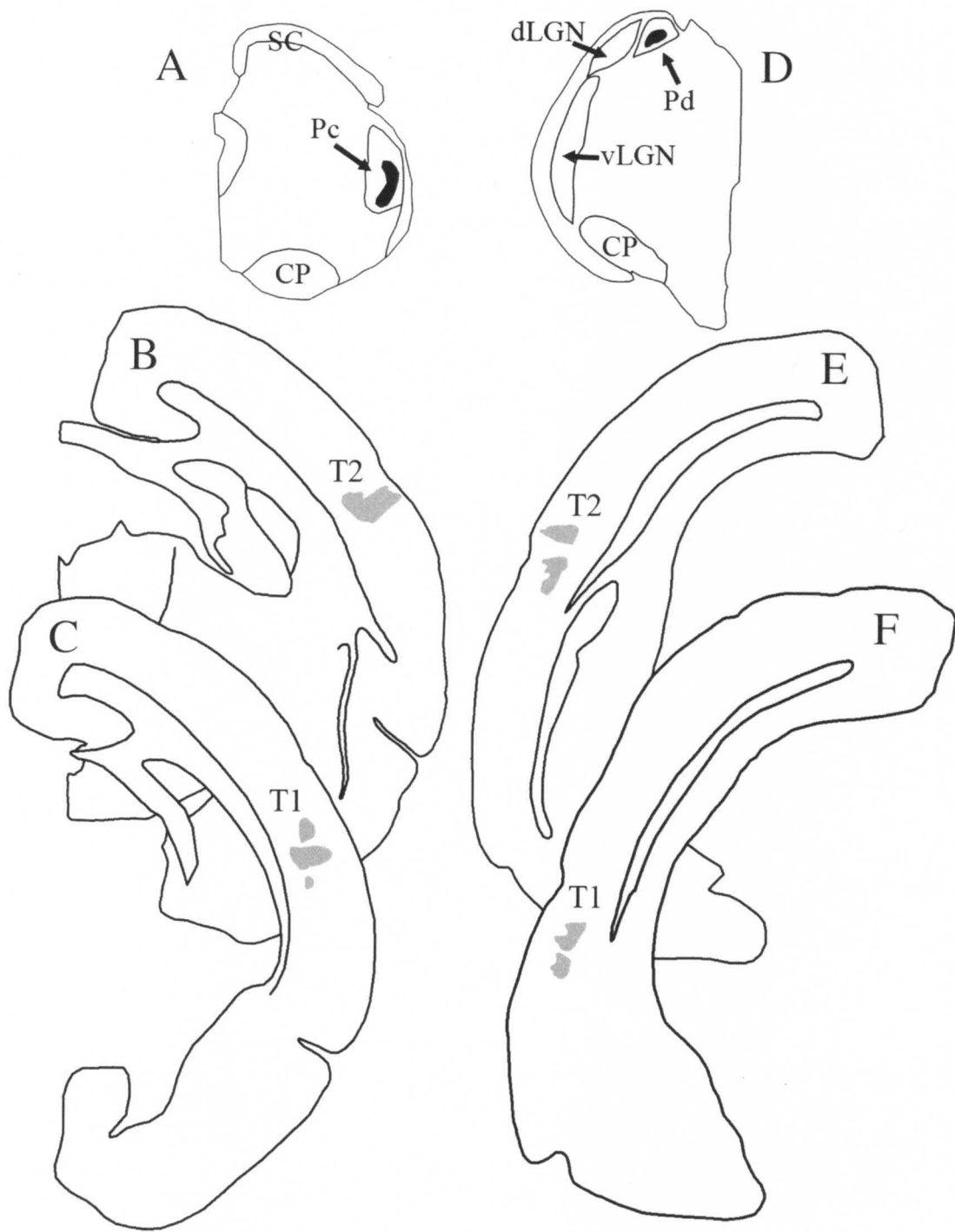


**Figure 5.**

Single injections of biotinylated dextran amine in the pulvinar nucleus label 2 terminal foci in the temporal cortex (T1 and T2). Three-dimensional reconstructions (lateral views) illustrate the location of injections in the Pc (A) and Pd (B) and the resulting distribution of pulvinocortical terminals (C). Each color indicates a single injection site in the pulvinar nucleus and the resulting 2 foci of pulvinocortical terminals. C, caudal, D, dorsal, R, rostral, V, ventral, V1/V1, primary and secondary visual cortex. Scale for (A) and (B) = 0.5 mm, scale for (C) = 1 mm.

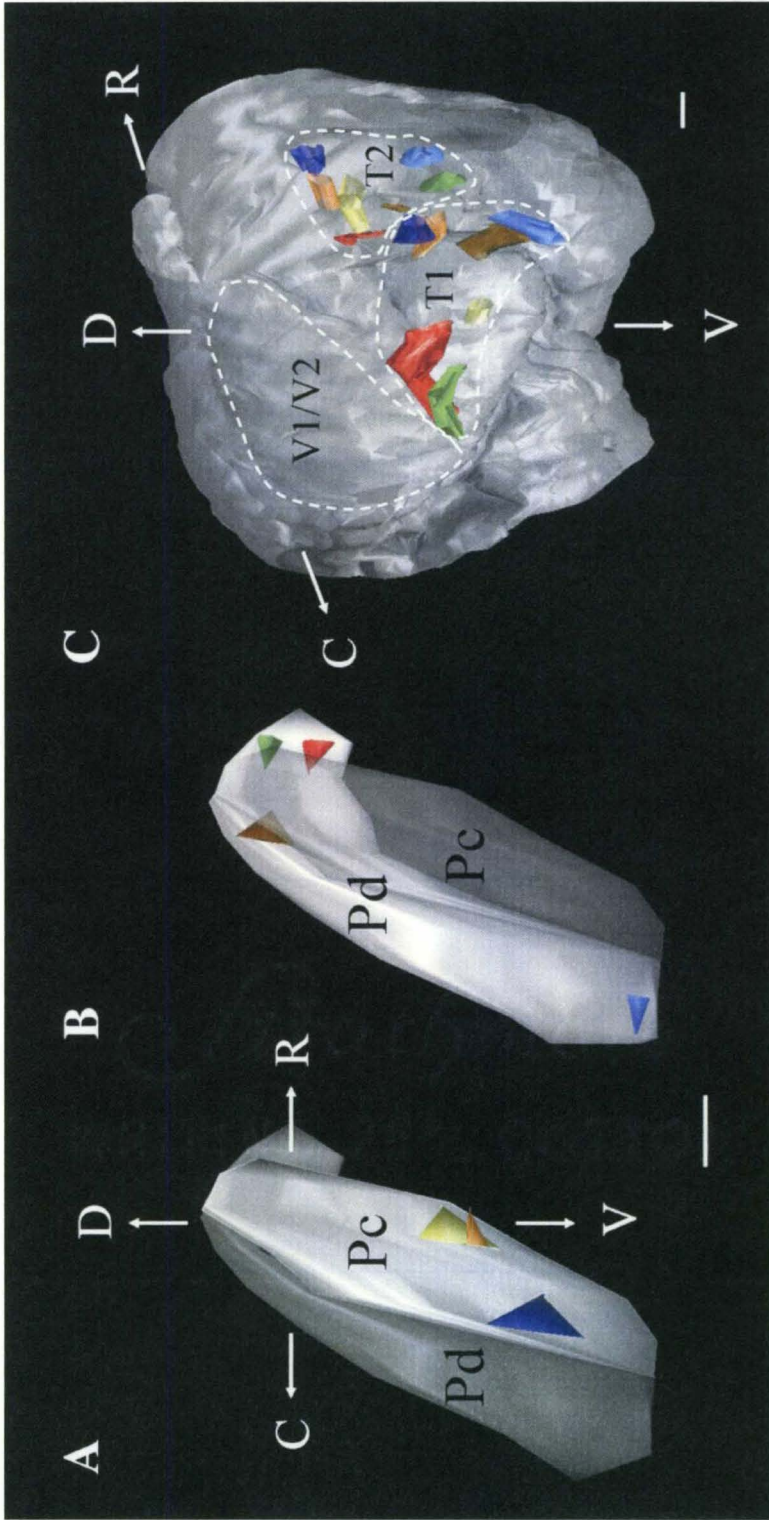


**Figure 6.**

Corticopulvinar and pulvinocortical projections are topographically organized. A fluorogold injection that included both the Pd and Pc (A) labeled cells in layer VI of restricted regions of the temporal cortex (B). A fluorogold injection in the posterior temporal cortex (T1, C) labeled cells in the dorsal/rostral Pc (D), whereas a fluorogold injection in the more rostral/dorsal temporal cortex (T2, E) labeled cells in the caudal/ventral Pc (F). Scale bar in (B)= 500  $\mu$ m and applies to (A), scale bar in (E)= 1 mm and applies to (C). Scale bar in F= 250  $\mu$ m and applies to D. LGN, lateral geniculate nucleus, LME, external medullary lamina., OT, optic tract, PUL, pulvinar nucleus, V1, striate cortex, V2, secondary visual cortex.

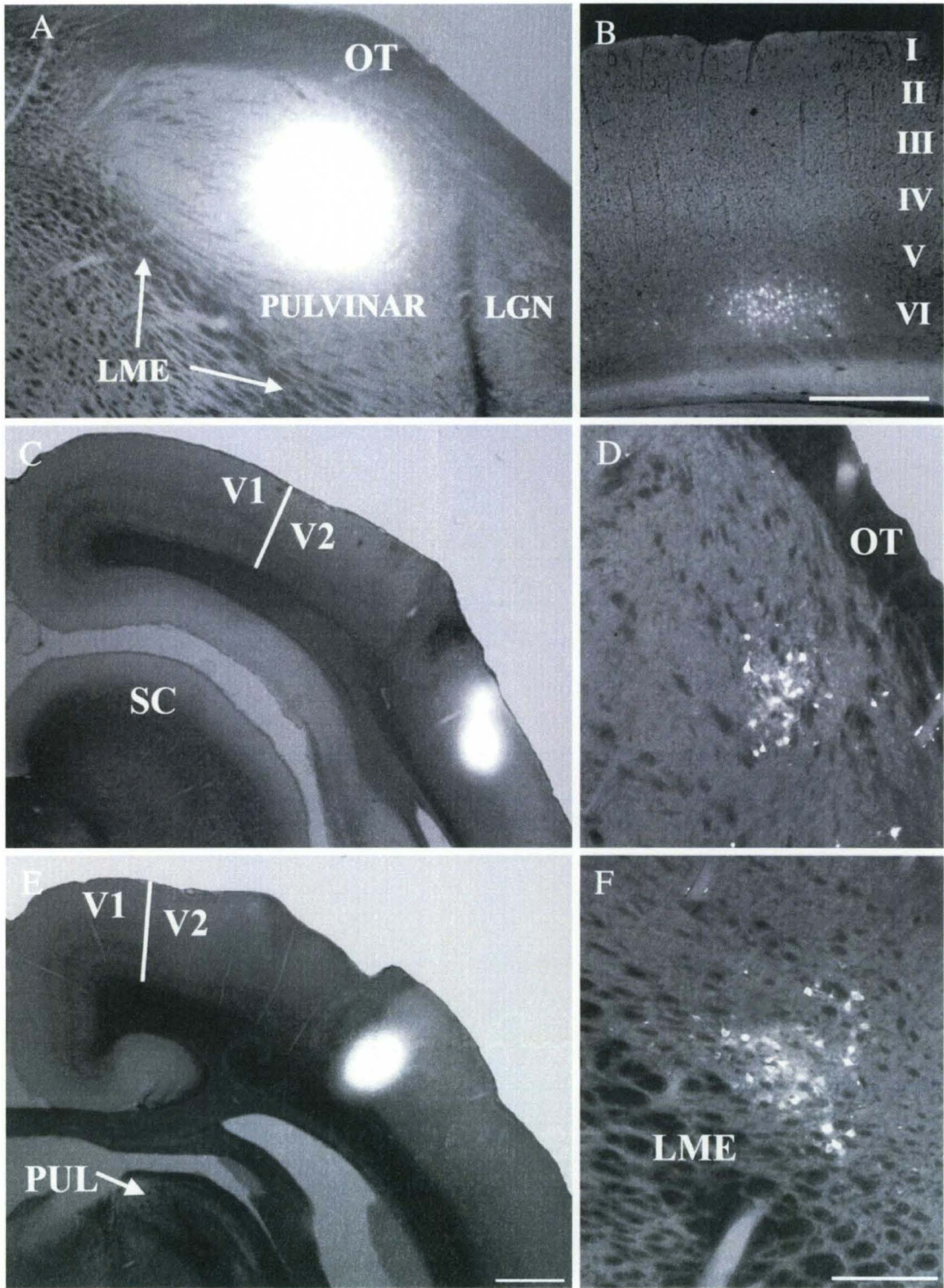




**Figure 7.**

Most pulvinocortical terminals contact (white arrows) non-GABAergic (low density of overlying gold particles) spines (identified by size and occasionally the presence of a spine apparatus, black arrows) with asymmetric synapses. The ultrastructure of pulvinocortical terminals in the T2 (A, B, and C) and T1 (D–H) is illustrated. Single (D, F) and perforated (A, B, E, H) synapses were identified, and some terminals contacted multiple profiles (C, G). Scale bar = 0.5  $\mu\text{m}$  and applies to all panels.

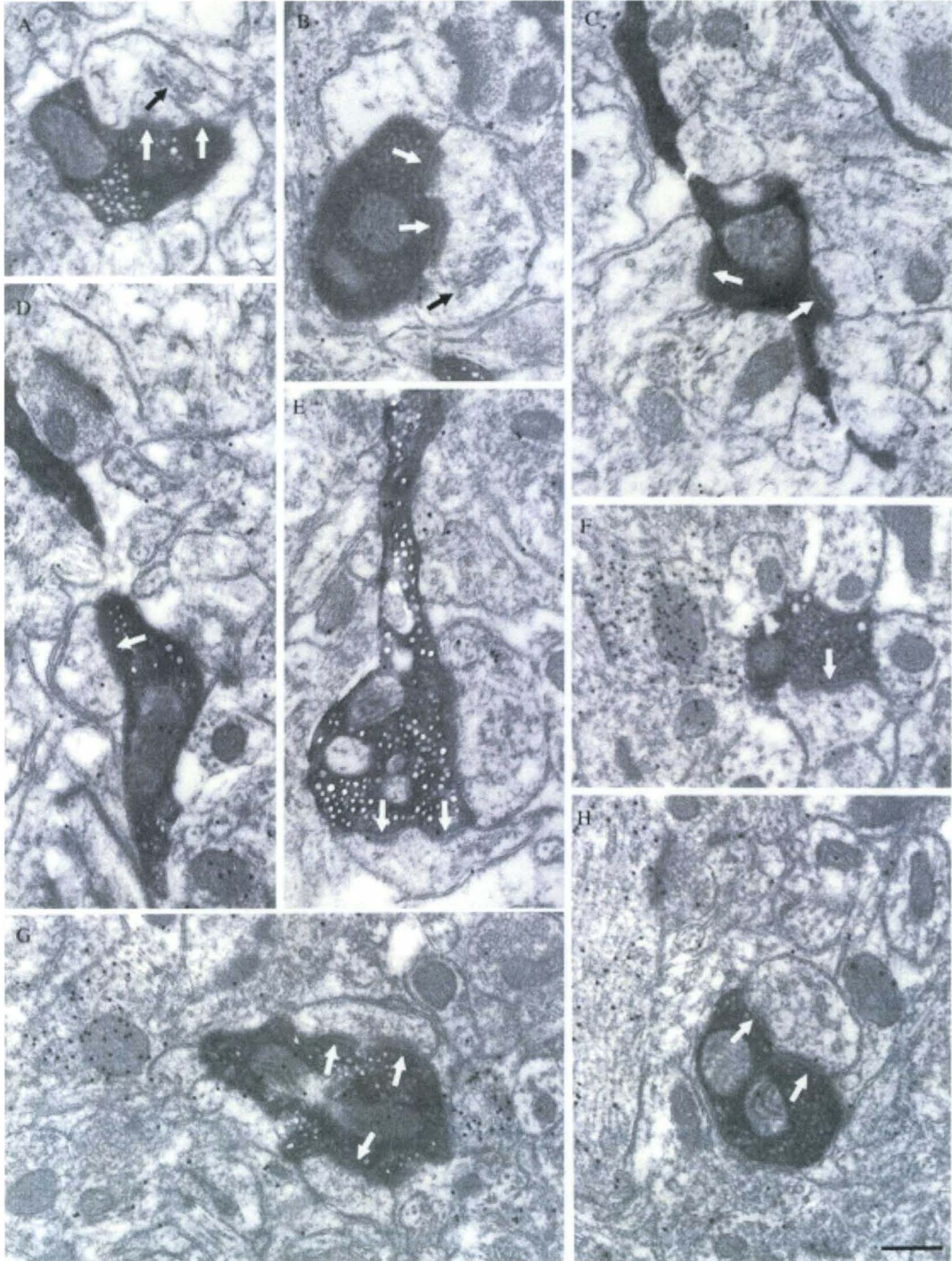


**Figure 8.**

Corticopulvinar cells (black dots) are labeled in layer VI of 2 zones T2 (A) and T1 (B) following single injections of fluorogold in the pulvinar nucleus (C), shown in black).

Scale bar = 1 mm.

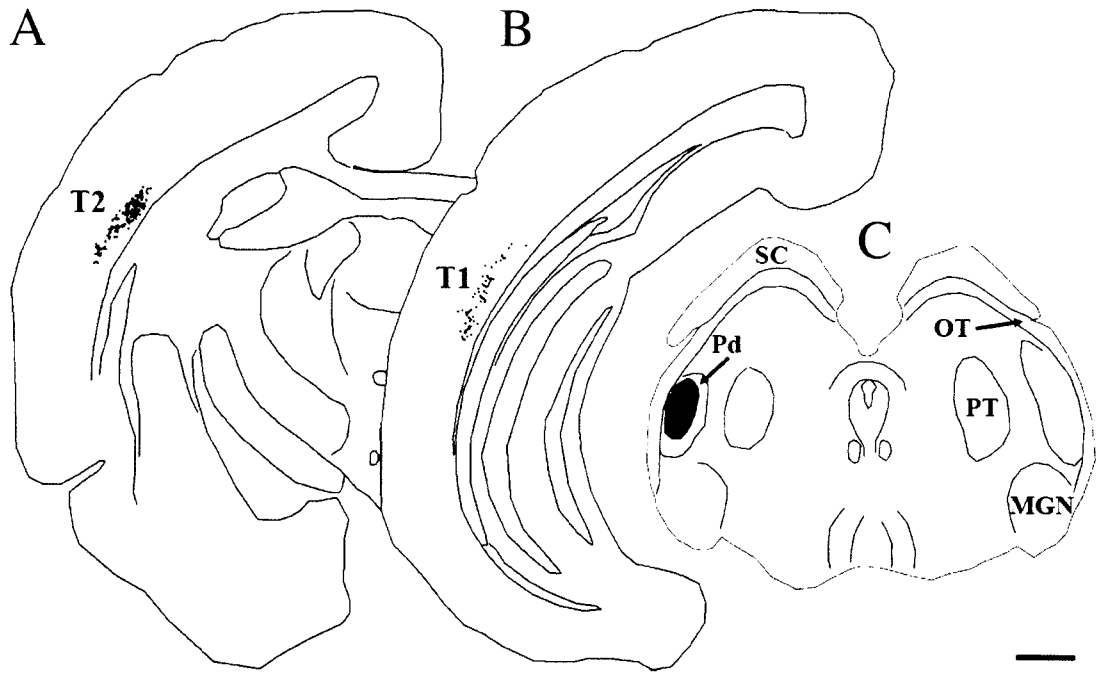


**Figure 9.**

The pulvinar nucleus and temporal cortex are reciprocally connected. (A) The confocal image of the temporal cortex illustrates the overlapping distributions of pulvinocortical terminals (purple, in layer IV) and corticopulvinar cells (green, in layer VI) labeled by a dual injection of biotinylated dextran amine and fluorogold in the tectorecipient pulvinar nucleus (PUL, yellow; injection site is depicted in orange in panel (C), also illustrated in Figure 1E, left pulvinar). (B) The confocal image of the pulvinar nucleus illustrates the overlapping distributions of pulvinocortical cells (green) and corticopulvinar terminals (purple) labeled by a dual injection of biotinylated dextran amine and CTB in the temporal cortex (injection site depicted in orange in panel F). Three-dimensional reconstructions of the case illustrated in panel (A) show the overlapping distributions of corticopulvinar cells (D, green) and pulvinocortical terminals (E, purple) which formed a band within T1 and T2. Tectopulvinar cells labeled from the same pulvinar injections site are distributed in a band that is restricted in the medio-lateral dimension (C, green). Three-dimensional reconstructions of the case illustrated in panel (B) show the distributions of pulvinocortical cells (G, green) and corticopulvinar terminals (H, purple) which overlapped within a restricted region of the pulvinar nucleus. C, caudal, D, dorsal, R, rostral, V, ventral, V1/V1, primary and secondary visual cortex. Scale bars in (A) and (B)= 10  $\mu$ m. Scale in (G)= 1 mm and applies to (C) and (H). Scale in (F)= 1 mm and applies to (D) and (E).

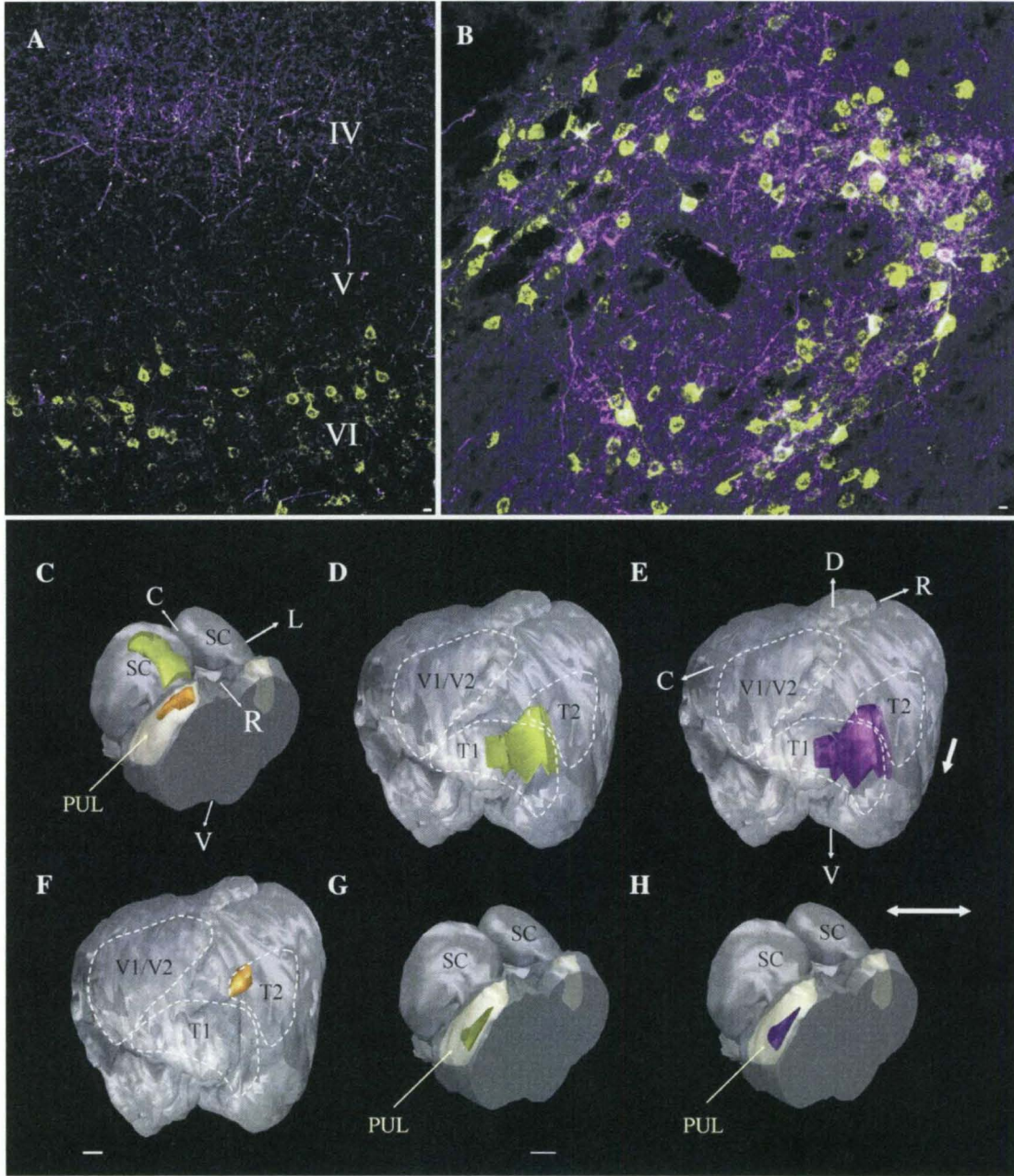


**Figure 10.**

The micrographs illustrate the morphology of axons and terminals labeled by an injection of BDA in the temporal cortex. In the pulvinar nucleus (A), the labeled axons are of fine caliber and give rise to small boutons. In the PT (B), axons labeled from the same cortical injection site are thicker and give rise to larger boutons. Scale bar = 30  $\mu\text{m}$  and applies to both panels.

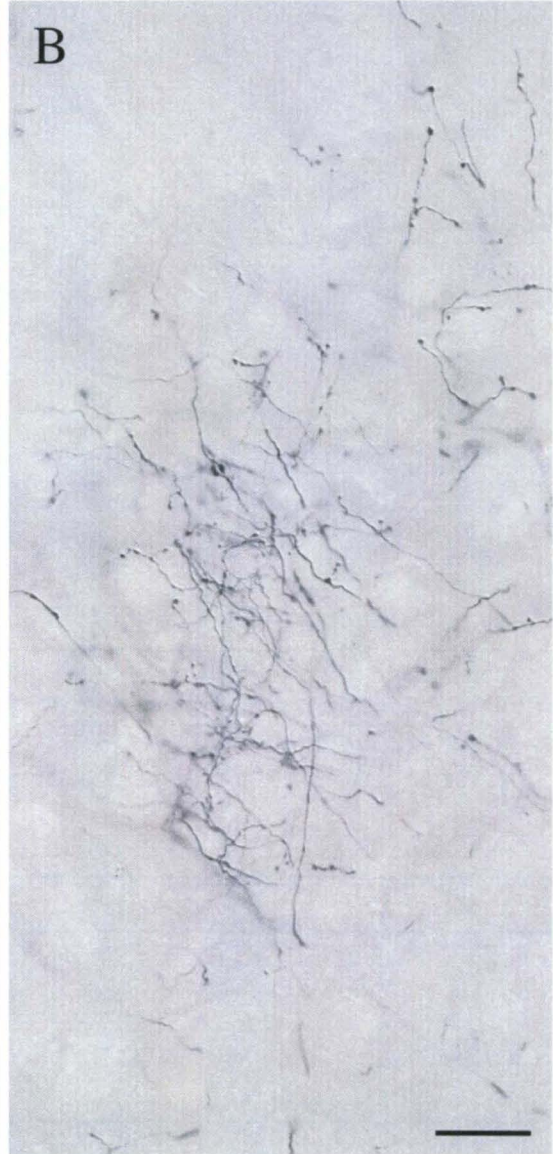




**Figure 11.**

Examples of the corticothalamic terminals in Pc labeled by the anterograde transport of BDA from T2. All terminals are small profiles and primarily contact (white arrows) GABA-negative (low density of the gold particles) profiles (B–G). A few contacts are made with GABA-positive (high density of the gold particles) profiles that contain synaptic vesicles (A). Scale bar = 0.5  $\mu\text{m}$ .

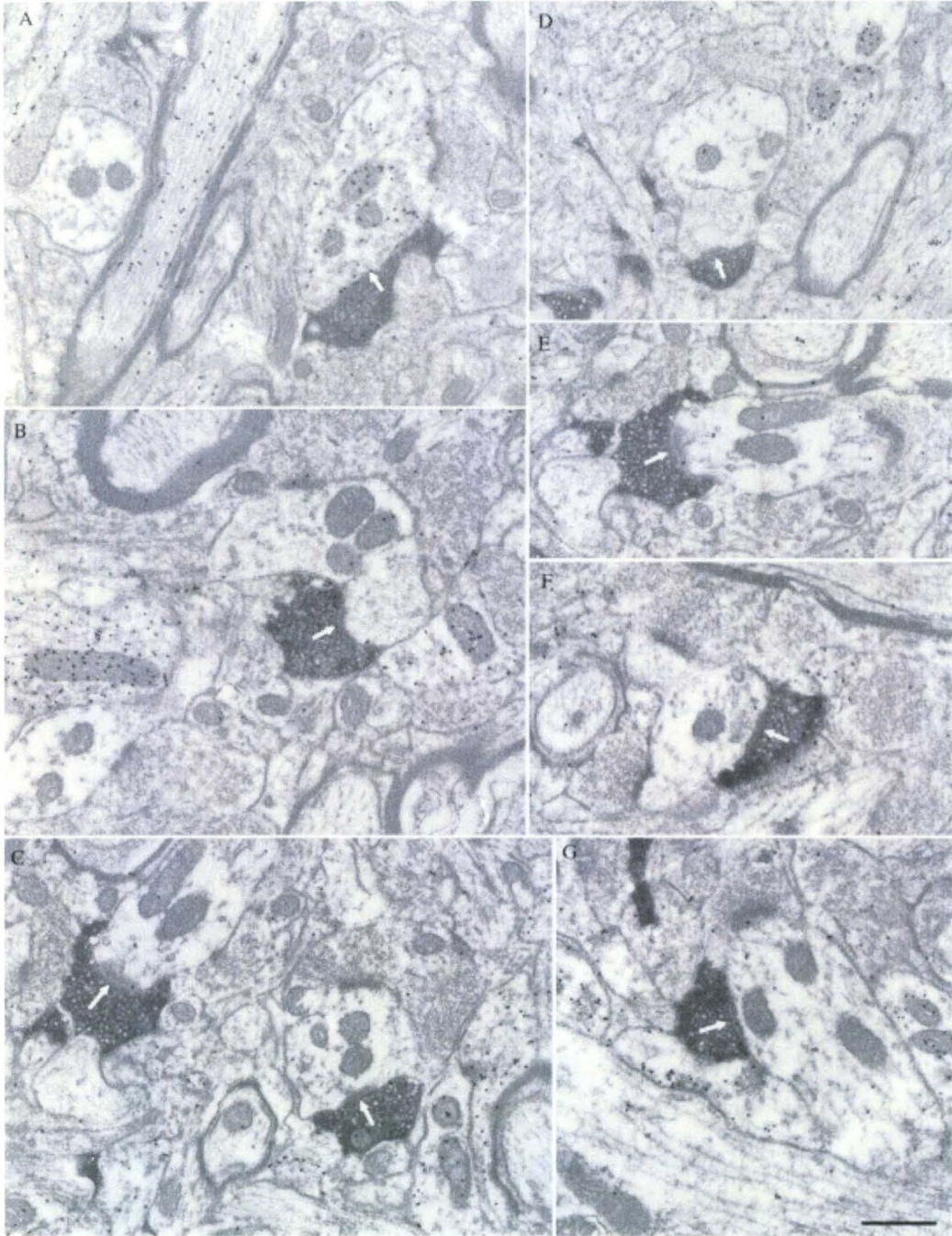
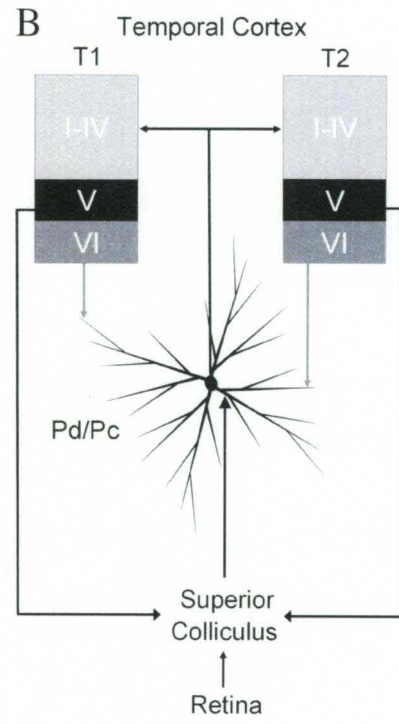
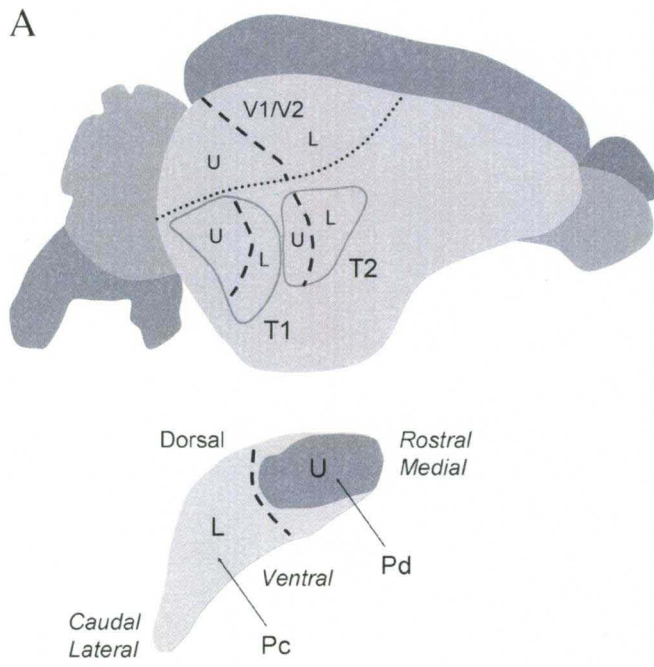


**Figure 12.**

A summary of the results of the current study and those of our previous study of tectopulvinar projections (Chomsung et al. 2008). (A) A schematic depiction of the visual field representations (U, upper visual field, L, lower visual field, dashed line, horizontal meridian) within the pulvinar nucleus and temporal cortex estimated from the location of tectopulvinar cells and pulvinocortical terminals labeled following small injections of BDA in the pulvinar nucleus. (B) The Pd and Pc are reciprocally connected to 2 regions of the temporal cortex (T1 and T2). The Pd and Pc project to layers I-IV of T1 and T2 where they contact spines. In the Pd and Pc, projection cells receive input from the SC on proximal dendrites, and input from layer VI temporal cortex cells on distal dendrites. Because the SC receives input from the retina as well as layer V cells in the striate and temporal cortex, the Pd and Pc can be categorized as “second order” nuclei to indicate their unique position in integrating ascending input from the periphery with descending input from the cortex. V1, striate cortex, V2, secondary visual cortex.



## CHAPTER III

### THALAMIC BURST FIRING PROPENSITY: A COMPARISON OF THE DORSAL LATERAL GENICULATE AND PULVINAR NUCLEI IN THE TREE SHREW

#### Outline

Neurons in all dorsal thalamic nuclei can fire with high frequency bursts of action potentials that ride the crest of voltage-dependent transient (T-type) calcium currents (low threshold spike; LTS). To explore potential nucleus-specific burst features, we compared the membrane properties of dorsal lateral geniculate nucleus (dLGN) and pulvinar nucleus (PUL) neurons using *in vitro* whole cell recording in juvenile and adult tree shrew (*Tupaia*) tissue. We injected current ramps of variable slope into neurons that were sufficiently hyperpolarized to de-inactivate T-type calcium channels. In a small percentage of juvenile PUL and dLGN neurons, an LTS could not be evoked. In the remaining juvenile neurons, and in all adult dLGN neurons, a single LTS could be evoked by current ramps. However, in the adult PUL, current ramps evoked multiple LTSs in over 70% of recorded neurons. Using immunohistochemistry, western blot techniques, unbiased stereology, confocal and electron microscopy, we found that the PUL contains a higher glia:neuron ratio than the dLGN, and PUL neurons express significantly more T-type calcium channels (Cav 3.2) than dLGN neurons. Neuron modeling revealed that the distinct firing modes could be replicated by manipulating T channel density, distribution, and kinetics. These results suggest that the membrane

properties of PUL neurons promote burst firing, potentially increasing the synaptic impact of pulvinar projections and/or synchronizing the activity of the multiple targets of the pulvinar nucleus.

## **Introduction**

Most dorsal thalamic neurons have been found to fire in at least two different modes: single action potentials (tonic mode), or high frequency bursts of action potentials (burst mode) that ride the crest of voltage-dependent transient (T-type) calcium currents (low threshold spike; LTS) (Llinas and Steriade, 2006). *In vivo* recordings have demonstrated that rhythmic burst firing in the thalamus is most common during sleep, while tonic firing is more common when animals are alert and attentive (Glenn and Steriade, 1982). Thus, proposed functions of thalamic burst firing include disruption of the propagation of sensory signals during sleep and/or consolidation of memory traces acquired during the waking state (Llinas and Steriade, 2006). Burst firing can also occur when animals are awake (Guido and Weyand, 1995; Bezdudnaya et al., 2006; Wang et al., 2007), and analysis of activity patterns in the dorsal lateral geniculate nucleus (dLGN) suggest that burst firing can provide a nonlinear amplification of sensory signals (Guido et al., 1995). Burst firing has also been shown to activate cortical neurons more efficiently than tonic firing, potentially providing a further amplification of the thalamocortical relay of sensory signals (Swadlow and Gusev, 2001; Boudreau and Ferster, 2005; Hull et al., 2009). Thus, it has been proposed that burst firing may additionally serve as a cortical “wake up call” for the detection of novel, previously unattended stimuli (Guido and Weyand, 1995).

Burst firing may also serve nucleus-specific functions. *In vitro* studies have revealed that the kinetics of LTSs in the thalamic reticular nucleus and centrolateral nucleus are distinct from those of most other dorsal thalamic nuclei (Huguenard and Prince, 1992; Steriade et al., 1993), and *in vivo* recordings have found significant variations across dorsal thalamic nuclei in the percentage of spikes fired as a part of a burst. In anesthetized guinea pigs burst firing was found to be much more common in the nonlemniscal versus the lemniscal medial geniculate nucleus (He and Hu, 2002) and in awake primates (Ramcharan et al., 2005) burst firing was found to be much more common in the mediodorsal nucleus and pulvinar nucleus (PUL) when compared the dLGN.

Identification of the mechanisms underlying nucleus-specific burst firing propensity is important not only for understanding the functions of the burst firing mode, but also for developing treatments for conditions that involve aberrant burst firing (Huguenard and McCormick, 1992; Graef et al., 2009; Uhlhaas and Singer, 2010). To begin to address this, we compared the firing properties of neurons in the dLGN and PUL of the tree shrew (*Tupaia belangeri*), a species in which the functional organization of the visual system is similar to that found in primates. By using *in vitro* electrophysiology, immunocytochemistry, western blot techniques, confocal and electron microscopy; stereology, and neuron modeling, our results suggest that, relative to the dLGN, PUL neurons display an increased propensity to fire in bursts because they express a greater density of T-type calcium channels.

## **Methods**

A total of 23 tree shrews (*Tupaia belangeri*); 14 adults (more than 3 months old) and 9 juveniles (3 weeks old), were used for these experiments. All procedures were approved by the Institutional Animal Care and Use Committee of the University of Louisville.

### ***Slice preparation***

Thalamic slices (400 $\mu$ m) were prepared from 7 juvenile and 5 adult male and female tree shrews (Li et al., 2003). Briefly, the animals were deeply anesthetized with carbon dioxide and decapitated, the brain was excised and a block of tissue containing the thalamus was removed and placed in a ice-cold oxygenated solution of modified artificial cerebrospinal fluid (ACSF) containing (in mM) 206 sucrose, 2.5 KCl, 1 CaCl<sub>2</sub>, 1 MgSO<sub>4</sub>, 1 MgCl<sub>2</sub>, 1.25 NaH<sub>2</sub>PO<sub>4</sub>, 26 NaHCO<sub>3</sub>, 10 glucose at a pH of 7.4 and equilibrated with 95% O<sub>2</sub>/5% CO<sub>2</sub>. Parasagittal slices were cut on a vibratome (Leica, VT 1000E, Deerfield, IL) at a thickness of 400 $\mu$ m and transferred into a holding chamber with ACSF containing (in mM) 124 NaCl, 2.5 KCl, 2 CaCl<sub>2</sub>, 1 MgSO<sub>4</sub>, 1.25 NaH<sub>2</sub>PO<sub>4</sub>, 26 NaHCO<sub>3</sub>, 10 glucose at a pH of 7.4 and equilibrated with 95% O<sub>2</sub>/5% CO<sub>2</sub>, where they incubated for at least 2 hours before recording.

### ***Electrophysiology***

Whole cell recordings were obtained from the dLGN and PUL. All recordings were carried out in the recording chamber maintained at 33°C with ACSF (with 10  $\mu$ M bicuculline and 2.5  $\mu$ M CGP55845 added; Tocris; Ellisville, MO) continually superfused at a rate of 2.0 ml/min. Pipettes were pulled from borosilicate glass (Sutter Instrument, Novato, CA) and had a tip resistance of 4-6 M $\Omega$  when filled with a solution containing (in mM) 115 K-gluconate, 2 MgCl<sub>2</sub>, 10 HEPES, 10 sodium phosphocreatine, 2 Na<sub>2</sub>-ATP,



20 KCl, 0.3 Na<sub>2</sub>-GTP with pH adjusted to 7.2 with KOH (osmolarity 290–295 mOsm). Biocytin (0.5%) was added to allow morphological reconstruction of the recorded neurons. Current-clamp recording were made with an Axoclamp 2B amplifier (Axon Instruments, Foster City, CA); the bridge was continually monitored and adjusted as needed. Data were digitized and stored on an IBM-compatible computer for off-line analyses. Only recordings showing a stable resting membrane potential more negative than -50 mV and over shooting action potentials were included in this study (n = 46). For a subset of these cells (4), a combination of tetrodotoxin (TTX; 3.1 μM, Tocris), tetraethylammonium chloride (TEA; 20 mM; Sigma Chemical Company, St Louis, MO) and 4-aminopyridine (4AP; 6 mM; Sigma) was applied (through the broken tip of a pipette located 2 mm from the recording pipette) after initial categorization of LTS responses to examine the properties of I<sub>T</sub>.

### ***Histochemistry***

A subset of neurons was filled with 0.5% biocytin by diffusion from the pipette during recording. At the end of each recording, slices were fixed at 4 °C overnight in 4% paraformaldehyde and rinsed several times in 0.1 M phosphate buffer saline (PB). Slices were then incubated in 10% methanol in PB with 3% hydrogen peroxide to react with the endogenous peroxidase activity of red blood cells. After several rinses in PB, slices were incubated overnight at 4 °C under agitation in a 1% solution of a complex of avidin and biotinylated-horseradish peroxidase (ABC Kit Standard, Vector Laboratories) prepared in 0.3% Triton X-100. The slices were subsequently rinsed, reacted with nickel-intensified 3,3'-diaminobenzidine (DAB) for 5 min, and washed in PB. After rinses in phosphate buffer, slices were mounted onto slides and reconstructed with a NeuroLucida system

(Micro Bright Field Inc., USA). In some cases, biocytin-filled neurons were revealed by incubating slices in a 1:100 dilution of streptavidin conjugated to Alexa Fluor 546 (Molecular Probes, Eugene, OR) and confocal images of the cell was obtained using an Olympus Fluoview laser scanning microscope (BX61W1).

### ***Western blot analysis***

Six frozen tree shrew brains (3 juvenile and 3 adults) were cut into 250  $\mu\text{m}$  sections using a cryostat (Leica), and mounted on slides. The dLGN and PUL were separately dissected from the sections and homogenized in ice cold RIPA buffer (50 mM Tris-HCl, 150 mM NaCl, 1% Igepal, 0.5% sodium deoxycholate, 0.1% SDS, pH 8.0, Sigma) with a cocktail of protease and phosphatase inhibitors (1:100 FabGennix, Frisco, TX, USA). Tissue was centrifuged at 4 °C under 14,000 r.p.m. for 30 min. The supernatant was collected and the protein concentration was estimated using a BCA kit (Pierce Biotechnology Inc., Rockford, IL, USA). Equal amounts (15  $\mu\text{g}$ ) of protein were separated by SDS-PAGE on 10% gels (Bio-Rad) and transferred to PVDF membranes (Milipore, Billerica, MA, USA). Membranes were blocked with 5% dry milk dissolved in Tris buffered saline pH 8.0 (TBS) plus 0.1% tween-20 (TBST), and incubated at 4 °C overnight with either a mouse anti- $\text{Ca}_v$  3.2 antibody (1:1000, NeuroMab, UC Davis) or mouse anti- $\beta$ -actin (1:10,000; Sigma) in 5% bovine serum albumin (BSA) dissolved in TBST. Antibody binding was detected with an anti-mouse antibody conjugated to horseradish peroxidase (1:10,000, Chemicon International) and enhanced chemiluminescence (ECL) Western blotting detection reagents (Amersham Life Science, Buckinghamshire, UK). For quantitative analysis, the density of the labeled bands was

measured with a computerized image analysis system (Alpha Innotech) as integrated density values, normalized to integrated density values of bands labeled for  $\beta$ -actin.

### ***Immunohistochemistry***

Three tree shrews (1 juvenile and 2 adults) were given an overdose of sodium pentobarbital (250 mg/kg) and were perfused through the heart with Tyrode solution, followed by a fixative solution of 4% paraformaldehyde in 0.1 M PB. The brain was removed from the skull, sectioned into 50- $\mu$ m-thick slices using a vibratome (Leica VT100E, Leica Microsystems, Bannockburn, IL) and collected in a solution of 0.1 M PB. The sections were incubated at 4 °C overnight with mouse monoclonal anti-Ca<sub>v</sub> 3.2 antibody (1:200, NeuroMab, UC Davis), and the following day the sections were rinsed in PB and incubated for 1 hour in an anti-mouse antibody conjugated to Alexafluor-488 (1:100, Invitrogen/Molecular Probes, Carlsbad, CA) and the fluorescent DNA marker 4',6-diamidino-2-phenylindole (DAPI). The sections were subsequently rinsed in PB and mounted on slides for confocal microscopic examination.

### ***Stereology***

Three tree shrews (1 juvenile and 2 adult) brains were fixed and sectioned into 50- $\mu$ m-thick slices using a vibratome (Leica VT100E, Leica Microsystems, Bannockburn, IL). The sections were incubated at 4 °C overnight with mouse monoclonal anti-NeuN antibody (1:200, Chemicon International), the following day the sections were rinsed in PB and incubated for 1 hour in an anti-mouse antibody conjugated to Alexafluor-488 (1:100, Invitrogen/Molecular Probes, Carlsbad, CA) with the fluorescent DNA marker 4',6-diamidino-2-phenylindole (DAPI 3 $\mu$ M, Invitrogen) for 1 hour. After being rinsed in PB, sections were mounted on slides for light and confocal microscopic examination.

Using the differential staining of neurons and glial cells with the NeuN antibody and DAPI, the densities of neurons and glia in the juvenile and adult dLGN and PUL were quantified using Stereo Investigator (version 7) software (MBF Bioscience, Williston, VT, USA). All experiments were blind to age of the animals. A contour was drawn around the dLGN or PUL under low magnification (4x) and, within each traced contour, the computer determined the placement of random counting frames. The depth (z-axis) of the counting frame was equal to the minimal thickness of the section, minus a total guard zone of 6  $\mu\text{m}$  (3  $\mu\text{m}$  from the top and bottom of the section). Neurons and glia were counted in the volume designated by each counting frame (25  $\mu\text{m}^2$ ) and were only counted once, when they first came into focus. The total numbers of neurons and glial cells were then estimated for the entire volume using the optical fractionator probe (MBF Bioscience).

#### ***Cell size analysis and electron microscopy***

Sections from juvenile (1) and adult (3) tree shrew brains containing the dLGN or PUL were postfixed in 2% osmium tetroxide, dehydrated in an ethyl alcohol series, and flat embedded in Durcupan resin between 2 sheets of Aclar plastic (Ladd Research, Williston, VT). Durcupan-embedded sections were first examined with a light microscope to select areas for further analysis. Selected areas of the dLGN or PUL were mounted on resin blocks, and cut into 1  $\mu\text{m}$  or ultrathin (70–80 nm, silver-gray interference color) sections with an ultramicrotome (Leica Ultracut E). One  $\mu\text{m}$  thick sections were collected on glass slides and stained with toluidine blue. A NeuroLucida system and tracing software (MicroBrightField, Inc., Williston, VT) were used to measure the soma areas of dLGN and PUL neurons. Neuronal somata were measured

only at the level where a clear nucleolus was visible in the section. Ultrathin sections were collected on Formvar-coated nickel slot grids. The grids were stained with a 10% solution of uranyl acetate in methanol for 30 min before examination with an electron microscope.

### ***Statistical Analysis***

Student t-tests or two-way analysis of variance (ANOVA) were used to test for statistical significance. Quantitative data are expressed as means  $\pm$  SD. The significance level was set at  $p < 0.05$  for all statistical comparisons.

### ***Neuronal modeling***

A model of a thalamic relay neuron was developed to investigate the hypothesis formulated by the experimental results. The model had three compartments, aiming at capture the soma, basal dendrites, and distal dendrites, with voltage-dependent conductances modeled using a Hodgkin-Huxley type of kinetic model (Hodgkin and Huxley, 1952).

The somatic compartment was capable of generating action potentials and contained a fast sodium current,  $I_{Na}$ , a potassium current,  $I_K$ , a leak current,  $I_{leak}$ , and a  $\text{Na}^+/\text{K}^+$  pump, as well as calcium dynamics. Kinetics of  $I_{Na}$  and  $I_K$  were taken from Traub and Miles (Traub et al., 1991), and had maximal conductances of  $g_{Na} = 100 \text{ mS/cm}^2$ , and  $g_K = 100 \text{ mS/cm}^2$ , and reversal potential of  $E_{Na} = 50 \text{ mV}$ , and  $E_K = -100 \text{ mV}$ . Dendritic compartments had a leak current,  $I_{leak}$ .

In addition, all compartments were embedded with the low-threshold calcium current,  $I_T$ . Because no data exist to constrain the localization and kinetics of  $I_T$  in the tree shrew, we used the kinetics of activation and inactivation of  $I_T$  in TC cells from rodents

(Huguenard and McCormick, 1992; Destexhe et al., 1998). That calcium current was described by Goldman-Hodgkin-Katz constant-field equations,

$$I_T = \bar{P}_{Ca} m^2 h G(V, Ca_i, Ca_o),$$

$$\dot{m} = -\frac{1}{\tau_m(V)} (m - m_\infty(V))$$

$$\dot{h} = -\frac{1}{\tau_h(V)} (h - h_\infty(V)),$$

where  $\bar{P}_{Ca}$  (cm/s) is the maximum permeability of the membrane to  $Ca^{2+}$  ions, and  $m$  and  $h$  are, respectively, the activation and inactivation variables.  $G(V, Ca_o, Ca_i)$  is a nonlinear function of voltage and ionic concentrations:

$$G(V, Ca_o, Ca_i) = \frac{Z^2 F^2 V Ca_i - Ca_o \exp\left(-\frac{Z F V}{R T}\right)}{R T \left(1 - \exp\left(-\frac{Z F V}{R T}\right)\right)},$$

Where  $Z = 2$  is the valence of calcium ions,  $F$  is the Faraday constant,  $R$  is the gas constant, and  $T$  is the temperature in Kelvin.  $Ca_i$  and  $Ca_o$  are the intracellular and extracellular  $Ca^{2+}$  concentrations (in M), respectively. Expressions for the steady-state activation and inactivation functions were taken from voltage-clamp experiments on dissociated TC cells (Huguenard and McCormick, 1992; Huguenard and Prince, 1992). The functions optimized to reproduce our experimental results in the presence of a slow depolarizing ramp were:

$$m_\infty(V) = \varphi^{-1} \left( 0.6 + \frac{1}{\exp\left(-\frac{(V + 132)}{16.7}\right) + \exp\left(\frac{(V + 16.8)}{18.2}\right)} \right),$$

$$h_\infty(V) = \frac{1}{1 + \exp\left(\frac{V - V_{1/2}}{4}\right)},$$

with  $\varphi = 5^{(cellular-24)/10}$ , and where  $V_{1/2} = -82$  mV for multiple occurrences of LTSs and  $V_{1/2} = -77$  for a single occurrence of a LTS. The voltage-dependent time constant for activation was

$$\tau_m(V) = \varepsilon \frac{0.204 + 0.333}{\exp\left[-\frac{V + 131}{16} \cdot 7\right] + \exp\left[\frac{V + 15.8}{18} \cdot 2\right]}$$

with  $\varepsilon = 1$  for multiple occurrences of LTSs and  $\varepsilon = 5$  for a single LTS. For inactivation, it was:

$$\tau_h(V) = \begin{cases} 0.333 \exp\left(\frac{V + 466}{66.6}\right), & \text{for } V \leq -81 \text{ mV} \\ 9.32 + 0.333 \exp\left(-\frac{V + 21}{10.5}\right), & \text{for } V \geq -81 \text{ mV} \end{cases}$$

These functions correspond to an external  $\text{Ca}^{2+}$  concentration of 2mM at a temperature of 36°C. Calcium handling was modeled by a first-order system representing  $\text{Ca}^{2+}$  transporters and buffers (McCormick and Huguenard, 1992), with a time constant of decay of  $\text{Ca}^{2+}$  of 5ms. At equilibrium, the free intracellular  $\text{Ca}^{2+}$  concentration was 240 nM and the extracellular  $\text{Ca}^{2+}$  concentration was 2mM (*i.e.*  $E_{\text{Ca}}=120$  mV). A range of T-current densities of  $0-2 \times 10^{-3}$  cm/s was simulated in perisomatic and dendritic compartments to reproduce the experimental observations.

Simulations were performed under the NEURON modeling environment software, with a Runge-Kutta fourth-order integration method. Analyses of computational data were carried out with MATLAB 7 (R2010).

## Results

### *Single- Multi- and No-LTS neurons in the PUL and dLGN*

Our electrophysiological results are based on whole cell recordings from 46

neurons in the dLGN and PUL from slices of juvenile (7) and adult (5) tree shrew brains. Figure 1A illustrates the location of the dLGN and PUL recordings in parasagittal slices. The individual dLGN lamina could not be accurately identified in the slices. Therefore recordings were obtained in the central regions of the dLGN, likely including layers 2-5. All recordings in the PUL were obtained from either the dorsal (Pd) or central (Pc) subdivisions, which receive input from the superior colliculus and temporal cortex (Chomsung et al., 2008; Chomsung et al., 2010). Biocytin was included in the recording pipette and all recovered cells displayed morphologies consistent with their identification as relay cells (Figure 1B). Burst and tonic firing (Figure 1C-E) could be induced in most neurons (37 of 46).

To activate LTSs in thalamic relay neurons, cells must be depolarized after they have been sufficiently hyperpolarized to de-inactivate  $I_T$ . To accomplish this, neurons were either injected with a series of hyperpolarizing 500 ms current steps of varying size (-200 pA to -50 pA; Figure 2 A-C), or with a series of depolarizing current ramps varying in slope (duration varied from 0.5s to 10s while the amplitude of the current ramp remained constant, Figure 3 A-C). For the ramp current injections, to ensure the full de-inactivation of  $I_T$ , the membrane potential of the recorded neurons was adjusted to -80mV before application of the current ramps. The amplitude of the current ramps was sufficient to pass through LTS activation zone and subsequently activate tonic firing.

As illustrated in Figures 2 and 3, based on the responses of neurons to hyperpolarizing current steps or ramps, 3 types of neurons were identified which exhibited significant variation in their propensity to fire with bursts. In some neurons within the juvenile dLGN and PUL (n = 9), we were unable to elicit any LTSs (Figure 2A



and 3A). In most neurons within the juvenile dLGN and PUL, as well as the adult dLGN ( $n = 27$ ), single LTSs could be elicited (Figure 2B and 3B). However, within the adult PUL, multiple LTSs were elicited by either current steps or ramps in the majority of the recorded neurons ( $n=6$ ; Figure 2C, 3C). The proportions of these 3 types of neurons within the adult dLGN and PUL are illustrated in Figure 2D.

### ***Comparison of single- and multi-LTS neurons***

To compare the burst firing properties of single- and multi-LTS neurons we quantified the effects of the slope ( $dV/dt$ ) of depolarizing current ramps on the number and interspike interval of action potentials initiated by the LTSs, and the maximum rate of rise of the elicited LTSs. In single-LTS neurons, a strong positive correlation was observed between the number of the action potentials riding the crest of the LTS and  $dV/dt$  (Figure 4A). This relationship is shown in Figure 4C, for 4 neurons in the juvenile and adult PUL and dLGN. The same relationship was observed between the maximum rate of rise of the LTS and ramp slope of depolarization in single LTS neurons (Figure 4E). To measure the maximum rate of rise of the LTS, TTX, 4-AP and TEA were applied and voltage response of the recorded cell to current ramps were obtained and temporally differentiated. In the differentiated trace, the voltage baseline was determined before the onset of current ramp, and the maximum rate of rise of the LTS was measured.

In contrast, in multi-LTS neurons, the number of the action potentials riding the crest of the first LTS elicited by each current ramp was constant (Figure 4B), i.e. there was no correlation between the number of the action potentials and  $dV/dt$  (Figure 4D), although there was still a positive correlation between the maximum rate of rise of the LTS and  $dV/dt$  (Figure 4E). In both single-LTS and multi-LTS neurons, interspike

intervals increase with the addition of action potentials to the burst sequence (Figure 4F).

### ***Burst properties of multi-LTS neurons***

In multi-LTS neurons, the number of LTSs evoked decreased with increases in  $dV/dt$  (Figure 5B, C). Although the number of action potentials riding the first LTS elicited by each current ramp was unrelated to  $dV/dt$  (Figure 4D and 5C), the number of action potentials riding each subsequent LTS decreased (Figure 5A, C).

### ***Cav 3.2 expression in the PUL and dLGN***

To determine whether the greater propensity of PUL neurons to fire in burst mode could be due to an increased density of calcium channels, we used an antibody against the alpha-1H subunit of the voltage-dependent T-type calcium channel (Cav 3.2) for immunocytochemistry and western blot techniques. As illustrated in Figure 6 (A-B), the Cav 3.2 antibody stains neurons in both the dLGN and PUL. Glial cells, identified by dense nuclear staining with DAPI (Figure 7), were not stained with the Cav 3.2 antibody.

We carried out a quantitative comparison of Cav 3.2 expression in samples of PUL and dLGN tissue collected from 3 juvenile and 3 adult brains. An antibody against beta actin was used to correct for sample loading discrepancies (Figure 6 C). This analysis revealed no significant difference between expression levels in juvenile versus adult tissue. However, at both ages, PUL tissue was found to contain a higher density of Cav 3.2 than that found in dLGN tissue (Figure 6D). This difference was found to be significant (Two-way ANOVA).

### ***Neuron size and density in the PUL and dLGN***

In order to relate the western blot results to neuronal Cav 3.2 channel density, we used unbiased stereology techniques to compare the neuron and glial cell density in the

dLGN and PUL. As illustrated in Figure 7, in neurons, regions of condensed chromatin (black asterisks A, B, E, F) surround nucleoli (white asterisks, B, F) or are sparsely distributed in the nucleus. In contrast, chromatin is relatively condensed through glial cell nuclei, resulting in intense staining of the entire nucleus with the DAPI stain (A, E). Using these staining characteristics to identify neurons and glial cells, as well as NeuN immunocytochemical staining as a second means to identify neurons, unbiased stereological techniques were used to count neurons and glial cells within the dLGN and PUL.

While there were no significant difference in cell density in each nucleus (Figure 7I), we found a nearly equal number of glia and neurons in the dLGN (glia:neuron ratio 1.21:1 in juvenile and 1.19:1 in adult), the PUL contained a higher percentage of glial cells (glia:neuron ratio 2.23:1 in juvenile and 2.72:1 in adult; Figure 7 J). Additionally, although there was no significant difference in the size of neurons in the juvenile dLGN and PUL, in the adult, dLGN cells were found to be significantly larger as a group when compared to PUL cells ( $P < 0.001$ ; 2-way ANOVA). Therefore the membrane density of T-type calcium channels expressed by PUL neurons may be significantly higher than that expressed by dLGN neurons.

### ***Neuronal Modeling***

To further assess our working hypothesis that a difference in burst firing propensity between dLGN and PUL neurons stems from a variation in the density of T-type calcium channel (Cav 3.2), we developed a computational model of a thalamic relay cell, composed of three compartments representing the soma, the apical dendrites, and the

distal dendrites, respectively, each of these embedded with T-type calcium channels (see *Methods*).

Depending on the density of T-channels simulated in the perisomatic areas or in the distal dendrites, we were able to reproduce five qualitatively distinct representative firing patterns in response to a depolarizing current ramp injection, namely (i) passive (P), (ii) subthreshold (S), (iii) single-LTS burst (LTS), (iv) multi-LTS bursts (MLTS), and (v) and spontaneous oscillatory (O). Figure 8 shows a space-plot diagram of the different firing patterns which were achieved in response to a 2 second current ramp as the density of T-type calcium channels was varied in the perisomatic areas and distal dendrite compartments. The controlling factor in shaping the firing pattern response was the T-current density in the distal dendritic compartment, in contrast to the density in the perisomatic compartments. Below a given value for distal dendritic density ( $10^{-3}$  cm/s in Fig.8), the neuron response was passive during the depolarizing ramp, being unable to elicit a full or a subthreshold calcium spike. In contrast, for a fixed value of the distal dendritic density, a systematic variation of the perisomatic density was unable to significantly alter the firing pattern regime. Whenever the perisomatic density was varied, it mostly affected the number of action potentials crowning the calcium spike (*data not shown*). Above a given value for the distal dendritic density ( $10^{-3}$  cm/s in Fig., 8), the neuron exhibited a spontaneous oscillatory regime by eliciting calcium spikes in the absence of external stimulation. A progressive increase of T-channel density in the distal dendrites caused a switch from a single-LTS response to multi-LTS (Fig. 8, green vs. orange areas). With the initial channel kinetics parameters used (cf. *Methods*), the single-LTS pattern that could be produced was systematically followed by one or multiple

subthreshold LTSs (see Figure 9A, *left panel*). This result is at odds with the experimental observations from Figure 3B that evidences a single-LTS with Na<sup>+</sup>-spikes, without the presence of obvious subsequent subthreshold (passive) LTSs. To cope with this discrepancy between the model and the empirical results, we modified the kinetics of the T-type calcium channel in the model, and observed that the best results were obtained by reducing  $V_{1/2}$  from -82 to -77 mV from the Boltzmann distribution of the steady-state inactivation variable,  $h_{\infty}$  (Figure 9B), and by a five-fold increase of the voltage-dependent time constant activation,  $\tau_{act}$  (Figure 9C). With this slower T-channel kinetics, we were able to produce a single-LTS response similar to Fig. 3B (see Figure 9A, *right panel*). The temporal evolutions of these kinetics variables for the T-type current during a current-ramp stimulation of 2 seconds are depicted in Figure 9E-G.

Using the combination of parameters for dendritic T-channel densities and the T-current kinetics described *supra*, we were able to faithfully reproduce the essential properties of the firing patterns from the experimental results reproduced in Figure 3. A passive response to a depolarization ramp (i.e. tonic firing without calcium spike) was obtained in presence of a weak density of T-channels in both somatic and dendritic compartments (Figure 10A - see legend for details). Because the channel density was low enough and failed to elicit any LTSs, the channel kinetics chosen were of little relevance. By inhomogeneously increasing the density of T-channels in all three compartments (i.e. the density in the distal dendrites mattered the most) with a slow channel kinetics, we were able to elicit a single-LTS without subthreshold calcium spikes for steep current ramps. The calcium spike became passive (subthreshold) for reduced ramp slope corresponding to 8-s and 10-s ramp stimulations (Figure 10B). Multi-LTS were elicited

upon further increase of T-channel densities in the distal dendrites, along with a modified, faster, channel kinetics (Figure 10C).

Finally, we looked at the relationships to the current ramp slope between the two major classes of TC neurons (single-LTS and multi-LTS). For single-LTS neurons, the slope of the current ramp,  $\frac{\Delta V}{\Delta t}$ , had a strong positive correlation with the number of action potentials crowning the isolated calcium spike, as shown in Figure 10D, where the LTS of the first four simulations in Figure 10B is expanded (i.e. 2s-, 4s-, 6s-, and 8s-current ramps). This proportional relationship was observed in the experiments as well. An increase of 100% of the current-ramp duration corresponded to a reduction by 50% of the number of action potentials riding the crest of the LTS. In contrast, the number of action potentials crowning the first LTS of multi-LTS neurons showed a more robust independence to the slope of the current ramp. As shown for the first three expanded traces in Figure 10E, an increase of 100% of the current-ramp duration only corresponded to an average reduction by 14.45% of the number of action potentials riding on top of the first LTS.

## **Discussion**

### ***PUL and dLGN burst propensity***

Our results support those of Ramcharan et al (Ramcharan et al., 2005) who found that PUL neurons fire with bursts more often than dLGN neurons, and further indicate that the increased T-type channel density of PUL neurons relative to dLGN neurons may underlie this phenomenon. *In vivo*, the increased T-type channel density of PUL neurons may work in concert with a variety of other factors to increase the propensity of PUL neurons to fire in bursts. For example, several *in vitro* studies in other species have noted

differences in the response of PUL and dLGN neurons to neurotransmitters such as serotonin and acetylcholine (Monckton and McCormick, 2002; Varela and Sherman, 2007, 2009), which may maintain PUL neurons in a more hyperpolarized state relative to dLGN neurons. In fact, Ramcharan et al (Ramcharan et al., 2005) found that *in vivo*, PUL neurons have a lower rate of spontaneous firing when compared to dLGN neurons, suggesting that they are relatively more hyperpolarized.

Ramcharan et al (Ramcharan et al., 2005) also found that in the awake state, PUL neurons can fire rhythmically, even during the execution of visual tasks, whereas rhythmic firing was never detected in the awake dLGN. Our results suggest that the membrane properties of PUL may also contribute to this phenomenon. We found that even in the *in vitro* situation, with all ascending and descending inputs transected, and all intrinsic GABAergic connections blocked pharmacologically, the PUL neurons could fire with a rhythmic burst pattern, and our neuronal modeling demonstrate that oscillatory activity can result from the increased T-channel density predicted by our western blot results.

### ***Developmental of burst firing***

Our comparison of the membrane properties of neurons recorded in juvenile and adult tissue suggest that the multi-LTS firing pattern displayed by PUL neurons develops after 3 weeks of age (possibly correlated with eye opening which occurs at that time in tree shrews). With our neuron model, we were able to closely replicate this firing pattern by increasing T-channel density within distal dendrites. However, a small change in channel kinetics was necessary to fully replicate the adult data. Previous studies have also

demonstrated developmental changes in channel kinetics (Ramoia and McCormick, 1994).

### ***Within-burst coding***

In contrast to previous studies which have observed little variation in the number of spikes elicited by each LTS (Zhan et al., 1999; Gutierrez et al., 2001), for single LTS neurons, we found significant correlations between the rate of rise of the current slope and the number of action potentials elicited, and for multi-LTS neurons correlations between the number of action potential elicited and the position of the LTS in a multi-LTS train. Our results suggest that rather than all-of-none events, significant information can be contained within the dynamics of each burst. Thus, variations in the T-channel density across nuclei could dramatically increase the coding repertoire of the thalamus.

### ***Neuron:glia ratio in the PUL and dLGN***

Our investigations of neuron density, which were carried out in order to more precisely interpret our western blot data, revealed an interesting difference in the structure of the dLGN and PUL. We found that the density of neurons is much lower in the PUL nucleus compared to the dLGN, but the overall cell density in each nucleus is similar. This is because the PUL nucleus contains a much higher density of glial cells relative to the dLGN. In the dLGN, neurons and glial cells are present in approximately equal numbers, while in the PUL, glial cells outnumber neurons by a ratio of 2.5:1.

The glia:neuron ratio varies considerably in the brain. A recent stereological study of human brain tissue found a 1:1 ratio for the thalamus as a whole, and a 7:1 for the cortex as a whole (Azevedo et al., 2009). Although we did not identify the subtypes of glial cells in the PUL, the majority are likely to be astrocytes, the processes of which



surround most synapses (Halassa et al., 2007b). Recent evidence suggests that astrocytes are quite important for the modulation of synaptic transmission and plasticity, and that gap junctions between astrocytes may enhance the rhythmic firing of adjacent neurons (Crunelli et al., 2002). Astrocytes are also thought to play major roles in disease states that may interfere with rhythmic firing, such as epilepsy and schizophrenia (Halassa et al., 2007a).

### ***Functional implications***

In contrast to the dLGN, which projects to single discrete sites within V1 (Conley et al., 1984), the regions of the PUL recorded in this study project to multiple targets within the temporal cortex (Chomsung et al., 2010), as well as the striatum and amygdala (Day-Brown et al., 2010). The prevalence of burst firing in the PUL could serve to synchronize the activity of these multiple widespread targets and/or function as a form of gain control (Saalmann and Kastner, 2009). The PUL neurons recorded in this study receive convergent input from superior colliculus axons that encircle their proximal dendrites, and convergent input from temporal cortex axons that innervates their distal dendrites (Chomsung et al., 2008; Chomsung et al., 2010). By amplifying synchronous tectal and cortical inputs, burst firing could enhance the relay of visual signals that match predicted sensory events. Such a mechanism could underlie the recent observation that PUL activity reflects the perceptual awareness of a visual stimulus (Wilke et al., 2009).

Finally, the unique membrane properties of PUL neurons may be relevant to the treatment of conditions that involve atypical brain rhythms. For example, schizophrenia is characterized by abnormal electroencephalograms, in both waking and sleeping states, which are thought to be related to the perceptual aberrations experienced by these

patients (Uhlhaas and Singer, 2010). The PUL and mediodorsal nucleus are reduced in size in schizophrenic brains when compared to controls (Byne et al., 2009) and PUL inactivation has been shown to affect cortical oscillations (Molotchnikoff and Shumikhina, 1996). Further study of the nucleus-specific properties of the dorsal thalamus may contribute to our understanding and treatment of anomalous thalamocortical interactions.

**Figure 1.**

*In vitro* recording methods. A) A parasagittal section of the tree shrew brain stained for Nissl substance illustrates the location of the whole cell recordings in either the dorsal lateral geniculate nucleus (dLGN, outlined in green) or the pulvinar nucleus (PUL, outlined in red). D, dorsal, R, rostral, SC, superior colliculus. B) A confocal image of a PUL cell filled with biocytin during recording (scale = 20  $\mu\text{m}$ ). All successfully filled cells exhibited morphologies consistent with their identification as relay cells. Voltage fluctuations were recorded in response to the injection of depolarizing or hyperpolarizing current steps of varying size (C) as well in response to depolarization (D) or hyperpolarization (E) of the membrane potential via constant current injection.

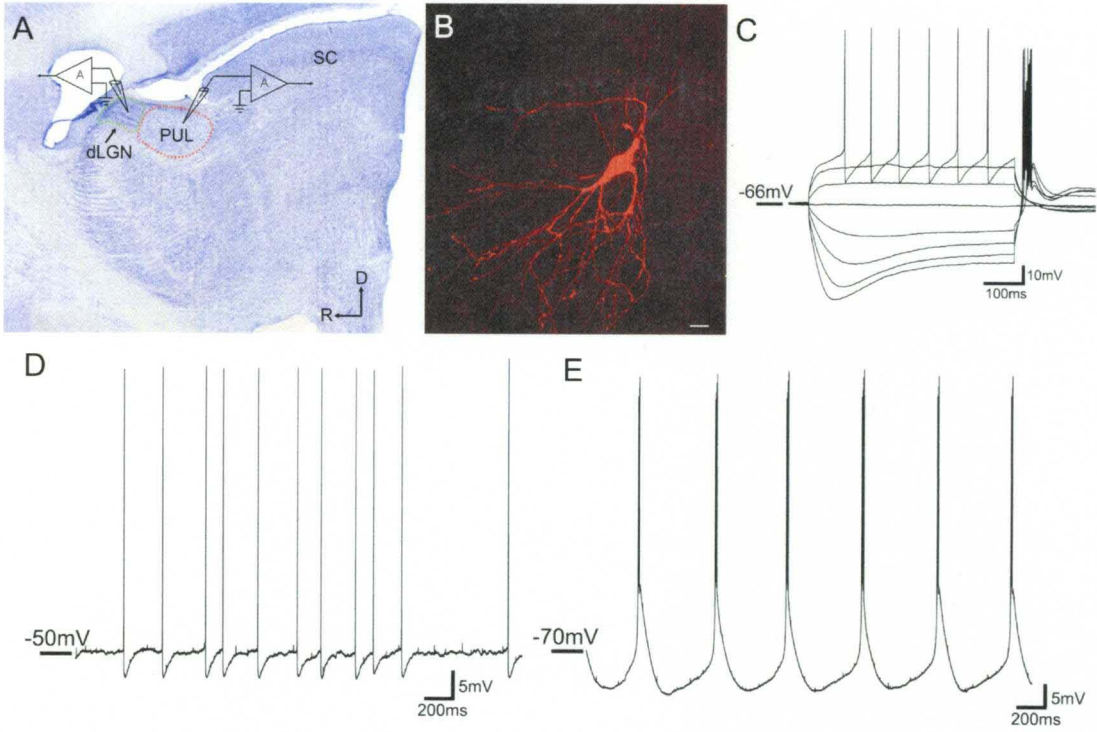


**Figure 2.**

Three types of neurons are distinguished by their responses to hyperpolarizing current steps. Injection of hyperpolarizing (-50pA to -200pA) current steps (500 ms in duration) revealed 3 categories of responses. A) No LTS: An LTS could not be elicited in a small percentage of neurons in both the juvenile dLGN and PUL. B) Single LTS: Most recorded neurons responded to hyperpolarizing current steps with a single "rebound" LTS. C) Multi LTS: Most neurons in the adult PUL responded to hyperpolarizing current steps with multiple LTSs. D) The proportion of the 3 types of cells recorded in the juvenile and adult dLGN.

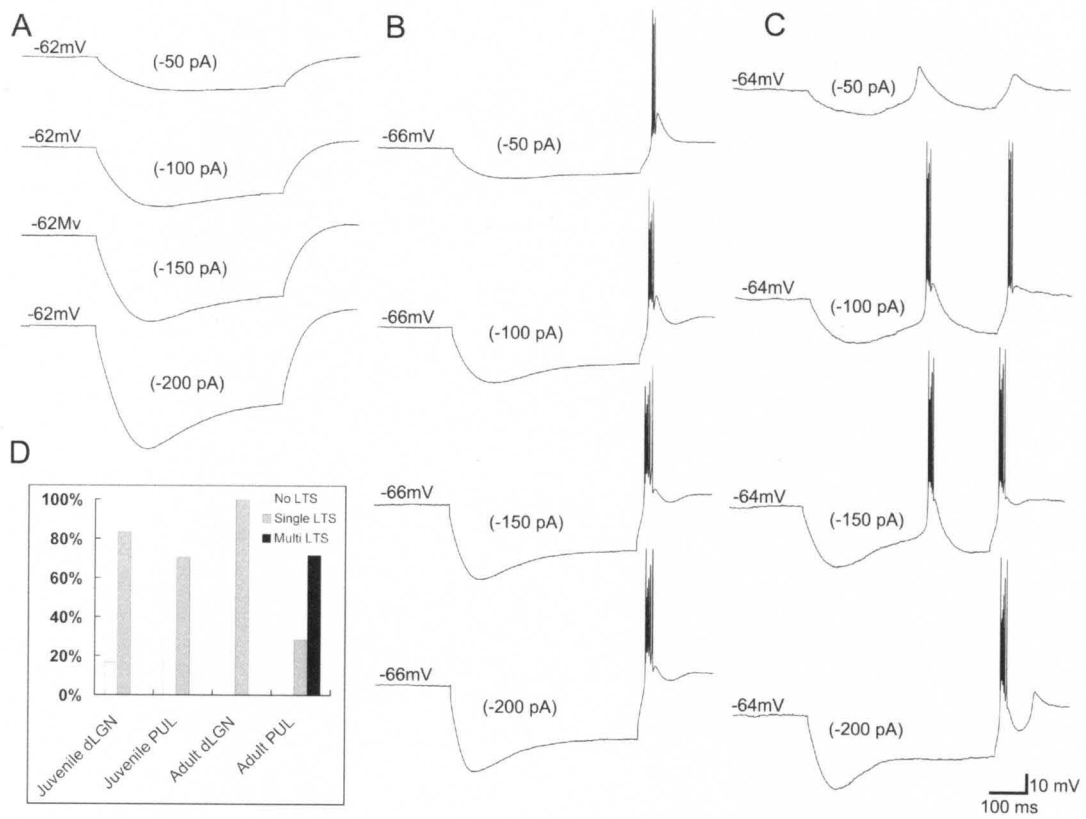


**Figure 3.**

Three types of neurons are distinguished by their responses to depolarizing current ramps. Current ramps of variable slope (durations varying from 2-10s) were injected into neurons that were sufficiently hyperpolarized to de-inactivate T-type calcium channels (-80mV). All cells were depolarized sufficiently to pass through the LTS activation window elicit tonic firing. A) No LTS neuron: current ramps evoke action potentials but no LTS. B) Single LTS neuron: steep current ramps evoke a single LTS. C) Multi LTS neuron: current ramps of variable slope evoke multiple LTSs.

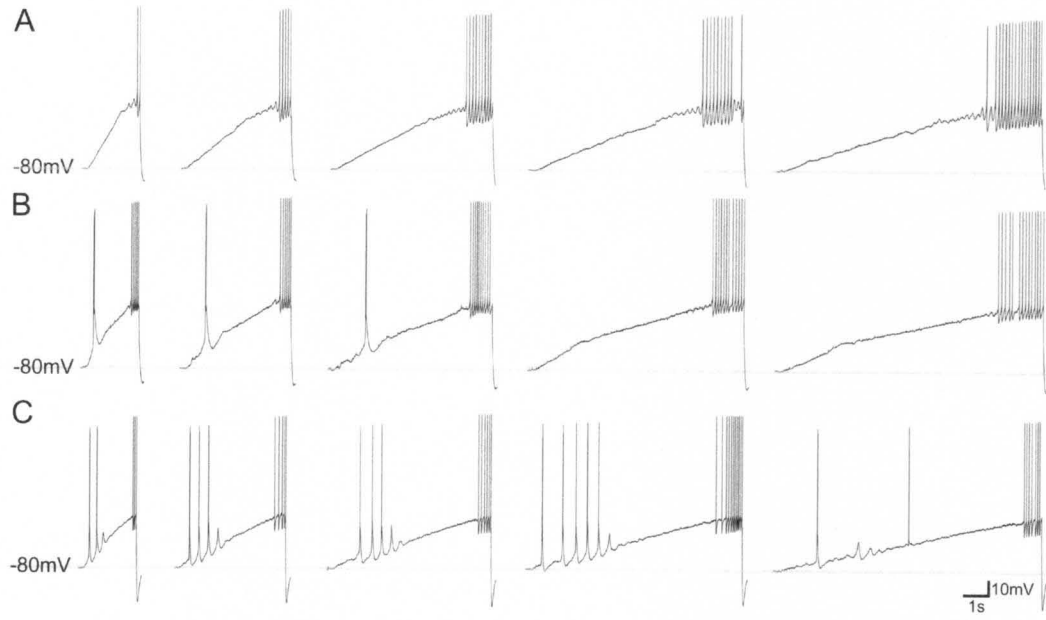




**Figure 4.**

Current ramps reveal distinct firing characteristics of single LTS and multi LTS neurons.

A) Expanded traces from a single LTS neuron. The number of action potentials that ride the crest of the LTS decreases with ramp slope. This phenomenon is plotted for 4 single LTS neurons in the juvenile and adult dLGN and PUL in panel C. B) Expanded traces from a multi LTS neuron. The number of action potentials that ride the crest of the first LTS initiated by variable current ramps remains constant. This phenomenon is plotted for multi LTS neurons in the adult PUL in panel D. E) The maximum slope of the LTS in single- and multi-LTS neurons increases with increasing ramp slope. F) In both single-LTS and multi-LTS neurons, interspike intervals increase with the addition of action potentials to the burst sequence.

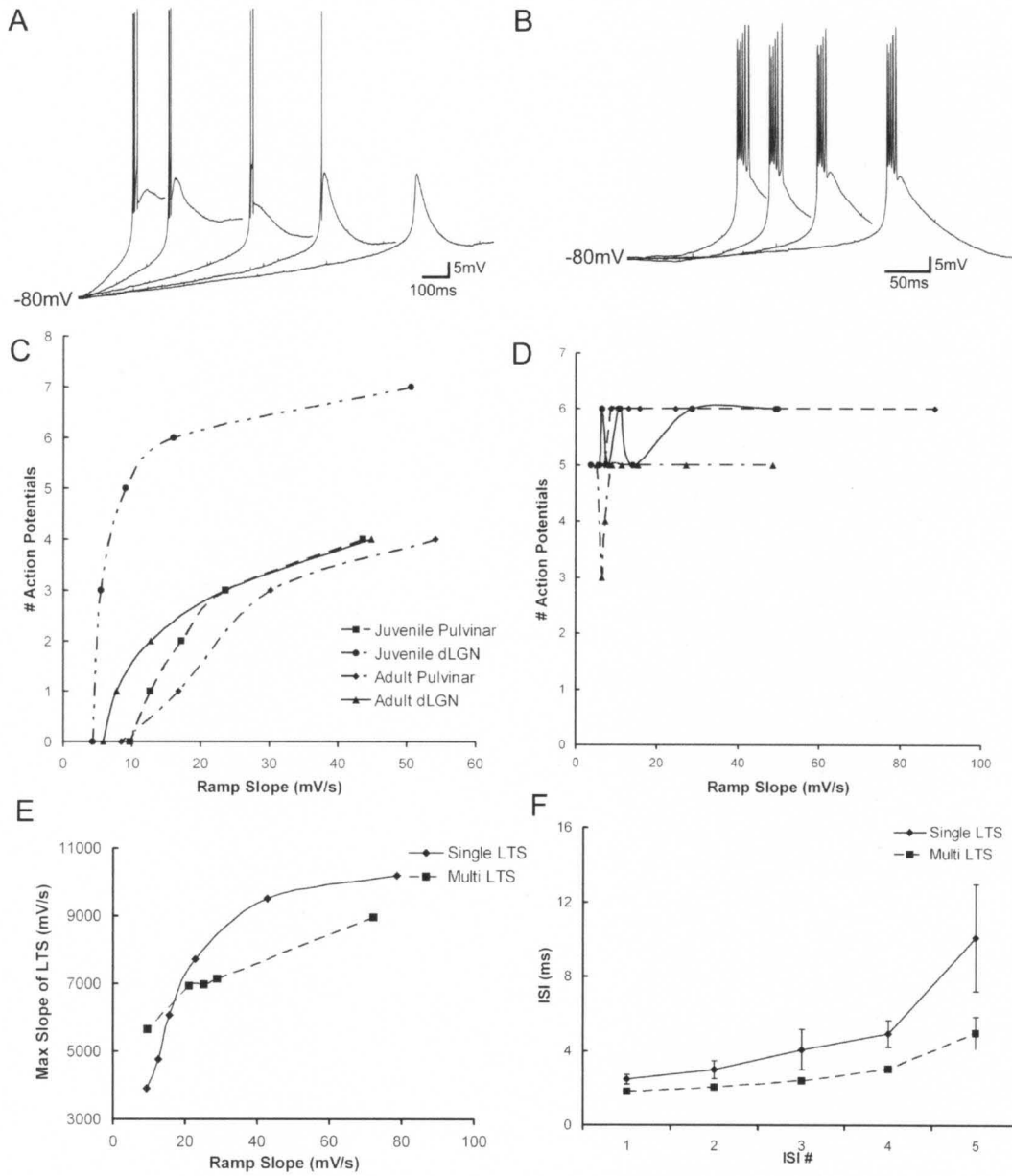


**Figure 5.**

Current ramps reveal further features of burst firing in multi LTS neurons. A) A train of LTSs evoked by a current ramp; a, b, and c indicate traces expanded below that evoke 6, 4, and 2 action potentials respectively. B) The number of LTSs evoked by current ramps of different slopes is plotted for 3 multi LTS neurons. The number of LTSs decreases with increasing ramp slope. C) The number of action potentials that ride the crest of each LTS is plotted as a function of ramp slope and the position of the LTS in a train sequence for one multi LTS neuron. Regardless of ramp slope, the number of action potentials that ride the crest of the first LTS of the train remains constant, but each subsequent LTS initiates decreasing numbers of action potentials.

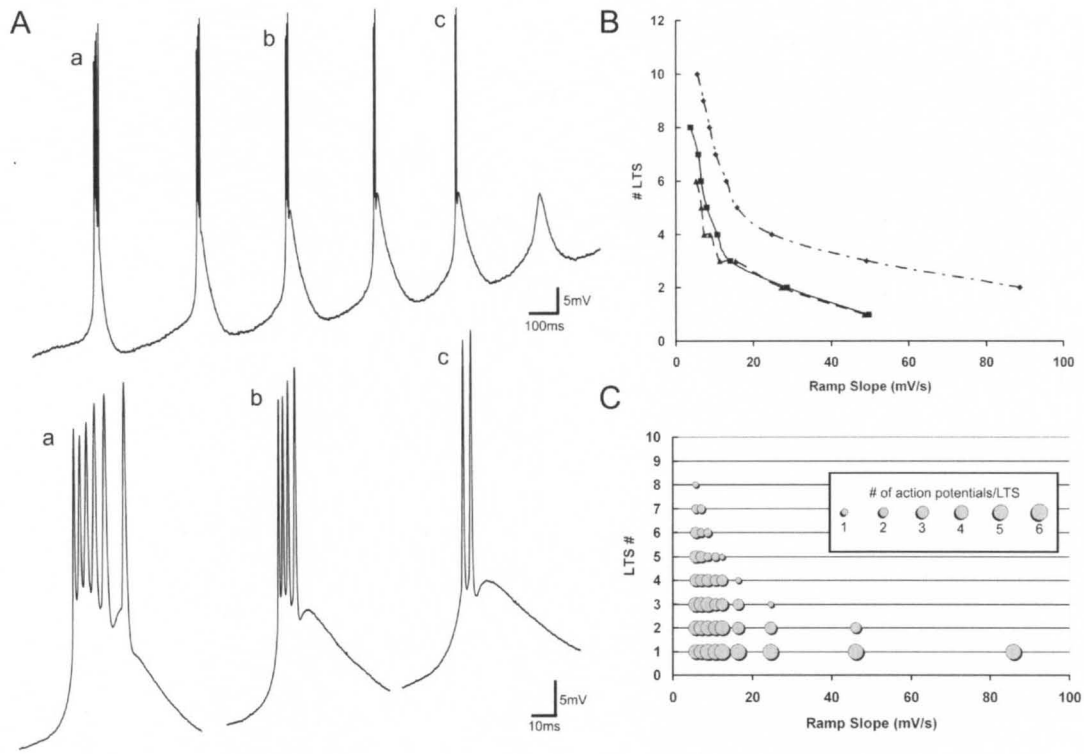


**Figure 6.**

The pulvinar nucleus contains more T-type calcium channels than the dLGN. Confocal images of the PUL (A) and dLGN (B) stained for the alpha-1H subunit of the T-type calcium channel (Cav 3.2, red) and DAPI (blue) illustrate Cav 3.2 labeling of neurons (asterisks, nuclei lightly stained with DAPI) but not glial cells (arrows, nuclei intensely stained with DAPI). C) Western blots of dLGN and PUL tissue samples from 3 juvenile and 3 adult animals illustrates greater staining intensity of the Cav 3.2 antibody in the PUL regardless of age. An antibody against beta actin was used to correct for loading errors. D) Quantification of the western blot signal intensities reveals significantly more intense staining in the PUL compared to the dLGN. PUL versus dLGN ( $p = 0.05$ ; 2-way ANOVA).

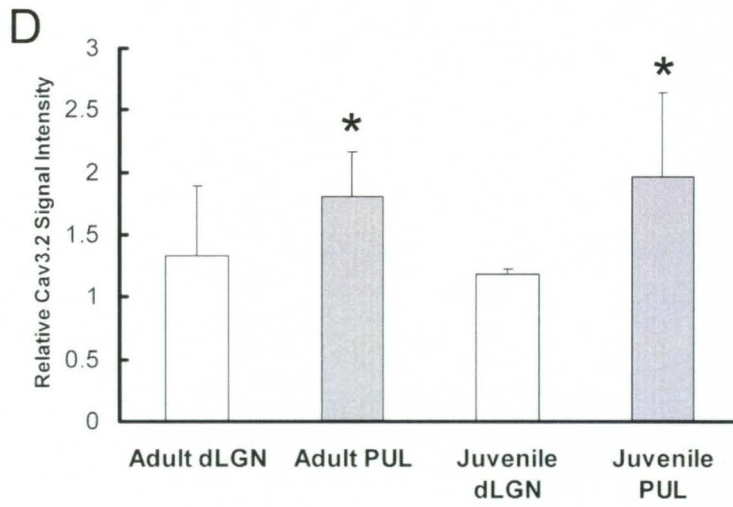
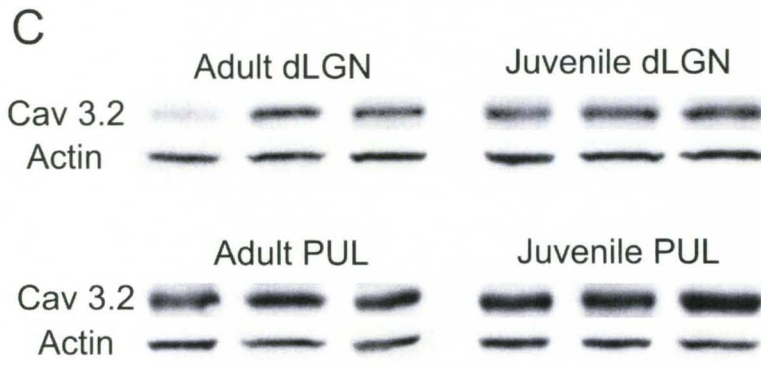
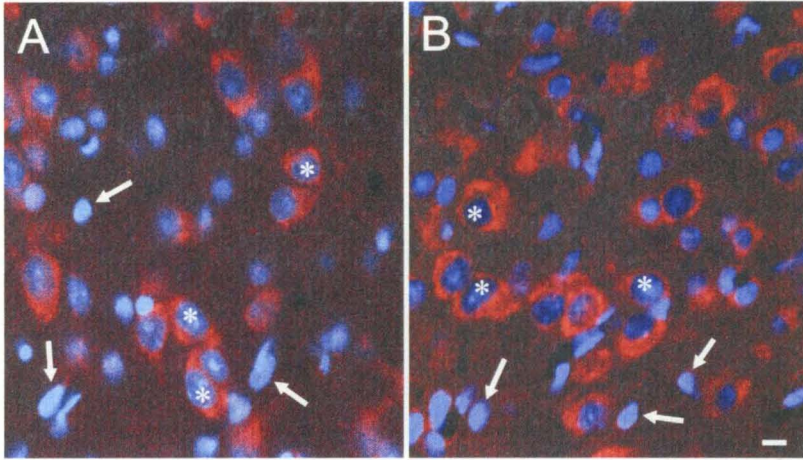


**Figure 7.**

The pulvinar nucleus contains fewer neurons than the dLGN. Correlation of light microscopic images of DAPI staining (A, E) and electron microscopic images (B-D, F) of the PUL (A-D) and dLGN (E,F) illustrates the distinct density and distribution of DNA within neuronal and glial cell nuclei. In neurons, regions of condensed chromatin (black asterisks A, B, E, F) surround nucleoli (white asterisks, B, F) or are sparsely distributed in the nucleus. In contrast, chromatin is relatively condensed through glial cell nuclei, resulting in intense staining of the entire nucleus with the DAPI stain (A, B). Using these staining characteristics to identify neurons and glial cells, as well as NeuN immunocytochemical staining as a second means to identify neurons, unbiased stereological techniques were used to count neurons and glial cells within the dLGN and PUL. Confocal images of the PUL (G) and dLGN (H) stained for DAPI (blue) and NeuN (red) illustrate examples of neurons (white asterisks) and glial cells (white arrows). I) There were no significant differences between the cell densities (neurons + glia) counted within the juvenile and adult dLGN and PUL. J) At each age, the glia:neuron ratio was significantly higher in the PUL when compared to the dLGN (t test, adult  $p = 0.036$ ; juvenile  $p = 0.0005$ ).

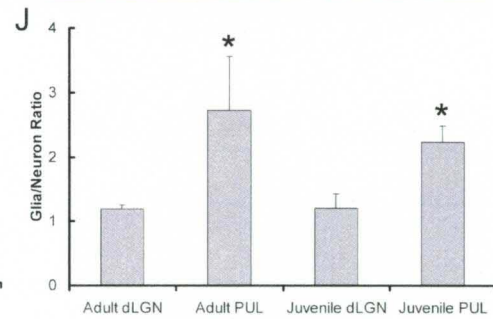
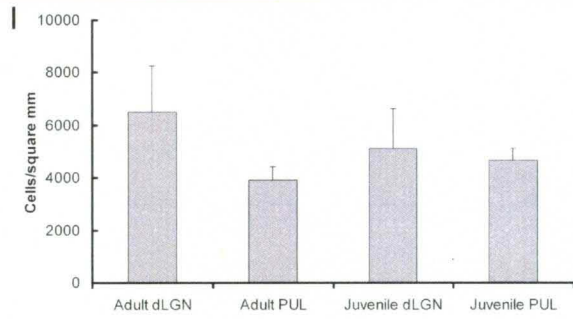
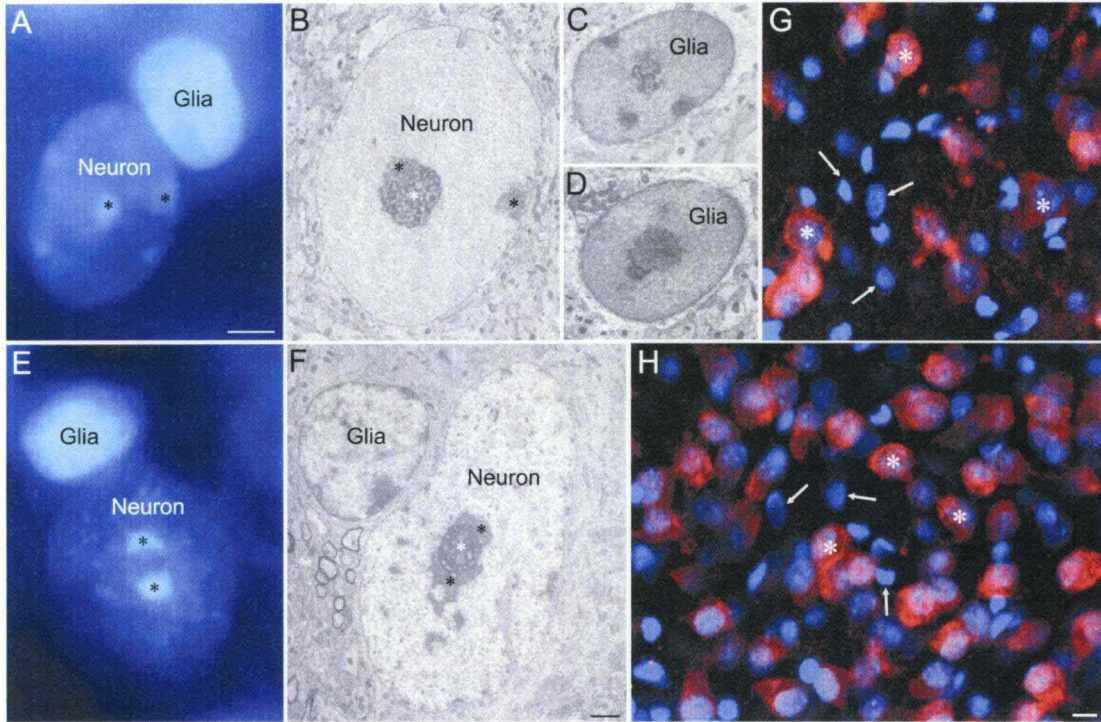
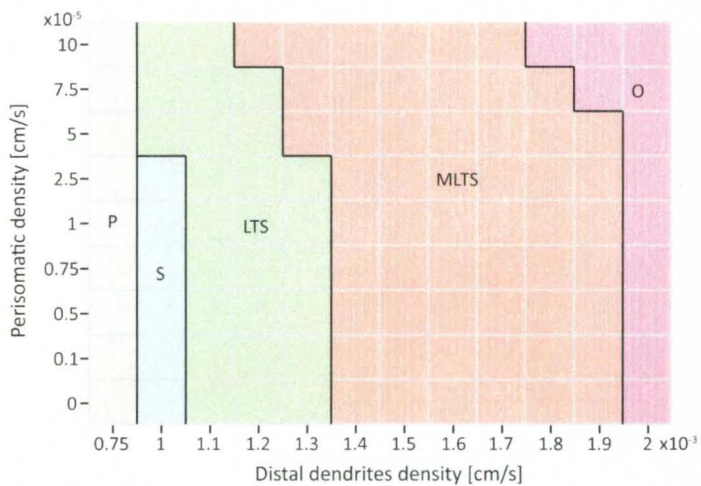




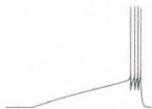
**Figure 8.**

Space-plot representation of the different burst regimes in function of the T-current distribution. Five representative types of response to depolarizing current injection (for a current ramp lasting 2s) from rest were obtained depending on the T-channel density simulated in the perisomatic area or in the distal dendrites: passive (P), subthreshold (S), single LTS burst (LTS), multiple LTS bursts (MLTS), and spontaneous oscillatory regime (O). Perisomatic densities were varied from 0 to  $10^{-5}$  cm/s and distal dendritic densities from  $0.75 \times 10^{-3}$  to  $2 \times 10^{-3}$  cm/s. The consequence of perisomatic T-current in shaping the burst response in TC cell was secondary compared to distal dendritic T-current density, which mostly controlled the nature of the response. For a given dendritic T-current density, the perisomatic density was mostly influencing in a proportional fashion the number of action potentials riding the crest of the first LTS.

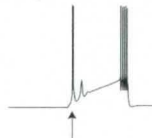
Differential LTS regimes in function of T-current distributions



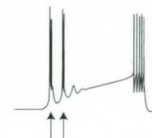
Passive response (P)



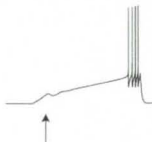
Single LTS burst response (LTS)



Multiple LTSs burst response (MLTS)



Subthreshold response (S)



Spontaneous oscillatory regime (O)

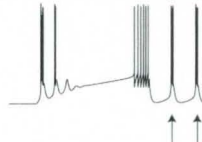


### Figure 9.

Single-LTS require different, slower, channel kinetics. A variation in T-current density cannot explain by itself the difference between single- and multi-LTS bursts. A) A reduced T-current density but the same channel kinetics than for multi-LTS creates an isolated LTS followed by one or multiple passive LTS bursts (*left*). But affecting the T-channel kinetics while keeping that reduced T-current density leads to the generation of a single-LTS without passive response (*right*). B) Differences in the steady-state kinetics variables to produce a single-LTS without passive response. The steady-state inactivation variable,  $h_{\infty}$ , was shifted towards more depolarized potential ( $V_{1/2} = -77$  mV (*red curve*) instead of -82 mV (*black curve*)) to produce the single-LTS from A, *right*. The steady-state activation variable was the same. C) The voltage-dependent activation time-constant was five times bigger (*red curve*) to generate panel A, *right* than the one (*black curve*) used to generate panel A, *left*. Consequently, the T-channel activation was much slower causing less passive responses. D) Peak amplitude of the T-current in the distal dendrites, during a depolarizing current-ramp lasting 2 seconds, for each three categories of TC neuron (passive, single-LTS, and multi-LTS). Several orders of magnitude distinguish the peak amplitude produced during a passive response, the generation of a single-LTS, or the generation of multiple-LTS, due to the difference of T-channel density in the dendrites and of channel kinetics. (*Note the different amplitude scales.*) E-G) Temporal evolution of parameter kinetics for the T-current during a 2s-depolarizing ramp for a passive response, a single-LTS response, and a multi-LTS response. Differences and similarities of the temporal evolution of voltage-dependent kinetics variables of IT are depicted in E for the activation ( $\tau_{act}$ ) and inactivation ( $\tau_{inact}$ ) steady-state variables, in F

for the activation time constant ( $\tau_{on}$ ), and in G for the inactivation time constant ( $\tau_{off}$ ).

Kinetics parameters for the activation time constant and the activation steady-state had to be varied to reproduce the differences observed between a single-LTS response and a multi-LTS response.

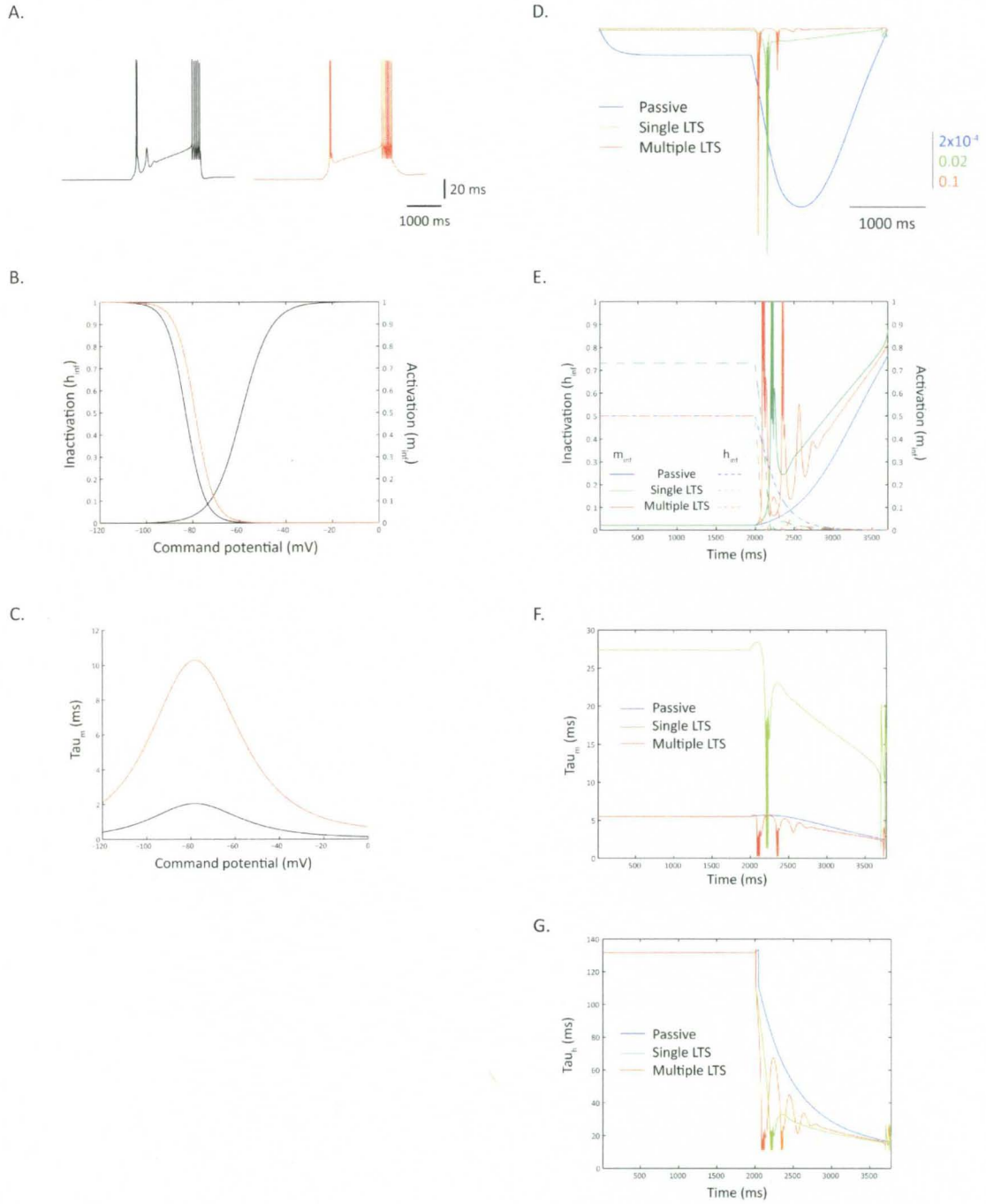
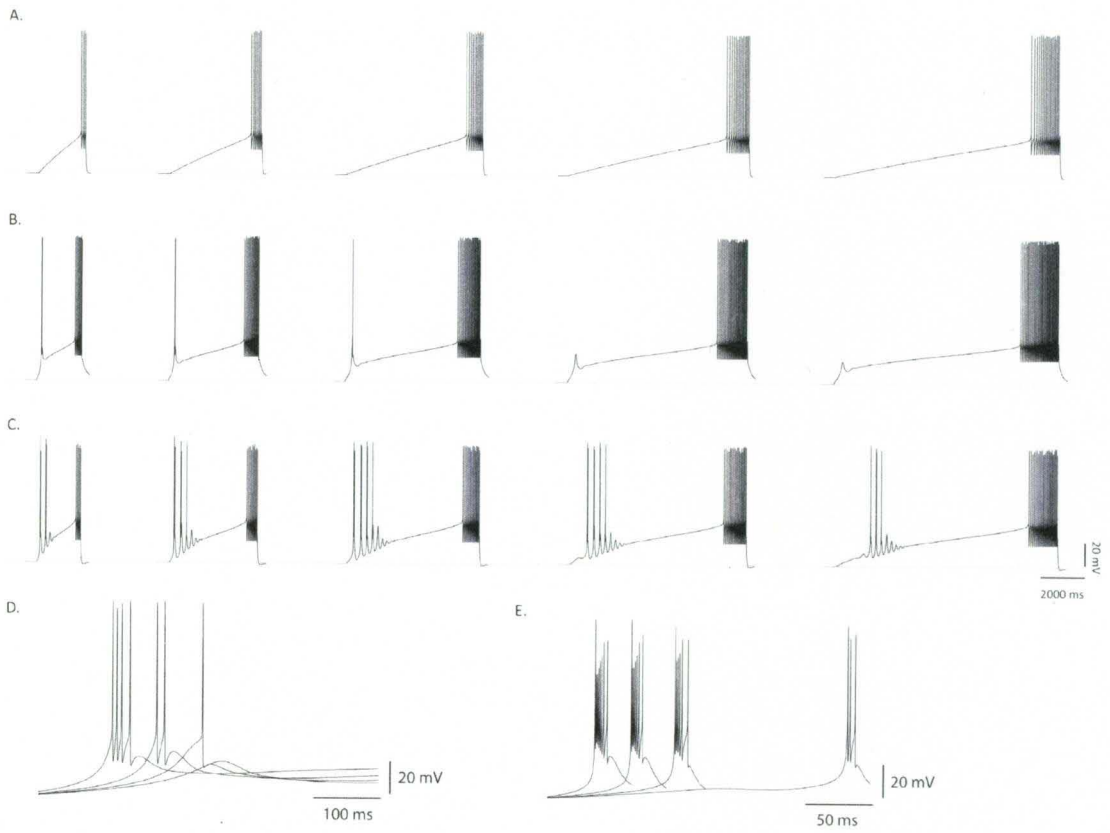


**Figure 10.**

Voltage-trace responses to depolarized current ramps of various durations in three different cell models reproducing the protocol and results of Figure 3. Current ramps of variable slope (duration varying from 2-10s) were simulated and injected into a computational model of a thalamic relay cell. Prior to the injection of the depolarized current ramp, the cell membrane voltage was maintained at a potential of -80 mV for 2 seconds to ensure proper de-inactivation of T-type calcium channels. All cells were depolarized sufficiently by the current ramp to elicit regular tonic firing. A) In the presence of a weak density of T-type calcium channels in both somatic and dendritic compartments, the current ramp failed to elicit any LTS. Tonic spiking was unaffected. (Perisomatic density:  $8.5 \times 10^{-6}$  cm/s; Dendritic density:  $3.78 \times 10^{-4}$  cm/s). B) Increasing the density of T-type calcium channels inhomogeneously in all three compartments of the cell model caused a single LTS to be elicited for steep current ramps. Note that a subthreshold calcium spike, but no sodium spikes, were generated when the ramp became more gradual. Distal dendrites had a T-current density significantly bigger than the proximal and somatic T-current densities (Perisomatic density:  $1.9 \times 10^{-5}$  cm/s; Dendritic density:  $1.0 \times 10^{-3}$  cm/s). C) Further increasing T-current densities and altering T-channel kinetics in both soma and dendrites led to the apparition of multiple LTSs in response to the application of the current ramp (Perisomatic density:  $1.9 \times 10^{-5}$  cm/s; Dendritic density:  $1.8 \times 10^{-3}$  cm/s). D) Expanded traces from B. The delay of apparition of the unique LTS which is triggered has an inversely proportional relationship to the slope of the current ramp and the number of action potentials crowning the LTS expresses a strong relationship with the ramp slope. E) Expanded traces from C. The time of apparition of

the first LTS is dependent on the ramp slope (inverse relationship), but unlike  $D$  the number of action potentials crowning the first LTS is more robust to the slope.





## CHAPTER IV

### DIFFUSE AND SPECIFIC TECTOPULVINAR EPSPS IN THE TREE SHREW: RELATION TO SYNAPSINS AND SYNAPTIC CLUSTERS

#### Outline

The pulvinar nucleus of the tree shrew receives both specific and diffuse projections from superior colliculus (Chomsung et al. 2008). We characterized the physiological properties of these synapses and describe two distinct types of excitatory postsynaptic potentials (EPSPs) that differed in amplitude, latency, and frequency-dependent plasticity. The first type of EPSP displayed shorter latencies and larger threshold amplitudes than the second type of EPSP. In response to repetitive stimulation (0.5–20 Hz), the first type of EPSP displayed frequency-dependent depression, whereas the amplitudes of the second type of EPSP were not changed by repetitive stimulation of up to 20Hz. Both types of EPSPs showed a graded increase in amplitude with increasing stimulation intensity, suggesting convergence. This convergence was further demonstrated by labeling tectopulvinar boutons by anterograde transport and staining the tissue with the type 2 vesicular glutamate transporter (vGLUT2, a marker for tectothalamic terminals). We also compared the synapsin content of terminals in the dorsal lateral geniculate (dLGN) and Pd and Pc by combining immunohistochemical staining for synapsin I or II with staining for vGLUT2 (a marker for tectothalamic and retinogeniculate terminals) or vGLUT1 (a marker for corticothalamic terminals). We

found that retinogeniculate terminals do not contain either synapsin I or synapsin II (Keilland et al., 2006), corticothalamic terminals in the dLGN, Pd and Pc contain synapsin I, but not synapsin II, whereas tectopulvinar terminals contain both synapsin I and synapsin II. These results suggests that different convergent synaptic arrangements allows tectopulvinar projection relay a dynamic range of visual signals from the SC to the cortex, striatum and amygdala in order to initiate and guide appropriate actions in response to visual signals.

### **Introduction**

Previous studies have identified three main types of glutamatergic terminals in the dorsal thalamus. All contain round synaptic vesicles, but can be distinguished based on their size as small (RS), medium (RM) and large (RL) profiles. Tract tracing and electron microscopic studies have revealed the distinct origins of each morphological terminal type: RS profiles originate from cortical layer VI (Guillery, 1969), RM profiles originate from the superior colliculus (Robson and Hall, 1977; Kelly et al., 2003; Chomsung et al., 2008; Masterson et al., 2009), while RL profiles are contributed by primary sensory inputs such as retinal ganglion cells (Szentagothai, 1963), neurons located in cortical layer V (Bourassa et al., 1995; Li et al., 2003b; Baldauf et al., 2005), and thalamocortical axon collaterals (Montero, 1989; Bickford et al., 2008).

The synaptic arrangements of RS, RM and RL profiles influence the properties of excitatory postsynaptic potentials (EPSPs) elicited by their activation. For example, both layer VI corticothalamic inputs (RS profiles) and SC inputs (RM profiles) innervate single cells with multiple convergent axons (Chomsung et al., 2008; Masterson et al., 2009). Therefore, *in vitro* studies have demonstrated that as more axons are activated by

increasing stimulation intensity, EPSPs elicited by activation of RS or RM profiles increase in a graded manner (Li et al., 2003a; Reichova and Sherman, 2004; Masterson et al., 2010). In contrast, activation of retinogeniculate terminals, or cortical layer V inputs (RL profiles), elicits EPSPs in an all-or-none manner (Turner and Salt, 1998; Li et al., 2003a; Reichova and Sherman, 2004), reflecting the fact that RL input to each cell originates from few axons (Cleland et al., 1971; Hamos et al., 1987).

RS, RM and RL profiles also display distinct short-term synaptic plasticity. The amplitudes of EPSPs elicited by stimulation of layer VI corticothalamic inputs (RS profiles) remain stable at low stimulation frequencies (<1 Hz), but facilitate with increasing stimulation frequency (Lindstrom and Wrobel, 1990; Turner and Salt, 1998; von Krosigk et al., 1999; Granseth et al., 2002). In contrast, the amplitudes of EPSPs generated by stimulation of ascending sensory inputs, or inputs that originate from cortical layer V (RL profiles), decrease in amplitude as the stimulation frequency is increased (Scharfman et al., 1990; Ramoa and McCormick, 1994; Kao and Coulter, 1997; Turner and Salt, 1998; Chen and Regehr, 2000; Chen et al., 2002; Li et al., 2003b; Arsenault and Zhang, 2006). Finally, the amplitudes of EPSPs elicited by stimulation of tectothalamic inputs (RM profiles) remain relatively stable at stimulation frequencies up to 10 Hz. (Smith et al., 2007; Masterson et al., 2010).

In addition to variations in the distribution of ionotropic and metabotropic glutamate receptors postsynaptic to RS, RM and RL profiles (Crunelli et al., 1987; Salt, 1987; Godwin et al., 1996), the synaptic properties of these terminal types are also dictated by differences in the expression of presynaptic proteins. For example, the frequency-dependent facilitation of EPSPs elicited by stimulation of RS profiles has been

found to be at least partly due to the presence of the synaptic vesicle-tethering proteins synapsin I and/or synapsin II. These proteins are absent in retinogeniculate terminals which show frequency-dependent depression, and corticogeniculate EPSPs in synapsin I/II knockout mice show alterations in their short-term plasticity (Kielland et al., 2006).

In the tree shrew (*Tupaia belangeri*), tectopulvinar terminals are classified as RM profiles, but they exhibit two different types of synaptic arrangements, referred to as “diffuse” and “specific” (Luppino et al., 1988; Chomsung et al., 2008). The specific projections are topographically arranged and distributed throughout both the dorsal (Updyke) and central (Pc) pulvinar nucleus. The diffuse projections are nontopographic projections that only innervate the Pd. Our recent tract tracing studies indicate both the Pd and Pc project to the temporal cortex and striatum, but only the Pd projects to the amygdala (Chomsung et al., 2010; Day-Brown et al., 2010). Thus, we have suggested that the specific projections relay topographic visual information from the SC to the cortex and striatum to aid in guiding precise movements, while the diffuse projection relays nontopographic visual information from the SC to the amygdala to alert the animal to potentially dangerous visual images.

In the current study, we characterized tectopulvinar EPSPs in the tree shrew to determine whether the unique organization of the diffuse and specific projections is reflected in differences in their synaptic properties. We also examined the distribution of presynaptic proteins expressed in glutamatergic RS, RM and RL terminals. We conclude that the short-term synaptic plasticity of RM profiles is distinct from that of RS or RL profiles because each terminal type contains a unique distribution of synapsins.

Furthermore, we conclude that the diffuse and specific tectopulvinar projections display subtle differences in short-term plasticity due to different patterns of convergence.

## **Methods**

A total of 16 tree shrews (*Tupaia belangeri*); 7 adults (more than 3 months old) and 9 juveniles (3 weeks old), were used for these experiments. Twelve tree shrews were used for in vitro physiology experiments, 1 tree shrew received injections of biotinylated dextran amine (BDA) in the SC, and tissue from 3 tree shrews was used immunocytochemistry. All procedures were approved by the Institutional Animal Care and Use Committee of the University of Louisville.

### ***Slice preparation***

Thalamic slices (400 $\mu$ m) were prepared from 9 juvenile and 3 adult male and female tree shrews (Li et al., 2003c). Briefly, the animals were deeply anesthetized with carbon dioxide and decapitated, the brain was excised and a block of tissue containing the thalamus was removed and placed in a ice-cold oxygenated solution of modified artificial cerebrospinal fluid (ACSF) containing (in mM) 206 sucrose, 2.5 KCl, 1 CaCl<sub>2</sub>, 1 MgSO<sub>4</sub>, 1 MgCl<sub>2</sub>, 1.25 NaH<sub>2</sub>PO<sub>4</sub>, 26 NaHCO<sub>3</sub>, 10 glucose at a pH of 7.4 and equilibrated with 95% O<sub>2</sub>/5% CO<sub>2</sub>. Parasagittal slices were cut on a vibratome (Leica, VT 1000E, Deerfield, IL) at a thickness of 400 $\mu$ m and transferred into a holding chamber with ACSF containing (in mM) 124 NaCl, 2.5 KCl, 2 CaCl<sub>2</sub>, 1 MgSO<sub>4</sub>, 1.25 NaH<sub>2</sub>PO<sub>4</sub>, 26 NaHCO<sub>3</sub>, 10 glucose at a pH of 7.4 and equilibrated with 95% O<sub>2</sub>/5% CO<sub>2</sub>, where they incubated for at least 2 hours before recording.

### ***Electrophysiology***

Whole cell recordings were obtained from the PUL. All recordings were carried out in the recording chamber maintained at 33°C with ACSF (with 10  $\mu$ M bicuculline and 2.5  $\mu$ M CGP55845 added; Tocris; Ellisville, MO) continually superfused at a rate of 2.0 ml/min. Pipettes were pulled from borosilicate glass (Sutter Instrument, Novato, CA) and had a tip resistance of 4-6 M $\Omega$  when filled with a solution containing (in mM) 115 K-gluconate, 2 MgCl<sub>2</sub>, 10 HEPES, 10 sodium phosphocreatine, 2 Na<sub>2</sub>-ATP, 20 KCl, 0.3 Na<sub>2</sub>-GTP with pH adjusted to 7.2 with KOH (osmolarity 290–295 mOsm). Biocytin (0.5%) was added to allow morphological reconstruction of the recorded neurons. Current-clamp recording were made with an Axoclamp 2B amplifier (Axon Instruments, Foster City, CA); the bridge was continually monitored and adjusted as needed. Data were digitized and stored on an IBM-compatible computer for off-line analyses. Only recordings showing a stable resting membrane potential more negative than -50 mV and overshooting action potentials were included in this study (n = 46). To stimulate the tectothalamic fibers, as illustrated in Figure 1A, a multipolar stimulation electrode (matrix microelectrode; FHC, Bowdoin, ME) was placed in the superficial layers of the superior colliculus (SC). Stimulating electrodes were at least 2 mm away from the recording electrode, once a stable whole-cell recording was obtained, paired-pulse or train stimulation was produced by using any two adjacent electrodes (115 $\mu$ m apart) in the arrays until the best response was achieved.

### ***Histochemistry***

A subset of neurons was filled with 0.5% biocytin by diffusion from the pipette during recording. At the end of each recording, slices were fixed at 4 °C overnight in 4% paraformaldehyde and rinsed several times in 0.1 M phosphate buffer saline (Campbell).

Slices were then incubated in 10% methanol in PB with 3% hydrogen peroxide to react with the endogenous peroxidase activity of red blood cells. After several rinses in PB, slices were incubated overnight at 4 °C under agitation in a 1% solution of a complex of avidin and biotinylated-horseradish peroxidase (ABC Kit Standard, Vector Laboratories) prepared in 0.3% Triton X-100. The slices were subsequently rinsed, reacted with nickel-intensified 3,3'-diaminobenzidine (DAB) for 5 min, and washed in PB. After rinses in phosphate buffer, slices were mounted onto slides and reconstructed with a Neurolucida system (Micro Bright Field Inc., USA). In some cases, biocytin-filled neurons were revealed by incubating slices in a 1:100 dilution of streptavidin conjugated to Alexa Fluor 546 (Molecular Probes, Eugene, OR) and confocal images of the cell was obtained using an Olympus Fluoview laser scanning microscope (BX61W1).

### ***Tracer injections***

Tree shrews that received BDA (3,000 MW; Molecular Probes, Eugene, OR) injections were initially anesthetized with intramuscular injections of ketamine (100 mg/kg) and xylazine (6.7 mg/kg). Additional supplements of ketamine and xylazine were administered approximately every 45 minutes to maintain deep anesthesia through completion of the tracer injections. Prior to injection, the tree shrews were placed in a stereotaxic apparatus and prepared for sterile surgery. A small area of the skull overlying the superior colliculus was removed and the dura reflected, a glass pipette containing either BDA (5% in saline, tip diameter 3  $\mu$ m) was lowered vertically and the tracer was ejected iontophoretically (2  $\mu$ A positive current for 15–30 minutes). After a 7-day survival period, the tree shrews were given an overdose of ketamine (600 mg/kg) and

xylazine (130 mg/kg) and were perfused through the heart with Tyrode solution, followed by a fixative solution of 4% paraformaldehyde.

The BDA was revealed by incubating sections in a 1:100 dilution of avidin and biotinylated horseradish peroxidase (ABC; Vector Laboratories, Burlingame, CA) in phosphate-buffered saline (0.01 M PB with 0.9% NaCl, pH 7.4; PBS) with 1% normal goat serum (NGS) overnight at 4°C. The sections were subsequently rinsed, reacted with nickel-intensified 3,3'-diaminobenzidine (DAB) for 5 minutes, and washed in PB. For confocal microscopy, the BDA was revealed by incubating sections in a 1:100 dilution of streptavidin conjugated to Alexa Fluor 546 (Molecular Probes, Eugene, OR)

### ***Immunohistochemistry***

Three adult tree shrews and three adult long-evans rats were given an overdose of sodium pentobarbital (tree shrew) or ketamine/xylazine (Murata et al.) and were perfused through the heart with Tyrode solution, followed by a fixative solution of 4% paraformaldehyde in 0.1 M PB. The brain was removed from the skull, sectioned into 50- $\mu$ m-thick slices using a vibratome (Leica VT100E, Leica Microsystems, Bannockburn, IL) and collected in a solution of 0.1 M PB. The sections were incubated at 4 °C overnight with guinea pig monoclonal anti-vGLUT1 or anti-vGLUT2 antibodies (1:5000, Chemicon Temecula, CA) or rabbit monoclonal anti-synapsin I (1:1000, Millipore, Billerica, MA) or anti-synapsin II (1:500, Abcam, Cambridge, MA), and the following day the sections were rinsed in PB and incubated for 1 hour in an anti-guinea pig antibody conjugated to Alexafluor-488 (1:100, Invitrogen/Molecular Probes, Carlsbad, CA) or anti-rabbit antibody conjugated to Alexafluor-546 (1:100, Invitrogen/Molecular



Probes, Carlsbad, CA). The sections were subsequently rinsed in PB and mounted on slides for confocal microscopic examination.

### ***Statistical Analysis***

Student t-tests were used to test for statistical significance. Quantitative data are expressed as means  $\pm$  SD. The significance level was set at  $p < 0.05$  for all statistical comparisons.

## **Results**

### ***Location of recordings***

In 400  $\mu$ m thick parasagittal sections, whole cell recordings were obtained in the pulvinar nucleus and the rostral SC was stimulated to evoke EPSPs. The pulvinar EPSPs evoked by SC stimulation can be identified as tectopulvinar EPSPs because the cortical input to the Pd and Pc originates exclusively from layer VI (Chomsung/Wei et al., 2010) while cortical input to the SC originates exclusively from layer V (Casseday et al., 1979). Therefore SC stimulation can not activate corticopulvinar inputs. In addition, the pretectum does not project to the Pd or Pc (Chomsung et al., 2008), so current spread to this region does not activate any pulvinar inputs.

Figure 1A illustrates the approximate location of the recording pipette in the PUL and the location of the 8 electrode stimulation array in the SC. The array spanned a distance of 1 mm and stimulation could be produced between any two electrodes in the array; the anode and cathode positions were varied to obtain the best response. With this configuration, tectopulvinar EPSPs could be elicited with a high rate of success (28 of 46 cells) in the caudal PUL which, as illustrated in Figure 1 (and described by Lyon et al.) (Lyon et al., 2003), corresponds to the Pd. We were unable to elicit tectopulvinar

responses from more rostral regions of the PUL; in the parasagittal slice preparation these axons were most likely severed before they reached the Pc.

As illustrated in Figure 1B, in response to the injection of depolarizing or hyperpolarizing current steps, all recorded neurons fired with either tonic action potentials or low threshold calcium spikes respectively, firing properties exhibited by thalamic relay cells (McCormick and Huguenard, 1992). Biocytin was included in the recording pipette and all recovered cells displayed morphologies consistent with their identification as relay cells.

#### ***Tectopulvinar EPSPs can be divided into two groups based on latency and amplitude***

As illustrated in Figure 2, tectopulvinar EPSPs fell into two groups based on differences in their average latencies, as well as their threshold and peak amplitudes, suggesting that two different types of axon arbors were activated. EPSPs with the shortest latencies ( $2.11 \pm 0.10$  ms,  $n=17$ ) exhibited the largest threshold EPSP amplitudes ( $4.82 \pm 0.57$  mV,  $n=17$ ; Figure 2B) and EPSPs with longer latencies ( $3.20 \pm 0.15$  ms,  $n=8$ ) exhibited smaller threshold amplitudes ( $1.58 \pm 0.27$  mV,  $n=8$ ; Figure 2C). These parameters were found to be significantly different (latencies  $p < 0.05$ ; threshold amplitudes  $p < 0.05$ ), supporting the division of the tectopulvinar EPSPs into two groups.

#### ***The two types of tectopulvinar EPSPs display distinct short term plasticity***

The short-term plasticity of these two types of EPSPs was tested with trains of stimuli varying in frequency from 1Hz to 10 Hz, as well as paired-pulse stimuli with interstimulus intervals of 0.1s to 2s. For each type of EPSP we used stimulation currents sufficient to evoke EPSPs at 50% of maximum. The short latency/large amplitude EPSPs were depressed by high frequency stimulation (frequencies  $>1$ Hz, Fig. 3, A and B;  $n =$

10). With train stimuli, relative to the first EPSP of the train, the second EPSP decreased by  $16.67 \pm 2.35\%$  at 2.5 Hz,  $23.29 \pm 3.88\%$  at 5 Hz, and  $29.42 \pm 3.42\%$  at 10Hz. Similar values were observed using paired-pulse stimuli (a  $9.19 \pm 4.99\%$  reduction in the amplitude of the second pulse relative to the first pulse at interstimulus intervals of 0.6s;  $17.17 \pm 7.51\%$  at 0.2s and  $37.18 \pm 8.27\%$  at 0.1s; Fig. 4, A and B, n = 5). In contrast, for the slower latency/smaller amplitude EPSPs, there was no correlation between mean amplitudes and stimulation frequencies or paired-pulse interstimulus intervals (Fig. 3, C and D n = 6; Fig. 4, A and C, n = 4).

#### ***The two types of tectopulvinar EPSP display different degrees of convergence***

All recorded tectopulvinar EPSP amplitudes (n = 28) increased as the stimulation intensity was increased, suggesting that each postsynaptic cell receives input from multiple convergent tectal axons. However, the degree of convergence was found to be greatest for the slower/smaller/nondepressing EPSPs. The peak amplitudes of these EPSPs increased up to 3.34 fold above threshold amplitude values, while peak amplitudes of the faster/larger/depressing EPSPs increased to 2.11 fold above threshold values. As illustrated in Figure 2, the rate of amplitude increase as a function of stimulation current was greater for nondepressing EPSPs compared to the depressing EPSPs.

#### ***“Mixed” EPSPs***

For the majority of tectopulvinar EPSPs (25 of 28) the latencies did not change as the stimulation intensity was increased (Figure 2B, C). However, in some cases (n=3) EPSPs appeared to contain a mixture of the two EPSP types described above. The amplitude of these “mixed” EPSPs initially increased gradually as the stimulation current was increased, but then exhibited a sudden large increase in amplitude, suggesting that

the threshold was reached to recruit a different type of axon. Supporting this conclusion, there was a corresponding decrease in EPSP latency with the jump in EPSP amplitude (Fig. 5, A and B). Furthermore, for “mixed” EPSPs the amplitudes were unaffected by stimulus frequency when stimuli were delivered with threshold current levels, but frequency-dependent depression was observed when the stimuli were delivered with current levels that elicited the larger amplitude EPSPs.

### ***Tectopulvinar clusters and convergence***

In the tectorecipient thalamus, immunohistochemical staining for the type 2 vesicular glutamate transporter (vGLUT2) can be used as a marker for tectopulvinar terminals (Chomsung et al., 2008; Masterson et al., 2009). As illustrated in Figure 1, this marker reveals the distinct arrangements of tectal terminals in the Pd and Pc. The Pd contains dense clusters of tectal terminals, and tubular clusters line long lengths of dendrites (Figure 1C). In contrast, the Pc contains smaller more sparsely distributed clusters of tectal terminals (Figure 1D). Using electron microscopy, we have previously shown that the clusters of tectopulvinar terminals surround and synapse on central dendrites (Chomsung et al., 2008).

As previously reported (Chomsung et al., 2008), injections of biotinylated dextran amine (BDA) in the SC label tectopulvinar axons that form topographically organized clusters of boutons (“specific” projections; Figure 6A) as well as nontopographically organized axons that contribute more widespread boutons (“diffuse” projections; Figure 6B). By comparing BDA-labeled tectopulvinar synapses to synapses labeled by the vGLUT2 antibody, we previously concluded that both the diffuse and specific projections are convergent (Chomsung et al., 2008). We confirmed this by staining tissue that

contained BDA-labeled tectopulvinar axons with the vGLUT2 antibody. As illustrated in Figure 6C-G), for both types of tectopulvinar axons, the BDA-labeled terminals made up a small proportion of the total terminals within a vGLUT2-stained cluster. However, vGLUT2-stained clusters contained at most 1 bouton contributed by “diffuse” axons (Figure 6C), whereas “specific” axons contributed several boutons to each cluster (Figure 6D-G). This suggests the “diffuse” pathway exhibits a greater degree of convergence onto individual dendrites than does the “specific” pathway.

### ***Tectopulvinar terminals contain both synapsin I and synapsin II***

Because the expression of synapsins has been related to short-term plasticity (Keilland et al., 2006), we examined the synapsin content of RS, RM and RL profiles in the tree shrew by combining immunohistochemical labeling for synapsin I or synapsin II with immunohistochemical labeling for vGLUT2 (a marker for tectothalamic or retinogeniculate terminals)(Chomsung et al., 2008; Masterson et al., 2009) or vGLUT1 (a marker for corticothalamic terminals)(Fremeau et al., 2001; Herzog et al., 2001; Kaneko et al., 2002) in the dorsal lateral geniculate nucleus (dLGN, Figure 7), Pd (Figure 8) and Pc (Figure 9) of the tree shrew. As illustrated in Figure 7, we found that retinogeniculate terminals (RL profiles labeled with the vGLUT2 antibody) do not contain either synapsin I or synapsin II (as previously reported in the mouse, Keilland et al., 2006). We also found that corticothalamic terminals in the dLGN, Pd and Pc (RS profiles labeled with the vGLUT1 antibody) contain synapsin I but not synapsin II (Figures 7-9). Finally tectopulvinar terminals (RM profiles labeled with the vGLUT2 antibody) contain both synapsin I and synapsin II (Figure 8 and 9). We found a similar distribution of synapsins

in vGLUT1- and vGLUT2-labeled terminals in the rat dLGN and lateral posterior nucleus (data not shown). These results are summarized in Table 1.

## **Discussion**

### ***Diffuse and specific EPSPs***

Based on differences in their convergence patterns, we conclude that the slower latency, smaller amplitude EPSPs represent activation of diffuse tectopulvinar projections, while the faster, larger amplitude EPSPs represent activation of specific tectopulvinar projections. This conclusion is also based on comparisons to our previous study of EPSPs elicited by stimulation of tectothalamic axons in the rat. Tectothalamic projections in the rodents are nontopographic (Mooney et al., 1984) and EPSP amplitudes remain stable at stimulation frequencies of up to 20Hz (Masterson et al., 2010). The lack of short-term frequency-dependent plasticity in the rat tectothalamic pathway is similar to that exhibited by the slower latency, smaller amplitude tectopulvinar EPSPs of the tree shrew. In contrast, the faster, larger amplitude tectopulvinar EPSPs of the tree shrew exhibited a small frequency-dependent depression (29.42% at 10Hz), a feature which was not observed in our studies of the rat tectothalamic EPSPs.

At threshold, specific EPSPs may be larger than diffuse EPSPs because stimulation of a single specific axon activates clusters of terminals that innervate the same dendrite, while stimulation of a single diffuse axon activates unitary inputs. Alternatively, the glutamate release probability may be higher for specific terminals than diffuse terminals. This would help to explain why the specific EPSPs are depressed at high rates of stimulation; the pool of synaptic vesicles ready for release in specific tectopulvinar terminals may not be fully replenished during short interstimulus intervals.

Diffuse tectopulvinar EPSPs may exhibit relative stability because their vesicles are not depleted as rapidly.

***Synapsin distribution varies in glutamatergic terminals of the thalamus***

Synapsins have been associated with the tethering of synaptic vesicles to cytoskeletal elements (Schiebler et al., 1986; De Camilli et al., 1990; Benfenati et al., 1991; Greengard et al., 1993; Pieribone et al., 1995; Rosahl et al., 1995; Gitler et al., 2004; Samigullin et al., 2004) and are thought to regulate the equilibrium of a reserve pool of synaptic vesicles and a population of vesicles that are docked for ready release (Llinas et al., 1985; Hilfiker et al., 1999). It has been hypothesized that synapsins are necessary to sustain the release of neurotransmitter at high rates of synaptic transmission (Greengard et al., 1993; Pieribone et al., 1995; Rosahl et al., 1995). In the dLGN of synapsin I/II knockout mice, the short-term frequency-dependent facilitation of corticogeniculate EPSPs was increased, while long-term post-tetanic potentiation was decreased (Kielland et al., 2006). This change presumably occurred because fewer vesicles were tethered to retain a reserve pool.

We found that, within the visual thalamus of the tree shrew and rat, tectothalamic terminals are the only glutamatergic terminals that contain both synapsin I and synapsin II. Retinogeniculate terminals contained neither synapsin, and corticothalamic terminals contained synapsin I, but not synapsin II. These distributions correlate with the distinct synaptic properties of these terminal types. Retinogeniculate EPSPs exhibit strong frequency-dependent depression (Turner and Salt, 1998; Chen et al., 2002; Kielland and Heggelund, 2002), corticothalamic EPSPs exhibit strong frequency-dependent facilitation (Lindstrom and Wrobel, 1990; Turner and Salt, 1998; von Krosigk et al., 1999), while

tectothalamic EPSP amplitudes remain relatively stable during high frequency stimulation (Masterson et al., 2010). Even the (specific) tectopulvinar EPSPs that showed a small decrease in amplitude high stimulation frequencies (29.42% decrease at 10Hz) stimulation, are more stable than retinogeniculate EPSPs which can depress by as much as 60% at 10Hz (Turner and Salt, 1998).

Recent studies have suggested that synapsin IIa is a key regulator of the reserve pool of synaptic vesicles. Gitler et al. (Gitler et al., 2008) found that synapsin IIa was the only synapsin isoform that could increase the reserve pool of synaptic vesicles and slow synaptic depression in neurons obtained from synapsin I/II/III triple knock-out mice. The synapsin II content of tectopulvinar terminals may make them particularly resistant to fatigue and able to follow high rates of firing.

### ***Functional implications***

Tectopulvinar neurons are located in the lower stratum griseum superficiale (SGS) of the SC and extend widespread, obliquely-oriented dendrites throughout the retinorecipient SGS (wide-field vertical cells; (Graham and Casagrande, 1980; Chomsung et al., 2008). Neurons in the lower SGS have large receptive fields, exhibit brisk responses to movement and are direction selective (Albano et al., 1978). Firing rates of up to 250Hz have been recorded in the tree shrew SGS. Moreover, many cells exhibit sustained activity as the leading or trailing edge of a stimulus moves across their receptive field (Albano et al., 1978). Therefore, tectopulvinar terminals must be uniquely equipped to sustain transmission from the SC to pulvinar neurons. We suggest that the convergent synaptic arrangements, as well as the synapsin content of tectopulvinar terminals, allows them to relay a dynamic range of visual signals from the SC to the



cortex, striatum and amygdala in order to initiate and guide the appropriate actions in response to the movements of predator or prey.

**Figure 1.**

*In vitro* recording methods. A) A parasagittal section of the tree shrew brain stained for the type 2 vesicular glutamate transporter (vGLUT2) illustrates the location of the whole cell recordings in the caudal pulvinar nucleus (Smith and Populin) and the location of the 8 electrode stimulus array in the superior colliculus (SC). B) Voltage fluctuations recorded in response to the injection of depolarizing or hyperpolarizing current steps of varying size revealed that all recorded cells fired with both tonic action potentials, and low threshold calcium bursts. C, D) High magnification views of the Pd and Pc illustrated in panel A. In the PUL, immunohistochemical staining for vGLUT2 is a marker for tectopulvinar terminals (Chomsung et al., 2008) and reveals the distinct arrangements of tectal terminals in the dorsal (Pd) central (Pc) pulvinar nucleus. The Pd contains dense clusters of tectal terminals and tubular clusters line long lengths of dendrites (C). In contrast, the Pc contains smaller more sparsely distributed clusters of tectal terminals (D). Scale in A = 1 mm. Scale in C = 30  $\mu$ m and also applies to D. dLGN, dorsal lateral geniculate nucleus.

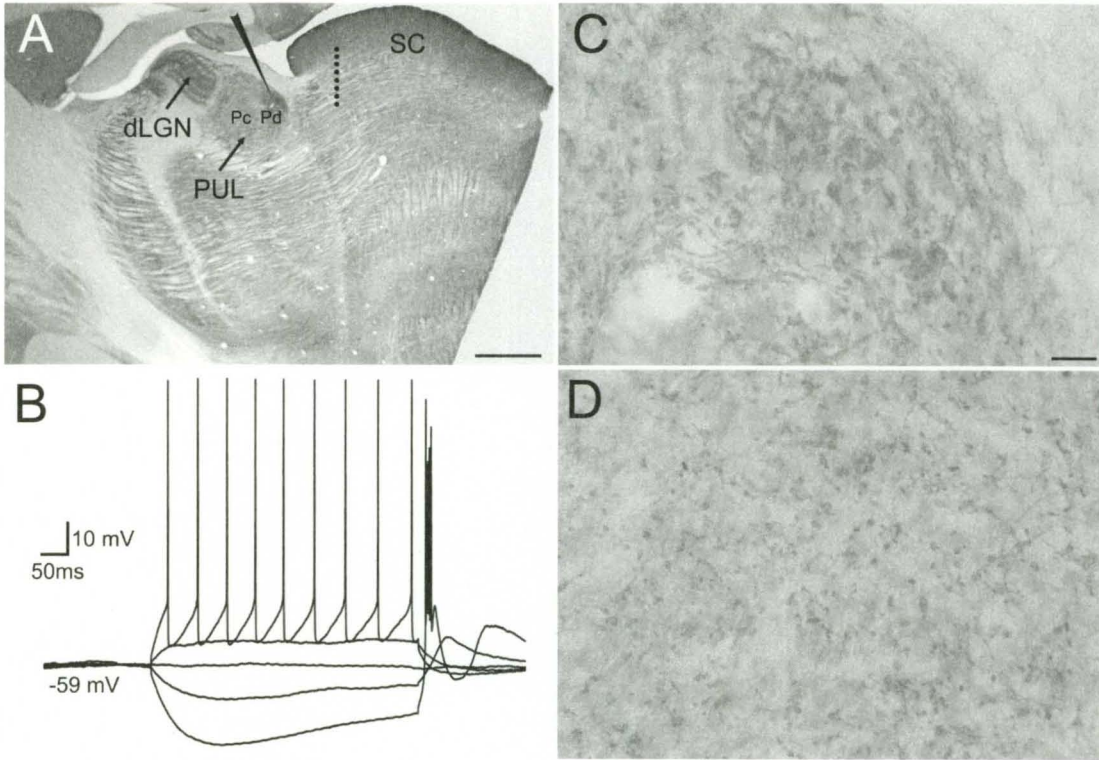


**Figure 2.**

Two types of EPSPs. *A*: with increasing stimulation intensity, tecto-pulvinar EPSPs show a graded increase in amplitude. *B*: average first type EPSP amplitudes and latencies as a function of stimulation intensity (n=17), graph show a graded increase in peak amplitude correlate to the increase in stimulation current but the latency of the EPSP is not relative to stimulation current. *C*: average second type EPSP amplitudes and latencies as a function of stimulation intensity (n=8), second type EPSP show a graded increase in peak amplitude and no change in latency with increasing stimulation intensity, but the threshold amplitude was smaller and latency was longer (p<0.05).

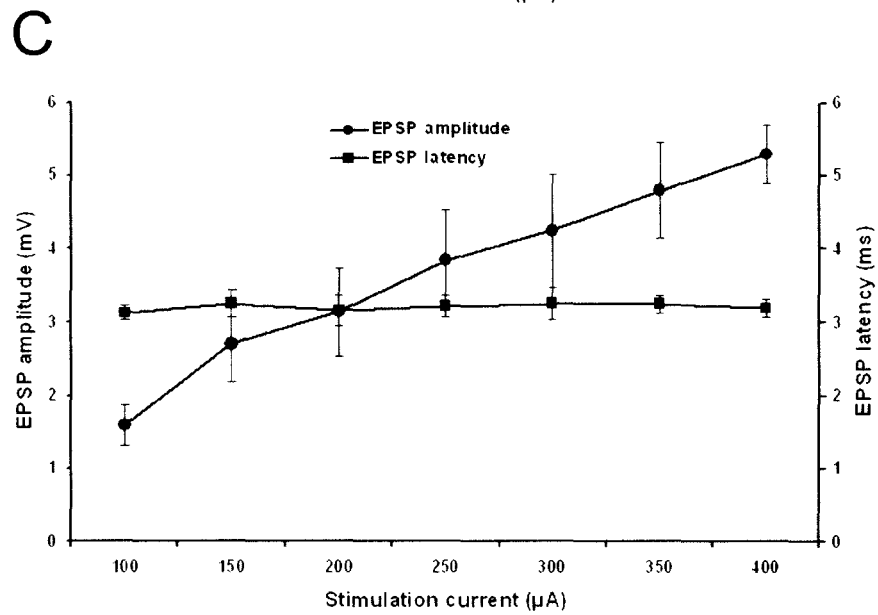
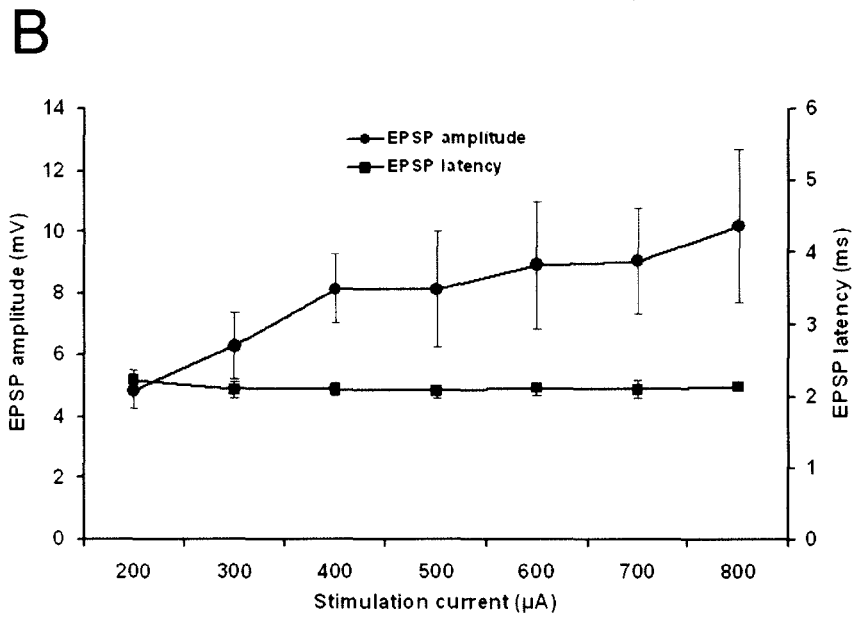
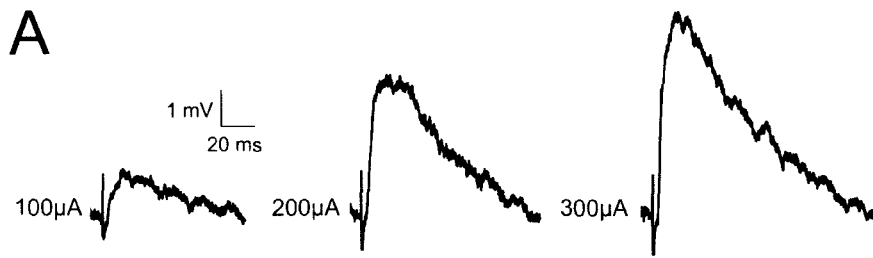


**Figure 3.**

Two types of EPSPs display distinct frequency-dependent short-term plasticity. *A*: train stimulation consisted of 8 pulses at 1Hz, 1.25Hz, 2.5Hz, 5Hz and 10 Hz, 1<sup>st</sup>, 3<sup>rd</sup> and 5<sup>th</sup> EPSPs from the train stimulation of first type tecto-pulvinar fiber showed frequency-dependent depression, recorded at resting membrane potential of -58mV. *B*: 1<sup>st</sup>, 3<sup>rd</sup> and 5<sup>th</sup> EPSPs from the train stimulation of second type tecto-pulvinar fiber produced EPSPs with stable amplitudes, recorded at resting membrane potential of -59mV. *C* and *D*: normalized average EPSPs evoked in 14 cells by 8 pulses at 1Hz, 1.25Hz, 2.5Hz, 5Hz and 10 Hz, each point was normalized by dividing the EPSP amplitude of that pulse in the train (EPSP<sub>n</sub>) to the amplitude of the first EPSP of the train (EPSP<sub>1</sub>), *C*: stimulation of the first type tecto-pulvinar fiber showed change in EPSP peak amplitudes of the 8 EPSPs evoked by the stimulus train at various frequencies. *D*: stimulation of the second type tecto-pulvinar fiber showed stable EPSP peak amplitudes of the 8 EPSPs evoked by the stimulus train at various frequencies.

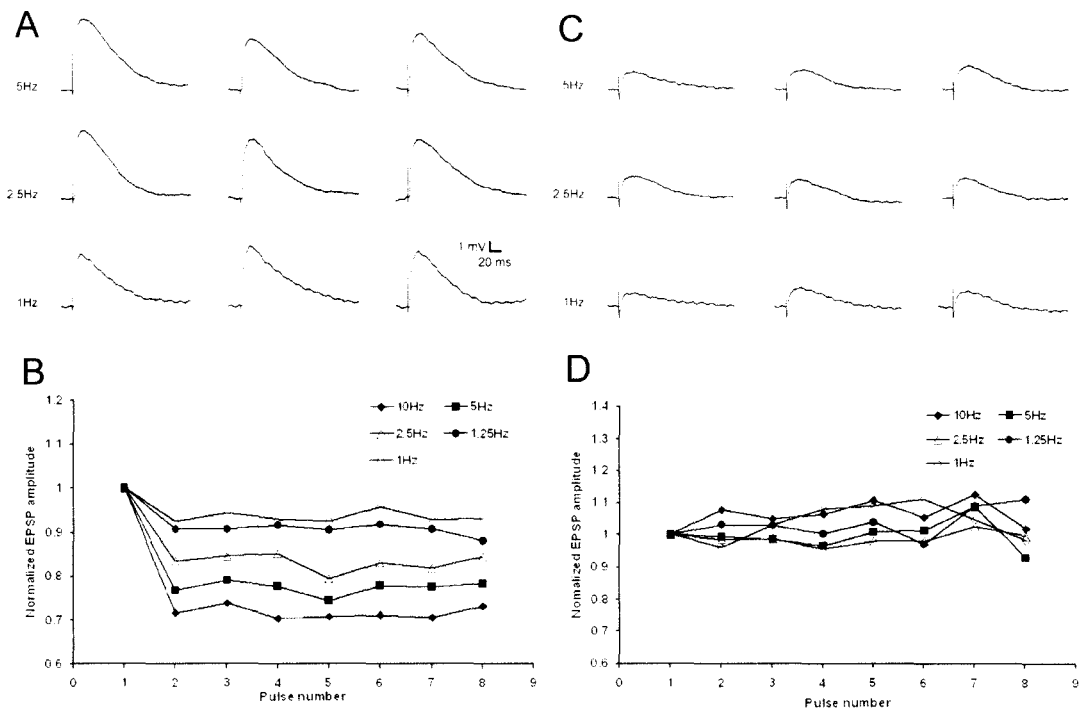


**Figure 4.**

Two types of EPSPs display distinct short-term plasticity by paired-pulse stimulation. *A*: left panel showed 1<sup>st</sup> and 2<sup>nd</sup> EPSP evoked by paired pulse stimulation of first type tecto-pulvinar fiber at 200ms time interval, traces were recorded at resting membrane potential at -58mV (upper panel) or -70mV under voltage-clamp mode (lower panel), both traces showed paired-pulse depression. Right panel showed 1<sup>st</sup> and 2<sup>nd</sup> EPSP evoked by paired pulse stimulation of second type tecto-pulvinar fiber at 200ms time interval, traces were recorded at resting membrane potential at -59mV (upper panel) or -70mV under voltage-clamp mode (lower panel), both traces showed stable EPSP amplitudes. *B*: plots of paired-pulse ratio (EPSP2 amplitude/EPSP1 amplitude) as a function of inter-stimulus intervals (0.1s, 0.2s, 0.3s, 0.4s, 0.6s, 0.8s, 1s, 2s) by stimulation of first type tecto-pulvinar fiber, showed gradual increase of paired-pulse ratio. *C*: plots of paired-pulse ratio (EPSP2 amplitude/EPSP1 amplitude) as a function of inter-stimulus intervals (0.1s, 0.2s, 0.3s, 0.4s, 0.6s, 0.8s, 1s, 2s) by stimulation of second type tecto-pulvinar fiber, showed stable paired-pulse ratio.



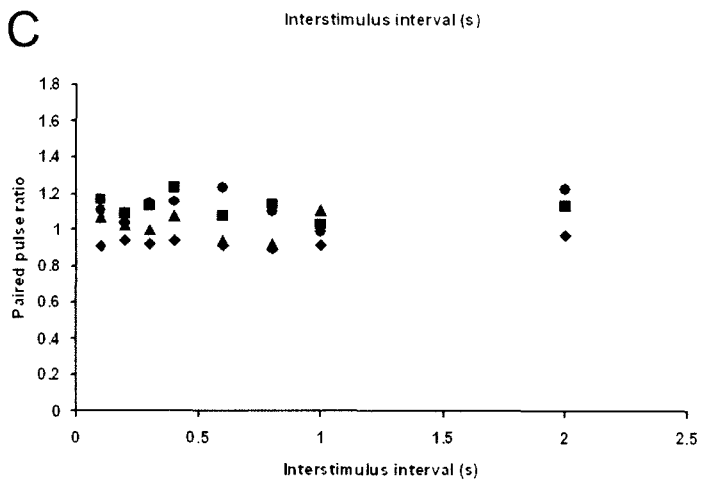
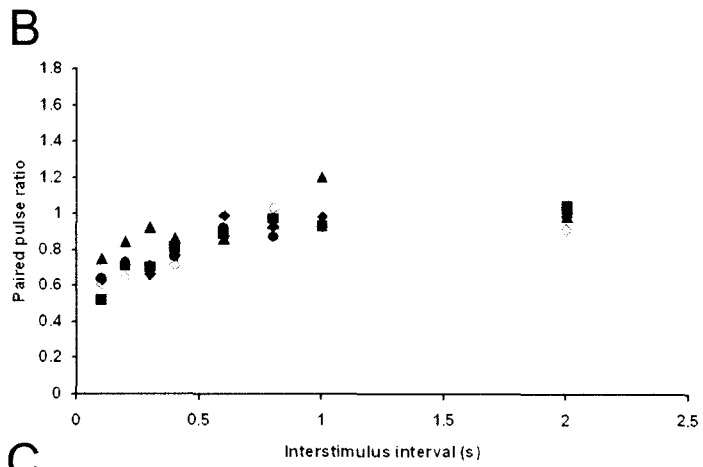
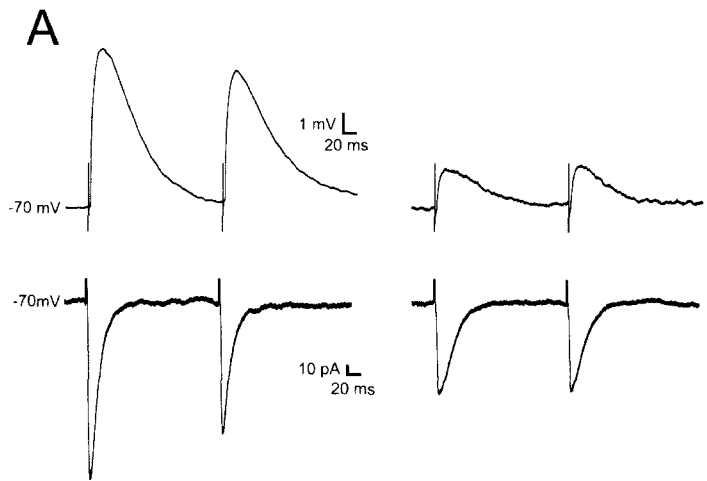


**Figure 5.**

“Mixed” EPSP show characteristics of two types of EPSPs. *A*: “mixed” EPSPs show small amplitude with small stimulation currents, followed by a large increase in amplitude and corresponding decrease in latency at larger stimulation currents. *B*: plots of “mixed” EPSP amplitudes and latencies as a function of stimulation intensity, showed graded increase in amplitude with small stimulation currents followed by a large increase in amplitude and corresponding decrease in latency at larger stimulation currents.

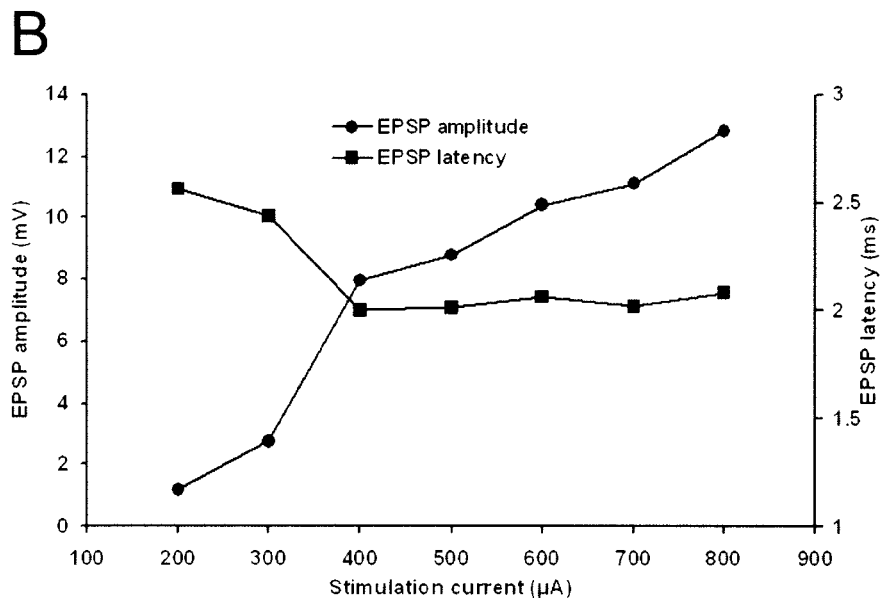
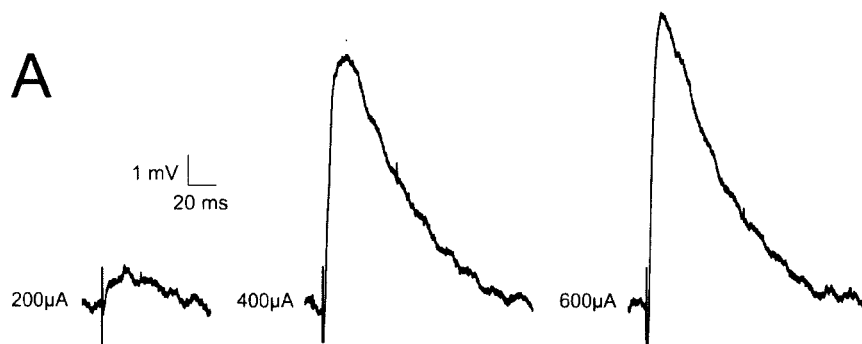


**Figure 6.**

Convergence of tectopulvinar terminals. Injections of biotinylated dextran amine (BDA) in the SC labels tectopulvinar axons that form widespread (“diffuse”) axons and boutons (A) as well as more discrete clustered (“specific”) boutons (B). C-G) Confocal images illustrate tectopulvinar terminals labeled with BDA (purple) and tectopulvinar terminals labeled with antibodies against the type 2 vesicular glutamate transporter (vGLUT2, green). Terminals labeled with both BDA and vGLUT2 appear white. Clusters of vGLUT2-stained terminals contain at most 1 bouton contributed by “diffuse” axons (C) while “specific” axons contributed several boutons to each cluster (D-G) Scale in B = 10  $\mu\text{m}$  and applies to A-F. Scale in G = 2  $\mu\text{m}$ .

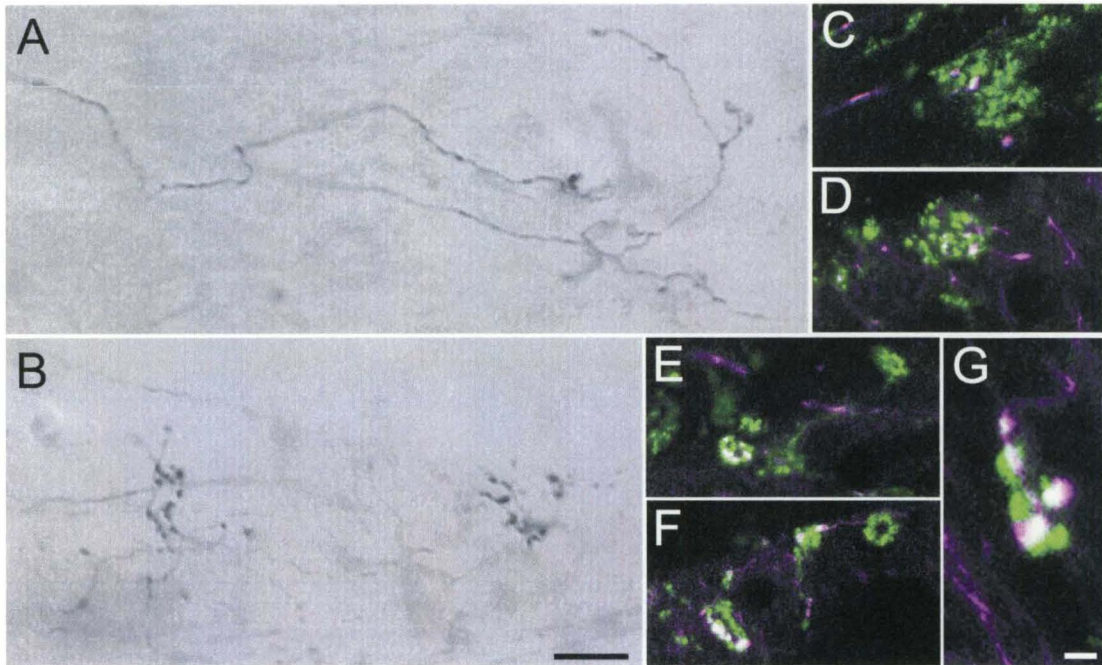


**Figure 7.**

Confocal images of dLGN tissue labeled with antibodies against synapsin I or II (purple), and vGLUT1 or 2 (green). Profiles that are labeled with two antibodies appear white. Retinogeniculate terminals (RL profiles labeled with the vGLUT2 antibody, right panels) do not contain either synapsin I or synapsin II. Corticothalamic terminals in the dLGN (RS profiles labeled with the vGLUT1 antibody, left panels) contain synapsin I, but not synapsin II. Scale = 10  $\mu$ m.

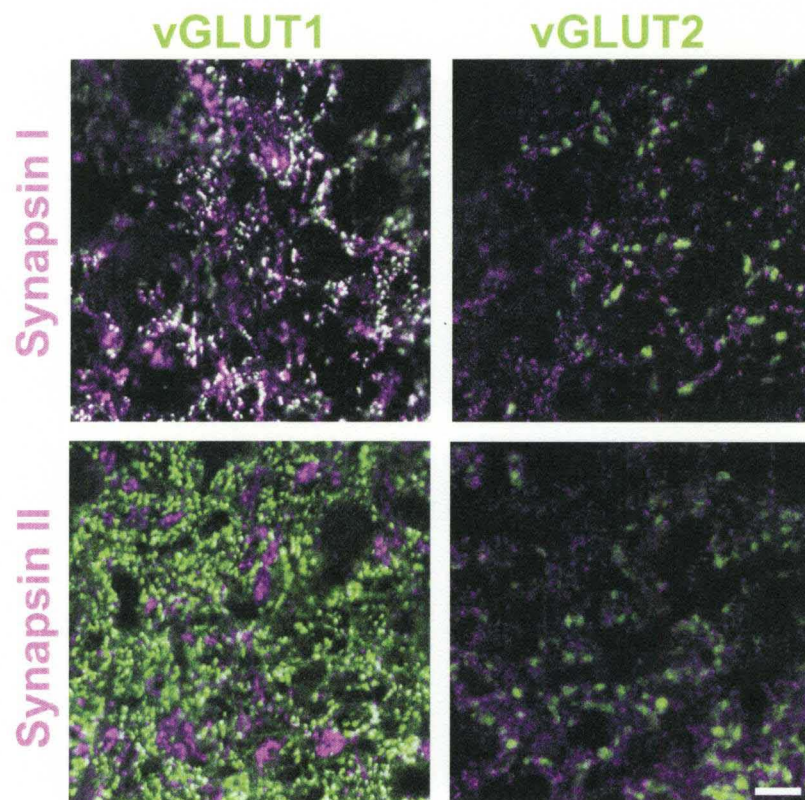


**Figure 8.**

Confocal images of Pd tissue labeled with antibodies against synapsin I or II (purple), and vGLUT1 or 2 (green). Profiles that are labeled with two antibodies appear white. Tectopulvinar terminals (RM profiles labeled with the vGLUT2 antibody, right panels) contain both synapsin I and synapsin II. Corticothalamic terminals in the Pd (RS profiles labeled with the vGLUT1 antibody, left panels) contain synapsin I, but not synapsin II. Scale = 10  $\mu$ m.



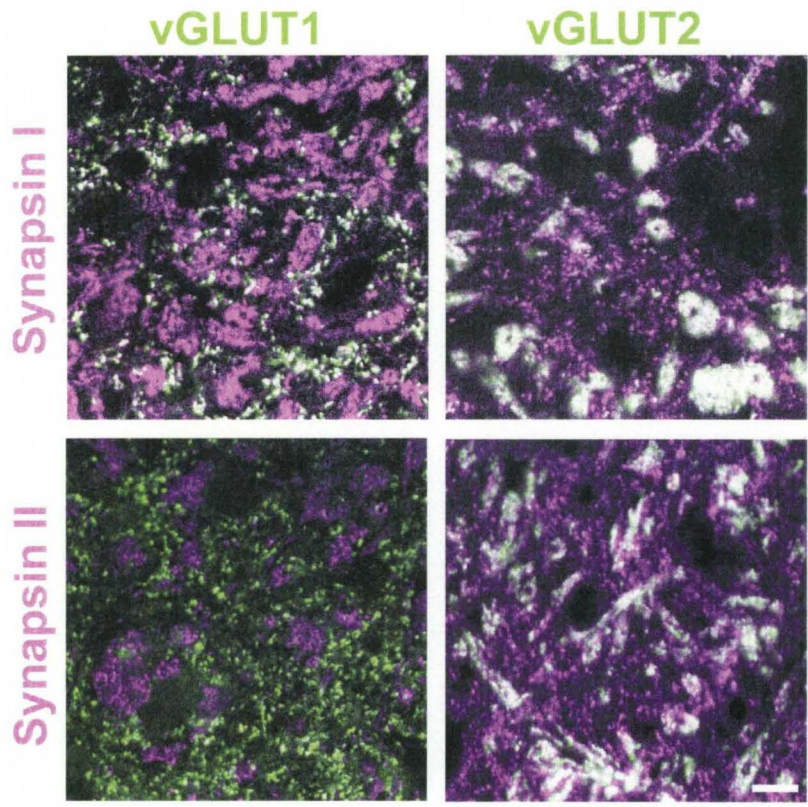


**Figure 9.**

Confocal images of Pc tissue labeled with antibodies against synapsin I or II (purple), and vGLUT1 or 2 (green). Profiles that are labeled with two antibodies appear white. Tectopulvinar terminals (RM profiles labeled with the vGLUT2 antibody, right panels) contain both synapsin I and synapsin II. Corticothalamic terminals in the Pc (RS profiles labeled with the vGLUT1 antibody, left panels) contain synapsin I, but not synapsin II. Scale = 10  $\mu$ m.

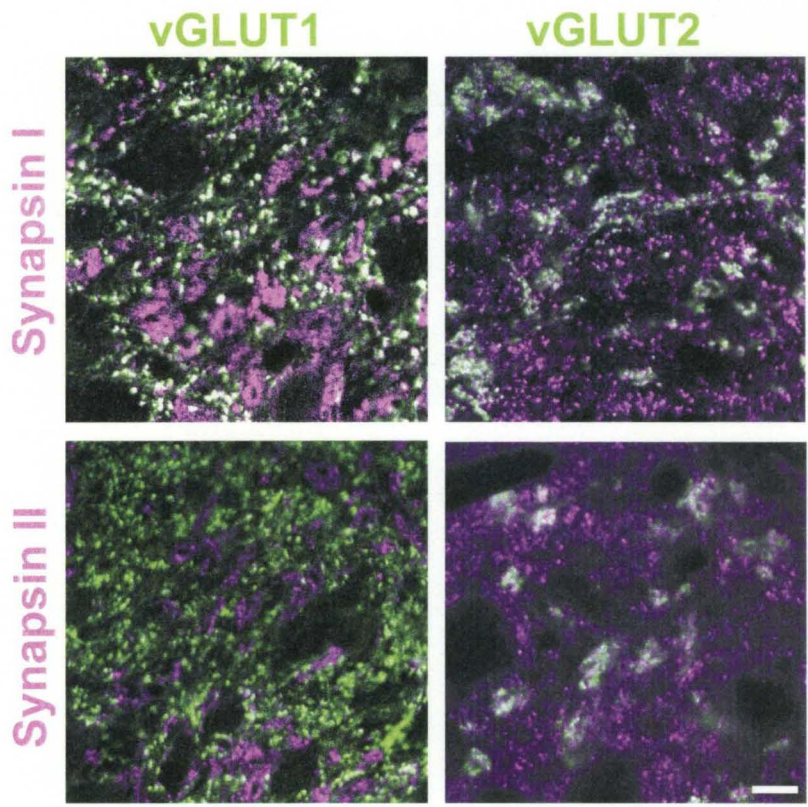


**Table 1.**

Characteristics of glutamatergic terminals in the visual thalamus.

Table 1: Characteristics of glutamatergic terminals in the visual thalamus								
Type	Species origin-target	Terminal size	EPSP <i>in vitro</i> latency	EPSP threshold amplitude	current vs EPSP amplitude	10Hz stim effect	synapsin content	vGLUT content
<b>RS</b>	rat cortex-dLGN	0.28 ± 0.13 μm <sup>2</sup>			graded	facilitation	type I	type I
	rat cortex-caudal LP	0.27 ± 0.12 μm <sup>2</sup>	4.2 ± 0.7 ms		graded	facilitation	type I	type I
	rat cortex-rostral LP	0.34 ± 0.11 μm <sup>2</sup>	4.3 ± 0.8 ms	≤ 1 mV	graded	facilitation	type I	type I
	mouse cortex-dLGN	0.22 ± 0.01 μm <sup>2</sup>				facilitation	type I &/or II	
<b>RM</b>	rat SC-caudal LP	0.71 ± 0.32 μm <sup>2</sup>	3.7 ± 0.63 ms		graded	none	type I & II	type 2
	Tree shrew SC diffuse-pulvinar	0.62 ± 0.22 μm <sup>2</sup>	3.20 ± 0.15 ms	1.58 ± 0.27 mV	graded	none	type I & II	type 2
	TS SC specific pulvinar	0.62 ± 0.21 μm <sup>2</sup>	2.11 ± 0.10 ms	4.82 ± 0.57 mV	graded	mild depression	type I & II	type 2
<b>RL</b>	rat cortex rostral LP	2.72 ± 1.27 μm <sup>2</sup>	1.6 ± 0.5 ms	~ 8 mV	all-or-none	depression	none	type 2
	rat retina-dLGN	3.73 ± 1.92 μm <sup>2</sup>			all-or-none	depression	none	type 2
	mouse retina-dLGN	1.74 μm <sup>2</sup>				depression	none	
References: Granseth et al., 2002; Kielland and Heggelund, 2002; Fujiyama et al., 2003; Li et al., 2003a; Li et al., 2003b; Kielland et al., 2006; Masterson et al., 2009; Bickford et al., 2010; Masterson et al., 2010; current study.								

## **CHAPTER V**

### **SUMMARY AND FUTURE DIRECTIONS**

The previous chapters describe investigations of several anatomical and physiological properties of tecto-pulvino-cortical pathways. By using a combination of neuroanatomical techniques, we characterized the synaptic organization of pulvinocortical projections. This is the first morphological description of the synaptic connections of pulvinocortical terminals. We found that the Pd and Pc subdivisions of the pulvinar nucleus, which receive visual input from the SC, innervate large regions of both the posterior and dorsal temporal cortex, forming 2 topographic maps. Within these regions, pulvinocortical terminals innervate layers I-IV. Our ultrastructural analysis of these terminals revealed that they all contact nonGABAergic spines of pyramidal cells. In addition, we found that the Pd and Pc receive input from layer VI cells in the temporal cortex and that the axons of these cells form small terminals (type I terminals) that innervate small caliber dendrites in the Pd and Pc. We found that the Pd and Pc do not receive input from cortical layer V (type II terminals). We also found that all pulvinar connections with the temporal cortex appear to be reciprocal. Therefore, it does not appear that the Pd and Pc can be considered “higher order” nuclei, which are defined by their input from cortical layer V, and their potential to receive input from one cortical area and transfer this information to other cortical areas (Guillery 1995; Guillery and Sherman 2002). We hypothesize that the receptive field properties of Pd and Pc cells are

created by the integration of convergent input from the SC and temporal cortex and that the pulvinocortical projections may influence the perception of visual stimuli and/or the activation subcortical visuomotor circuits.

A number of different pyramidal cell types can be found in the pulvinocortical projection zones and could be potentially targeted by pulvinar terminals. These include cells that project to the striatum, claustrum, SC, pretectum and/or thalamus, as well as corticocortical cells that form local intrinsic connections or project to other cortical areas (Katz 1987; Schofield et al., 1987; Bourassa and Deschênes, 1995). The identity of the cells targeted by pulvinocortical terminals is a critical piece of information for understanding the function of the pulvinar nucleus. One possibility is that the pulvinar nucleus modulates the perception of visual stimuli via contacts on corticocortical cells. In particular, corticocortical cells that project from the temporal cortex to V1 are primarily distributed in layer V and extend their apical dendrites to layer I (unpublished data). Therefore these cells could potentially be targeted by pulvinocortical terminals. It is also possible that corticotectal or corticostriatal cells are the primary pulvinar targets, which might suggest that the pulvinar plays a more direct role in coordinating movements in response to visual stimuli. Future anatomical and/or physiological studies are necessary to identify the cell types that are postsynaptic to pulvinocortical terminals.

In the dLGN, Guido et al (1995) demonstrated that the tonic firing mode faithfully reflects changes in retinal ganglion cell firing, while the burst firing mode provides a nonlinear amplification of retinal signals. Recent *in vitro* experiments have shown that layer IV thalamocortical synapses on both regular spiking cells and fast spiking interneurons exhibit paired pulse depression (Hull et al., 2009). These studies suggest that

the effects of pulvinar input on cortical activity will not only depend on the cell types targeted, but also on the properties of the firing patterns and the postsynaptic potentials elicited. If pulvinocortical potentials are depressed during high frequency stimulation, cortical circuits may be more effectively activated when pulvinar neurons fire in burst mode. On the other hand, if pulvinocortical potentials are enhanced by high frequency stimulation, cortical circuits may be more effectively activated when pulvinar neurons fire in tonic mode. This information is needed to understand how pulvinar firing modes affect cortical processing.

Our physiology studies suggest that burst firing is an important component of pulvinar function. Using *in vitro* whole cell recording techniques, immunohistochemistry, western blot techniques, unbiased stereology, confocal and electron microscopy, and computational modeling we explored nucleus-specific features of burst firing in the dLGN and pulvinar nucleus neurons. We found that intrinsic membrane properties of the pulvinar neurons promote burst firing, pulvinar neurons can fire with bursts more often than dLGN neurons, and an increased density of T-type channels in pulvinar neurons relative to dLGN neurons may underlie this phenomenon. The contribution of burst firing to pulvinar function could potentially be examined by injecting T channel blockers into the pulvinar of primates to examine the effects on the performance of behavioral tasks.

Our comparison of the membrane properties of neurons recorded in juvenile and adult tissue suggest that the development of the burst firing in both dLGN and pulvinar neurons correlate with a developmental change in T-channel density and could be possibly correlated with eye opening, which occurs at postnatal week 3 in tree shrews. With our neuron model, we were able to closely replicate the recorded changes in firing



patterns by increasing T-channel density within distal dendrites. However, a small change in channel kinetics was necessary to fully replicate the experimental data. Previous studies have also demonstrated developmental changes in channel kinetics (Ramoia and McCormick, 1994). More detailed studies of T channel kinetics in the juvenile and adult tissue will be necessary to fully understand the mechanisms underlying the development of multi-burst firing in the pulvinar nucleus. Dark rearing or monocular deprivation studies could be carried out to determine whether the development of multi-burst firing is related to eye opening.

We characterized tectopulvinar EPSPs in the tree shrew to determine whether the unique organization of the diffuse and specific projections is reflected in differences in their synaptic properties. We found that the short-term synaptic plasticity of tectopulvinar terminals is distinct from that of corticothalamic or retinogeniculate terminals and that this difference could be due to the fact that each terminal type contains a unique distribution of synapsins. Furthermore, we found that the diffuse and specific tectopulvinar projections display subtle differences in short-term plasticity due to different patterns of convergence and/or glutamate release probability.

We suggest that convergent synaptic arrangements allow the tectopulvinar projection to relay a dynamic range of visual signals from the SC, through the pulvinar, to the cortex, striatum and amygdala in order to initiate and guide the appropriate actions in response to the movements. However, further physiological experiments are necessary to more fully understand the function of the tectopulvinar projection. The response properties of neurons in the tree shrew pulvinar nucleus as well as the tree shrew temporal cortex should be characterized using *in vivo* recording techniques. The effects

of deactivation of the SC or temporal cortex on the response properties of pulvinar neurons would help to elucidate their contributions to pulvinar activity patterns. Finally, the effects of inactivation of the Pd and/or Pc on visual discrimination tasks would help to determine the contribution of tectopulvinar pathways to vision. Recent inactivation studies in rhesus monkeys have revealed that the pulvinar is important for the planning of movements (Wilke et al., 2010), but it is difficult to target the tectorecipient zone of the pulvinar nucleus in this species. Therefore, continued studies of the tree shrew will help to resolve the function of tecto-pulvino-cortical pathways and potentially aid in the design of therapeutics to reduce symptoms caused by compromise of these pathways.

## REFERENCES

- Albano JE, Humphrey AL, Norton TT (1978) Laminar organization of receptive-field properties in tree shrew superior colliculus. *J Neurophysiol* 41:1140-1164.
- Anderson JC, da Costa NM, Martin KA (2009) The W cell pathway to cat primary visual cortex. *J Comp Neurol* 516:20-35.
- Arsenault D, Zhang ZW (2006) Developmental remodelling of the lemniscal synapse in the ventral basal thalamus of the mouse. *J Physiol* 573:121-132.
- Atencio FW, Diamond IT, Ward JP (1975) Behavioral study of the visual cortex of *Galago senegalensis*. *J Comp Physiol Psychol* 89:1109-1135.
- Azevedo FA, Carvalho LR, Grinberg LT, Farfel JM, Ferretti RE, Leite RE, Jacob Filho W, Lent R, Herculano-Houzel S (2009) Equal numbers of neuronal and nonneuronal cells make the human brain an isometrically scaled-up primate brain. *J Comp Neurol* 513:532-541.
- Baldauf ZB, Chomsung RD, Carden WB, May PJ, Bickford ME (2005) Ultrastructural analysis of projections to the pulvinar nucleus of the cat. I: Middle suprasylvian gyrus (areas 5 and 7). *J Comp Neurol* 485:87-107.
- Bender DB (1983) Visual activation of neurons in the primate pulvinar depends on cortex but not colliculus. *Brain Res* 279:258-261.
- Benevento LA, Fallon JH (1975) The ascending projections of the superior colliculus in the rhesus monkey (*Macaca mulatta*). *J Comp Neurol* 160:339-361.
- Benfenati F, Valtorta F, Greengard P (1991) Computer modeling of synapsin I binding to synaptic vesicles and F-actin: implications for regulation of neurotransmitter release. *Proc Natl Acad Sci U S A* 88:575-579.
- Berman RA, Wurtz RH (2008) Exploring the pulvinar path to visual cortex. *Prog Brain Res* 171:467-473.
- Bezudnaya T, Cano M, Bereshpolova Y, Stoelzel CR, Alonso JM, Swadlow HA (2006) Thalamic burst mode and inattention in the awake LGNd. *Neuron* 49:421-432.

- Bickford ME, Wei H, Eisenback MA, Chomsung RD, Slusarczyk AS, Dankowski AB (2008) Synaptic organization of thalamocortical axon collaterals in the perigeniculate nucleus and dorsal lateral geniculate nucleus. *J Comp Neurol* 508:264-285.
- Bickford ME, Slusarczyk A, Dilger EK, Krahe TE, Kucuk C, Guido W (2010) Synaptic development of the mouse dorsal lateral geniculate nucleus. *J Comp Neurol* 518:622-635.
- Bloomfield SA, Sherman SM (1989) Dendritic current flow in relay cells and interneurons of the cat's lateral geniculate nucleus. *Proc Natl Acad Sci U S A* 86:3911-3914.
- Bloomfield SA, Hamos JE, Sherman SM (1987) Passive cable properties and morphological correlates of neurones in the lateral geniculate nucleus of the cat. *J Physiol* 383:653-692.
- Boudreau CE, Ferster D (2005) Short-term depression in thalamocortical synapses of cat primary visual cortex. *J Neurosci* 25:7179-7190.
- Bourassa J, Pinault D, Deschenes M (1995) Corticothalamic projections from the cortical barrel field to the somatosensory thalamus in rats: a single-fibre study using biocytin as an anterograde tracer. *Eur J Neurosci* 7:19-30.
- Brittain P, Ffytche DH, McKendrick A, Surguladze S (2010) Visual processing, social cognition and functional outcome in schizophrenia. *Psychiatry Res* 178:270-275.
- Byne W, Hazlett EA, Buchsbaum MS, Kemether E (2009) The thalamus and schizophrenia: current status of research. *Acta Neuropathol* 117:347-368.
- Campbell CBG (1980) The nervous system of tupaiidae: its bearing on phyletic relationships. In: *Comparative biology and evolutionary relationships of tree shrews* (Luckett WP, ed), pp 219-242. New York: Plenum Press.
- Campos-Ortega JA, Hayhow WR (1972) On the organisation of the visual cortical projection to the pulvinar in *Macaca mulatta*. *Brain Behav Evol* 6:394-423.
- Casagrande VA, Diamond IT (1974) Ablation study of the superior colliculus in the tree shrew (*Tupaia glis*). *J Comp Neurol* 156:207-237.
- Casagrande VA, Xu X (2004) Parallel Visual Pathways: A Comparative Perspective. In: *The Visual Neurosciences* (Chalupa L, Werner JS, eds), pp 494-506: MIT Press.
- Casanova C, Molotchnikoff S (1990) Influence of the superior colliculus on visual responses of cells in the rabbit's lateral posterior nucleus. *Exp Brain Res* 80:387-396.

- Casseday JH, Jones DR, Diamond IT (1979) Projections from cortex to tectum in the tree shrew, *Tupaia glis*. *J Comp Neurol* 185:253-291.
- Cavada C, Goldman-Rakic PS (1993) Multiple visual areas in the posterior parietal cortex of primates. *Prog Brain Res* 95:123-137.
- Chalupa LM, Coyle RS, Lindsley DB (1976) Effect of pulvinar lesions on visual pattern discrimination in monkeys. *J Neurophysiol* 39:354-369.
- Chen C, Regehr WG (2000) Developmental remodeling of the retinogeniculate synapse. *Neuron* 28:955-966.
- Chen C, Blitz DM, Regehr WG (2002) Contributions of receptor desensitization and saturation to plasticity at the retinogeniculate synapse. *Neuron* 33:779-788.
- Chen Y, Bidwell LC, Holzman PS (2005) Visual motion integration in schizophrenia patients, their first-degree relatives, and patients with bipolar disorder. *Schizophr Res* 74:271-281.
- Chomsung RD, Petry HM, Bickford ME (2008) Ultrastructural examination of diffuse and specific tectopulvinar projections in the tree shrew. *J Comp Neurol* 510:24-46.
- Chomsung RD, Wei H, Day-Brown JD, Petry HM, Bickford ME (2010) Synaptic organization of connections between the temporal cortex and pulvinar nucleus of the tree shrew. *Cereb Cortex* 20:997-1011.
- Cleland BG, Dubin MW, Levick WR (1971) Sustained and transient neurones in the cat's retina and lateral geniculate nucleus. *J Physiol* 217:473-496.
- Conley M, Fitzpatrick D, Diamond IT (1984) The laminar organization of the lateral geniculate body and the striate cortex in the tree shrew (*Tupaia glis*). *J Neurosci* 4:171-197.
- Cowey A (2010) The blindsight saga. *Exp Brain Res* 200:3-24.
- Crunelli V, Kelly JS, Leresche N, Pirchio M (1987) On the excitatory post-synaptic potential evoked by stimulation of the optic tract in the rat lateral geniculate nucleus. *J Physiol* 384:603-618.
- Crunelli V, Blethyn KL, Cope DW, Hughes SW, Parri HR, Turner JP, Toth TI, Williams SR (2002) Novel neuronal and astrocytic mechanisms in thalamocortical loop dynamics. *Philos Trans R Soc Lond B Biol Sci* 357:1675-1693.

- Cusick CG, Steindler DA, Kaas JH (1985) Corticocortical and collateral thalamocortical connections of postcentral somatosensory cortical areas in squirrel monkeys: a double-labeling study with radiolabeled wheatgerm agglutinin and wheatgerm agglutinin conjugated to horseradish peroxidase. *Somatosens Res* 3:1-31.
- Cusick CG, Scriptor JL, Darensbourg JG, Weber JT (1993) Chemoarchitectonic subdivisions of the visual pulvinar in monkeys and their connectional relations with the middle temporal and rostral dorsolateral visual areas, MT and DLr. *J Comp Neurol* 336:1-30.
- Dankowski A, Bickford ME (2003) Inhibitory circuitry involving Y cells and Y retinal terminals in the C laminae of the cat dorsal lateral geniculate nucleus. *J Comp Neurol* 460:368-379.
- Datskovskaia A, Carden WB, Bickford ME (2001) Y retinal terminals contact interneurons in the cat dorsal lateral geniculate nucleus. *J Comp Neurol* 430:85-100.
- Day-Brown JD, Chomsung RD, Petry HM, Bickford ME (2007) Synaptic organization of striate cortex projections to the tree shrew dorsal thalamus. In: *Soc Neurosci Abstr*, p 392.397:112.
- Day-Brown JD, Wei H, Chomsung RD, Petry HM, Bickford ME (2010) Pulvinar projections to the striatum and amygdala. *Frontiers in Neuroanatomy*.
- De Camilli P, Benfenati F, Valtorta F, Greengard P (1990) The synapsins. *Annu Rev Cell Biol* 6:433-460.
- De Lima AD, Singer W (1987) The brainstem projection to the lateral geniculate nucleus in the cat: identification of cholinergic and monoaminergic elements. *J Comp Neurol* 259:92-121.
- Dean P, Redgrave P, Westby GW (1989) Event or emergency? Two response systems in the mammalian superior colliculus. *Trends Neurosci* 12:137-147.
- Deschenes M, Paradis M, Roy JP, Steriade M (1984) Electrophysiology of neurons of lateral thalamic nuclei in cat: resting properties and burst discharges. *J Neurophysiol* 51:1196-1219.
- Destexhe A, Neubig M, Ulrich D, Huguenard J (1998) Dendritic low-threshold calcium currents in thalamic relay cells. *J Neurosci* 18:3574-3588.
- Diamond IT, Hall WC (1969) Evolution of neocortex. *Science* 164:251-262.
- Diamond IT, Snyder M, Killackey H, Jane J, Hall WC (1970) Thalamo-cortical projections in the tree shrew (*Tupaia glis*). *J Comp Neurol* 139:273-306.

- Ding Y, Casagrande VA (1998) Synaptic and neurochemical characterization of parallel pathways to the cytochrome oxidase blobs of primate visual cortex. *J Comp Neurol* 391:429-443.
- Einstein G, Davis TL, Sterling P (1987) Ultrastructure of synapses from the A-laminae of the lateral geniculate nucleus in layer IV of the cat striate cortex. *J Comp Neurol* 260:63-75.
- Erisir A, Dreusicke M (2005) Quantitative morphology and postsynaptic targets of thalamocortical axons in critical period and adult ferret visual cortex. *J Comp Neurol* 485:11-31.
- Erisir A, Van Horn SC, Sherman SM (1997) Relative numbers of cortical and brainstem inputs to the lateral geniculate nucleus. *Proc Natl Acad Sci U S A* 94:1517-1520.
- Erisir A, Van Horn SC, Bickford ME, Sherman SM (1997) Immunocytochemistry and distribution of parabrachial terminals in the lateral geniculate nucleus of the cat: a comparison with corticogeniculate terminals. *J Comp Neurol* 377:535-549.
- Feig S, Harting JK (1998) Corticocortical communication via the thalamus: ultrastructural studies of corticothalamic projections from area 17 to the lateral posterior nucleus of the cat and inferior pulvinar nucleus of the owl monkey. *J Comp Neurol* 395:281-295.
- Fitzpatrick D, Diamond IT, Raczkowski D (1989) Cholinergic and monoaminergic innervation of the cat's thalamus: comparison of the lateral geniculate nucleus with other principal sensory nuclei. *J Comp Neurol* 288:647-675.
- Fremeau RT, Jr., Troyer MD, Pahner I, Nygaard GO, Tran CH, Reimer RJ, Bellocchio EE, Fortin D, Storm-Mathisen J, Edwards RH (2001) The expression of vesicular glutamate transporters defines two classes of excitatory synapse. *Neuron* 31:247-260.
- Fujiyama F, Hioki H, Tomioka R, Taki K, Tamamaki N, Nomura S, Okamoto K, Kaneko T (2003) Changes of immunocytochemical localization of vesicular glutamate transporters in the rat visual system after the retinofugal denervation. *J Comp Neurol* 465:234-249.
- Geneser-Jensen FA, Blackstad TW (1971) Distribution of acetyl cholinesterase in the hippocampal region of the guinea pig. I. Entorhinal area, parasubiculum, and presubiculum. *Z Zellforsch Mikrosk Anat* 114:460-481.
- Gitler D, Cheng Q, Greengard P, Augustine GJ (2008) Synapsin IIa controls the reserve pool of glutamatergic synaptic vesicles. *J Neurosci* 28:10835-10843.

- Gitler D, Takagishi Y, Feng J, Ren Y, Rodriguiz RM, Wetsel WC, Greengard P, Augustine GJ (2004) Different presynaptic roles of synapsins at excitatory and inhibitory synapses. *J Neurosci* 24:11368-11380.
- Glendenning KK, Hall JA, Diamond IT, Hall WC (1975) The pulvinar nucleus of *Galago senegalensis*. *J Comp Neurol* 161:419-458.
- Glenn LL, Steriade M (1982) Discharge rate and excitability of cortically projecting intralaminar thalamic neurons during waking and sleep states. *J Neurosci* 2:1387-1404.
- Godwin DW, Van Horn SC, Eriir A, Sesma M, Romano C, Sherman SM (1996) Ultrastructural localization suggests that retinal and cortical inputs access different metabotropic glutamate receptors in the lateral geniculate nucleus. *J Neurosci* 16:8181-8192.
- Graef JD, Nordskog BK, Wiggins WF, Godwin DW (2009) An acquired channelopathy involving thalamic T-type Ca<sup>2+</sup> channels after status epilepticus. *J Neurosci* 29:4430-4441.
- Graham J, Casagrande VA (1980) A light microscopic and electron microscopic study of the superficial layers of the superior colliculus of the tree shrew (*Tupaia glis*). *J Comp Neurol* 191:133-151.
- Granseth B, Ahlstrand E, Lindstrom S (2002) Paired pulse facilitation of corticogeniculate EPSCs in the dorsal lateral geniculate nucleus of the rat investigated in vitro. *J Physiol* 544:477-486.
- Greengard P, Valtorta F, Czernik AJ, Benfenati F (1993) Synaptic vesicle phosphoproteins and regulation of synaptic function. *Science* 259:780-785.
- Guido W, Weyand T (1995) Burst responses in thalamic relay cells of the awake behaving cat. *J Neurophysiol* 74:1782-1786.
- Guido W, Lu SM, Vaughan JW, Godwin DW, Sherman SM (1995) Receiver operating characteristic (ROC) analysis of neurons in the cat's lateral geniculate nucleus during tonic and burst response mode. *Vis Neurosci* 12:723-741.
- Guillery RW (1969) The organization of synaptic interconnections in the laminae of the dorsal lateral geniculate nucleus of the cat. *Z Zellforsch Mikrosk Anat* 96:1-38.
- Guillery RW (1995) Anatomical evidence concerning the role of the thalamus in corticocortical communication: a brief review. *J Anat* 187 ( Pt 3):583-592.
- Guillery RW, Sherman SM (2002) Thalamic relay functions and their role in corticocortical communication: generalizations from the visual system. *Neuron* 33:163-175.



- Guillery RW, Feig SL, Van Lieshout DP (2001) Connections of higher order visual relays in the thalamus: a study of corticothalamic pathways in cats. *J Comp Neurol* 438:66-85.
- Gutierrez C, Cox CL, Rinzel J, Sherman SM (2001) Dynamics of low-threshold spike activation in relay neurons of the cat lateral geniculate nucleus. *J Neurosci* 21:1022-1032.
- Hajdu F, Hassler R, Somogyi G (1982) Neuronal and synaptic organization of the lateral geniculate nucleus of the tree shrew, *Tupaia glis*. *Cell Tissue Res* 224:207-223.
- Halassa MM, Fellin T, Haydon PG (2007) The tripartite synapse: roles for gliotransmission in health and disease. *Trends Mol Med* 13:54-63.
- Halassa MM, Fellin T, Takano H, Dong JH, Haydon PG (2007) Synaptic islands defined by the territory of a single astrocyte. *J Neurosci* 27:6473-6477.
- Hamos JE, Van Horn SC, Raczkowski D, Sherman SM (1987) Synaptic circuits involving an individual retinogeniculate axon in the cat. *J Comp Neurol* 259:165-192.
- Harting JK, Diamond IT, Hall WC (1973) Anterograde degeneration study of the cortical projections of the lateral geniculate and pulvinar nuclei in the tree shrew (*Tupaia glis*). *J Comp Neurol* 150:393-440.
- Harting JK, Glendenning KK, Diamond IT, Hall WC (1973) Evolution of the primate visual system: anterograde degeneration studies of the tecto-pulvinar system. *Am J Phys Anthropol* 38:383-392.
- He J, Hu B (2002) Differential distribution of burst and single-spike responses in auditory thalamus. *J Neurophysiol* 88:2152-2156.
- Herrick CJ (1918) *An Introduction to Neurology*. Philadelphia: W. B. Saunders.
- Herzog E, Bellenchi GC, Gras C, Bernard V, Ravassard P, Bedet C, Gasnier B, Giros B, El Mestikawy S (2001) The existence of a second vesicular glutamate transporter specifies subpopulations of glutamatergic neurons. *J Neurosci* 21:RC181.
- Hilfiker S, Pieribone VA, Czernik AJ, Kao HT, Augustine GJ, Greengard P (1999) Synapsins as regulators of neurotransmitter release. *Philos Trans R Soc Lond B Biol Sci* 354:269-279.
- Hodgkin AL, Huxley AF (1952) A quantitative description of membrane current and its application to conduction and excitation in nerve. *J Physiol* 117:500-544.

- Houser CR, Vaughn JE, Barber RP, Roberts E (1980) GABA neurons are the major cell type of the nucleus reticularis thalami. *Brain Res* 200:341-354.
- Huerta MF, Weber JT, Rothstein LR, Harting JK (1985) Subcortical connections of area 17 in the tree shrew: an autoradiographic analysis. *Brain Res* 340:163-170.
- Huguenard JR, McCormick DA (1992) Simulation of the currents involved in rhythmic oscillations in thalamic relay neurons. *J Neurophysiol* 68:1373-1383.
- Huguenard JR, Prince DA (1992) A novel T-type current underlies prolonged Ca(2+)-dependent burst firing in GABAergic neurons of rat thalamic reticular nucleus. *J Neurosci* 12:3804-3817.
- Hull C, Isaacson JS, Scanziani M (2009) Postsynaptic mechanisms govern the differential excitation of cortical neurons by thalamic inputs. *J Neurosci* 29:9127-9136.
- Huppe-Gourgues F, Bickford ME, Boire D, Ptito M, Casanova C (2006) Distribution, morphology, and synaptic targets of corticothalamic terminals in the cat lateral posterior-pulvinar complex that originate from the posteromedial lateral suprasylvian cortex. *J Comp Neurol* 497:847-863.
- Jahnsen H, Llinas R (1984) Ionic basis for the electro-responsiveness and oscillatory properties of guinea-pig thalamic neurones in vitro. *J Physiol* 349:227-247.
- Jahnsen H, Llinas R (1984) Electrophysiological properties of guinea-pig thalamic neurones: an in vitro study. *J Physiol* 349:205-226.
- Johnson BD, Hockerman GH, Scheuer T, Catterall WA (1996) Distinct effects of mutations in transmembrane segment IVS6 on block of L-type calcium channels by structurally similar phenylalkylamines. *Mol Pharmacol* 50:1388-1400.
- Jones EG, Powell TP (1969) An electron microscopic study of the mode of termination of cortico-thalamic fibres within the sensory relay nuclei of the thalamus. *Proc R Soc Lond B Biol Sci* 172:173-185.
- Jones BE, Yang TZ (1985) The efferent projections from the reticular formation and the locus coeruleus studied by anterograde and retrograde axonal transport in the rat. *J Comp Neurol* 242:56-92.
- Kaas J (2002) Convergences in the modular and areal organization of the forebrain of mammals: implications for the reconstruction of forebrain evolution. *Brain Behav Evol* 59:262-272.
- Kaas JH, Preuss TM (1993) Archontom affinities as reflected in the visual system. In: *Mammal phylogeny: placentals* (Szalay R, Novacek M, Mckenna M, eds), pp 115-128. New York: Springer-Verlag.

- Kaas JH, Lyon DC (2007) Pulvinar contributions to the dorsal and ventral streams of visual processing in primates. *Brain Res Rev* 55:285-296.
- Kaneko T, Fujiyama F, Hioki H (2002) Immunohistochemical localization of candidates for vesicular glutamate transporters in the rat brain. *J Comp Neurol* 444:39-62.
- Kao CQ, Coulter DA (1997) Physiology and pharmacology of corticothalamic stimulation-evoked responses in rat somatosensory thalamic neurons in vitro. *J Neurophysiol* 77:2661-2676.
- Katz LC (1987) Local circuitry of identified projection neurons in cat visual cortex brain slices. *J Neurosci* 7:1223-1249.
- Kaufman EF, Rosenquist AC, Raczkowski D (1984) The projections of single thalamic neurons onto multiple visual cortical areas in the cat. *Brain Res* 298:171-174.
- Kawamura S, Diamond IT (1978) The laminar origin of descending projections from the cortex to the thalamus in *Tupaia glis*. *Brain Res* 153:333-339.
- Kelly LR, Li J, Carden WB, Bickford ME (2003) Ultrastructure and synaptic targets of tectothalamic terminals in the cat lateral posterior nucleus. *J Comp Neurol* 464:472-486.
- Kielland A, Heggelund P (2002) AMPA and NMDA currents show different short-term depression in the dorsal lateral geniculate nucleus of the rat. *J Physiol* 542:99-106.
- Kielland A, Erisir A, Walaas SI, Heggelund P (2006) Synapsin utilization differs among functional classes of synapses on thalamocortical cells. *J Neurosci* 26:5786-5793.
- Killackey H, Diamond IT (1971) Visual attention in the tree shrew: an ablation study of the striate and extrastriate visual cortex. *Science* 171:696-699.
- Killackey H, Snyder M, Diamond IT (1971) Function of striate and temporal cortex in the tree shrew. *J Comp Physiol Psychol* 74:Suppl 2:1-29.
- Kleinhans NM, Richards T, Johnson LC, Weaver KE, Greenson J, Dawson G, Aylward E (2011) fMRI evidence of neural abnormalities in the subcortical face processing system in ASD. *Neuroimage* 54:697-704.
- Kovacs K, Sik A, Ricketts C, Timofeev I (2010) Subcellular distribution of low-voltage activated T-type Ca<sup>2+</sup> channel subunits (Ca<sub>v</sub>3.1 and Ca<sub>v</sub>3.3) in reticular thalamic neurons of the cat. *J Neurosci Res* 88:448-460.

- Lane RH, Allman JM, Kaas JH (1971) Representation of the visual field in the superior colliculus of the grey squirrel (*Sciurus carolinensis*) and the tree shrew (*Tupaia glis*). *Brain Res* 26:277-292.
- Latawiec D, Martin KA, Meskenaite V (2000) Termination of the geniculocortical projection in the striate cortex of macaque monkey: a quantitative immunoelectron microscopic study. *J Comp Neurol* 419:306-319.
- LeGros Clark WE (1934) *Early forerunners of man*. London: Baillere, Tyndall and Cox.
- LeVay S, Ferster D (1979) Proportion of interneurons in the cat's lateral geniculate nucleus. *Brain Res* 164:304-308.
- Leventhal AG, Rodieck RW, Dreher B (1985) Central projections of cat retinal ganglion cells. *J Comp Neurol* 237:216-226.
- Li J, Guido W, Bickford ME (2003) Two distinct types of corticothalamic EPSPs and their contribution to short-term synaptic plasticity. *J Neurophysiol* 90:3429-3440.
- Li J, Wang S, Bickford ME (2003) Comparison of the ultrastructure of cortical and retinal terminals in the rat dorsal lateral geniculate and lateral posterior nuclei. *J Comp Neurol* 460:394-409.
- Li J, Bickford ME, Guido W (2003) Distinct firing properties of higher order thalamic relay neurons. *J Neurophysiol* 90:291-299.
- Lin CS, Kaas JH (1979) The inferior pulvinar complex in owl monkeys: architectonic subdivisions and patterns of input from the superior colliculus and subdivisions of visual cortex. *J Comp Neurol* 187:655-678.
- Lindstrom S, Wrobel A (1990) Frequency dependent corticofugal excitation of principal cells in the cat's dorsal lateral geniculate nucleus. *Exp Brain Res* 79:313-318.
- Llano DA, Sherman SM (2008) Evidence for nonreciprocal organization of the mouse auditory thalamocortical-corticothalamic projection systems. *J Comp Neurol* 507:1209-1227.
- Llinas RR, Steriade M (2006) Bursting of thalamic neurons and states of vigilance. *J Neurophysiol* 95:3297-3308.
- Llinas R, McGuinness TL, Leonard CS, Sugimori M, Greengard P (1985) Intraterminal injection of synapsin I or calcium/calmodulin-dependent protein kinase II alters neurotransmitter release at the squid giant synapse. *Proc Natl Acad Sci U S A* 82:3035-3039.

- Lu SM, Guido W, Vaughan JW, Sherman SM (1995) Latency variability of responses to visual stimuli in cells of the cat's lateral geniculate nucleus. *Exp Brain Res* 105:7-17.
- Luppino G, Matelli M, Carey RG, Fitzpatrick D, Diamond IT (1988) New view of the organization of the pulvinar nucleus in Tupaia as revealed by tectopulvinar and pulvinar-cortical projections. *J Comp Neurol* 273:67-86.
- Lyon DC, Jain N, Kaas JH (1998) Cortical connections of striate and extrastriate visual areas in tree shrews. *J Comp Neurol* 401:109-128.
- Lyon DC, Jain N, Kaas JH (2003) The visual pulvinar in tree shrews I. Multiple subdivisions revealed through acetylcholinesterase and Cat-301 chemoarchitecture. *J Comp Neurol* 467:593-606.
- Lyon DC, Jain N, Kaas JH (2003) The visual pulvinar in tree shrews II. Projections of four nuclei to areas of visual cortex. *J Comp Neurol* 467:607-627.
- Masterson SP, Li J, Bickford ME (2009) Synaptic organization of the tectorecipient zone of the rat lateral posterior nucleus. *J Comp Neurol* 515:647-663.
- Masterson SP, Li J, Bickford ME (2010) Frequency-dependent release of substance P mediates heterosynaptic potentiation of glutamatergic synaptic responses in the rat visual thalamus. *J Neurophysiol* 104:1758-1767.
- Mathers LH (1972) The synaptic organization of the cortical projection to the pulvinar of the squirrel monkey. *J Comp Neurol* 146:43-60.
- Matsuzaki R, Kyuhou S, Matsuura-Nakao K, Gemba H (2004) Thalamo-cortical projections to the posterior parietal cortex in the monkey. *Neurosci Lett* 355:113-116.
- McCormick DA (1993) Actions of acetylcholine in the cerebral cortex and thalamus and implications for function. *Prog Brain Res* 98:303-308.
- McCormick DA, Huguenard JR (1992) A model of the electrophysiological properties of thalamocortical relay neurons. *J Neurophysiol* 68:1384-1400.
- Miceli D, Reperant J, Marchand L, Ward R, Vesselkin N (1991) Divergence and collateral axon branching in subsystems of visual cortical projections from the cat lateral posterior nucleus. *J Hirnforsch* 32:165-173.
- Molotchnikoff S, Shumikhina S (1996) The lateral posterior-pulvinar complex modulation of stimulus-dependent oscillations in the cat visual cortex. *Vision Res* 36:2037-2046.

- Monckton JE, McCormick DA (2002) Neuromodulatory role of serotonin in the ferret thalamus. *J Neurophysiol* 87:2124-2136.
- Montero VM (1987) Ultrastructural identification of synaptic terminals from the axon of type 3 interneurons in the cat lateral geniculate nucleus. *J Comp Neurol* 264:268-283.
- Montero VM (1989) Ultrastructural identification of synaptic terminals from cortical axons and from collateral axons of geniculo-cortical relay cells in the perigeniculate nucleus of the cat. *Exp Brain Res* 75:65-72.
- Mooney RD, Fish SE, Rhoades RW (1984) Anatomical and functional organization of pathway from superior colliculus to lateral posterior nucleus in hamster. *J Neurophysiol* 51:407-431.
- Muly EC, Fitzpatrick D (1992) The morphological basis for binocular and ON/OFF convergence in tree shrew striate cortex. *J Neurosci* 12:1319-1334.
- Murphy PC, Sillito AM (1996) Functional morphology of the feedback pathway from area 17 of the cat visual cortex to the lateral geniculate nucleus. *J Neurosci* 16:1180-1192.
- Nahmani M, Erisir A (2005) VGluT2 immunocytochemistry identifies thalamocortical terminals in layer 4 of adult and developing visual cortex. *J Comp Neurol* 484:458-473.
- Norton TT (1982) Changing concepts of the nervous system. In: *Geniculate and extrageniculate visual systems in the tree shrew*, pp 377-409. New York: Academic Press, Inc.
- O'Donnell BF, Bismark A, Hetrick WP, Bodkins M, Vohs JL, Shekhar A (2006) Early stage vision in schizophrenia and schizotypal personality disorder. *Schizophr Res* 86:89-98.
- Ogren MP, Hendrickson AE (1979) The morphology and distribution of striate cortex terminals in the inferior and lateral subdivisions of the Macaca monkey pulvinar. *J Comp Neurol* 188:179-199.
- Ohara PT, Lieberman AR (1985) The thalamic reticular nucleus of the adult rat: experimental anatomical studies. *J Neurocytol* 14:365-411.
- Pape HC, Budde T, Mager R, Kisvarday ZF (1994) Prevention of Ca(2+)-mediated action potentials in GABAergic local circuit neurones of rat thalamus by a transient K<sup>+</sup> current. *J Physiol* 478 Pt 3:403-422.

- Patel NC, Bickford ME (1997) Synaptic targets of cholinergic terminals in the pulvinar nucleus of the cat. *J Comp Neurol* 387:266-278.
- Perry VH, Cowey A (1984) Retinal ganglion cells that project to the superior colliculus and pretectum in the macaque monkey. *Neuroscience* 12:1125-1137.
- Pieribone VA, Shupliakov O, Brodin L, Hilfiker-Rothenfluh S, Czernik AJ, Greengard P (1995) Distinct pools of synaptic vesicles in neurotransmitter release. *Nature* 375:493-497.
- Pinault D, Deschenes M (1998) Projection and innervation patterns of individual thalamic reticular axons in the thalamus of the adult rat: a three-dimensional, graphic, and morphometric analysis. *J Comp Neurol* 391:180-203.
- Raczkowski D, Diamond IT (1980) Cortical connections of the pulvinar nucleus in Galago. *J Comp Neurol* 193:1-40.
- Raczkowski D, Diamond IT (1981) Projections from the superior colliculus and the neocortex to the pulvinar nucleus in Galago. *J Comp Neurol* 200:231-254.
- Raczkowski D, Fitzpatrick D (1990) Terminal arbors of individual, physiologically identified geniculocortical axons in the tree shrew's striate cortex. *J Comp Neurol* 302:500-514.
- Ramcharan EJ, Gnadt JW, Sherman SM (2005) Higher-order thalamic relays burst more than first-order relays. *Proc Natl Acad Sci U S A* 102:12236-12241.
- Ramoas AS, McCormick DA (1994) Developmental changes in electrophysiological properties of LGNd neurons during reorganization of retinogeniculate connections. *J Neurosci* 14:2089-2097.
- Reichova I, Sherman SM (2004) Somatosensory corticothalamic projections: distinguishing drivers from modulators. *J Neurophysiol* 92:2185-2197.
- Rhodes PA, Llinas R (2005) A model of thalamocortical relay cells. *J Physiol* 565:765-781.
- Robinson DL, Petersen SE (1992) The pulvinar and visual salience. *Trends Neurosci* 15:127-132.
- Robson JA, Hall WC (1977) The organization of the pulvinar in the grey squirrel (*Sciurus carolinensis*). I. Cytoarchitecture and connections. *J Comp Neurol* 173:355-388.

- Robson JA, Hall WC (1977) The organization of the pulvinar in the grey squirrel (*Sciurus carolinensis*). II. Synaptic organization and comparisons with the dorsal lateral geniculate nucleus. *J Comp Neurol* 173:389-416.
- Rockland KS, Andresen J, Cowie RJ, Robinson DL (1999) Single axon analysis of pulvinocortical connections to several visual areas in the macaque. *J Comp Neurol* 406:221-250.
- Rosahl TW, Spillane D, Missler M, Herz J, Selig DK, Wolff JR, Hammer RE, Malenka RC, Sudhof TC (1995) Essential functions of synapsins I and II in synaptic vesicle regulation. *Nature* 375:488-493.
- Saalman YB, Kastner S (2009) Gain control in the visual thalamus during perception and cognition. *Curr Opin Neurobiol* 19:408-414.
- Salt TE (1987) Excitatory amino acid receptors and synaptic transmission in the rat ventrobasal thalamus. *J Physiol* 391:499-510.
- Samigullin D, Bill CA, Coleman WL, Bykhovskaia M (2004) Regulation of transmitter release by synapsin II in mouse motor terminals. *J Physiol* 561:149-158.
- Sanchez-Vives MV, Bal T, McCormick DA (1997) Inhibitory interactions between perigeniculate GABAergic neurons. *J Neurosci* 17:8894-8908.
- Scharfman HE, Lu SM, Guido W, Adams PR, Sherman SM (1990) N-methyl-D-aspartate receptors contribute to excitatory postsynaptic potentials of cat lateral geniculate neurons recorded in thalamic slices. *Proc Natl Acad Sci U S A* 87:4548-4552.
- Schiebler W, Jahn R, Doucet JP, Rothlein J, Greengard P (1986) Characterization of synapsin I binding to small synaptic vesicles. *J Biol Chem* 261:8383-8390.
- Schneider GE (1969) Two visual systems. *Science* 163:895-902.
- Schofield BR, Hallman LE, Lin CS (1987) Morphology of corticotectal cells in the primary visual cortex of hooded rats. *J Comp Neurol* 261:85-97.
- Sesma MA, Casagrande VA, Kaas JH (1984) Cortical connections of area 17 in tree shrews. *J Comp Neurol* 230:337-351.
- Sherman SM (2001) Tonic and burst firing: dual modes of thalamocortical relay. *Trends Neurosci* 24:122-126.
- Sherman SM, Spear PD (1982) Organization of visual pathways in normal and visually deprived cats. *Physiol Rev* 62:738-855.



- Sherman SM, Friedlander MJ (1988) Identification of X versus Y properties for interneurons in the A-laminae of the cat's lateral geniculate nucleus. *Exp Brain Res* 73:384-392.
- Sherman SM, Guillery RW (1996) Functional organization of thalamocortical relays. *J Neurophysiol* 76:1367-1395.
- Sherman SM, Guillery RW (1998) On the actions that one nerve cell can have on another: distinguishing "drivers" from "modulators". *Proc Natl Acad Sci U S A* 95:7121-7126.
- Sherman SM, Guillery RW (2006) Exploring the thalamus and its role in cortical function, Second Edition Edition. Cambridge: The MIT Press.
- Sillito AM, Cudeiro J, Jones HE (2006) Always returning: feedback and sensory processing in visual cortex and thalamus. *Trends Neurosci* 29:307-316.
- Smith PH, Populin LC (2001) Fundamental differences between the thalamocortical recipient layers of the cat auditory and visual cortices. *J Comp Neurol* 436:508-519.
- Smith PH, Bartlett EL, Kowalkowski A (2007) Cortical and collicular inputs to cells in the rat paralamina thalamic nuclei adjacent to the medial geniculate body. *J Neurophysiol* 98:681-695.
- Stepniewska I, Qi HX, Kaas JH (1999) Do superior colliculus projection zones in the inferior pulvinar project to MT in primates? *Eur J Neurosci* 11:469-480.
- Stepniewska I, Qi HX, Kaas JH (2000) Projections of the superior colliculus to subdivisions of the inferior pulvinar in New World and Old World monkeys. *Vis Neurosci* 17:529-549.
- Steriade M, Curro Dossi R, Contreras D (1993) Electrophysiological properties of intralaminar thalamocortical cells discharging rhythmic (approximately 40 HZ) spike-bursts at approximately 1000 HZ during waking and rapid eye movement sleep. *Neuroscience* 56:1-9.
- Steriade M, Jones EG, McCormick DA (1997) *Thalamus*. New York: Elsevier.
- Swadlow HA, Gusev AG (2001) The impact of 'bursting' thalamic impulses at a neocortical synapse. *Nat Neurosci* 4:402-408.
- Symonds LL, Kaas JH (1978) Connections of striate cortex in the prosimian, *Galago senegalensis*. *J Comp Neurol* 181:477-512.

- Szentagothai J (1963) The Structure of the Synapse in the Lateral Geniculate Body. *Acta Anat (Basel)* 55:166-185.
- Tong L, Spear PD (1986) Single thalamic neurons project to both lateral suprasylvian visual cortex and area 17: a retrograde fluorescent double-labeling study. *J Comp Neurol* 246:254-264.
- Traub RD, Wong RK, Miles R, Michelson H (1991) A model of a CA3 hippocampal pyramidal neuron incorporating voltage-clamp data on intrinsic conductances. *J Neurophysiol* 66:635-650.
- Turner JP, Salt TE (1998) Characterization of sensory and corticothalamic excitatory inputs to rat thalamocortical neurones in vitro. *J Physiol* 510 ( Pt 3):829-843.
- Tytgat J, Pauwels PJ, Vereecke J, Carmeliet E (1991) Flunarizine inhibits a high-threshold inactivating calcium channel (N-type) in isolated hippocampal neurons. *Brain Res* 549:112-117.
- Uhlhaas PJ, Singer W (2010) Abnormal neural oscillations and synchrony in schizophrenia. *Nat Rev Neurosci* 11:100-113.
- Ungerleider LG, Galkin TW, Mishkin M (1983) Visuotopic organization of projections from striate cortex to inferior and lateral pulvinar in rhesus monkey. *J Comp Neurol* 217:137-157.
- Van Horn SC, Sherman SM (2004) Differences in projection patterns between large and small corticothalamic terminals. *J Comp Neurol* 475:406-415.
- Varela C, Sherman SM (2007) Differences in response to muscarinic activation between first and higher order thalamic relays. *J Neurophysiol* 98:3538-3547.
- Varela C, Sherman SM (2009) Differences in response to serotonergic activation between first and higher order thalamic nuclei. *Cereb Cortex* 19:1776-1786.
- Vidnyanszky Z, Hamori J (1994) Quantitative electron microscopic analysis of synaptic input from cortical areas 17 and 18 to the dorsal lateral geniculate nucleus in cats. *J Comp Neurol* 349:259-268.
- Vidnyanszky Z, Borostyankoi Z, Gorcs TJ, Hamori J (1996) Light and electron microscopic analysis of synaptic input from cortical area 17 to the lateral posterior nucleus in cats. *Exp Brain Res* 109:63-70.
- von Krosigk M, Monckton JE, Reiner PB, McCormick DA (1999) Dynamic properties of corticothalamic excitatory postsynaptic potentials and thalamic reticular inhibitory postsynaptic potentials in thalamocortical neurons of the guinea-pig dorsal lateral geniculate nucleus. *Neuroscience* 91:7-20.

- Walker AE (1938) *The Primate Thalamus*. Chicago: University of Chicago Press.
- Wall JT, Symonds LL, Kaas JH (1982) Cortical and subcortical projections of the middle temporal area (MT) and adjacent cortex in galagos. *J Comp Neurol* 211:193-214.
- Wang S, Eisenback MA, Bickford ME (2002) Relative distribution of synapses in the pulvinar nucleus of the cat: implications regarding the "driver/modulator" theory of thalamic function. *J Comp Neurol* 454:482-494.
- Wang S, Eisenback M, Datskovskaia A, Boyce M, Bickford ME (2002) GABAergic pretectal terminals contact GABAergic interneurons in the cat dorsal lateral geniculate nucleus. *Neurosci Lett* 323:141-145.
- Wang X, Wei Y, Vaingankar V, Wang Q, Koepsell K, Sommer FT, Hirsch JA (2007) Feedforward excitation and inhibition evoke dual modes of firing in the cat's visual thalamus during naturalistic viewing. *Neuron* 55:465-478.
- Ware CB, Diamond IT, Casagrande VA (1974) Effects of ablating the striate cortex on a successive pattern discrimination: further study of the visual system in the tree shrew (*Tupaia glis*). *Brain Behav Evol* 9:264-279.
- Wilke M, Mueller KM, Leopold DA (2009) Neural activity in the visual thalamus reflects perceptual suppression. *Proc Natl Acad Sci U S A* 106:9465-9470.
- Williamson AM, Ohara PT, Ralston HJ, 3rd (1993) Electron microscopic evidence that cortical terminals make direct contact onto cells of the thalamic reticular nucleus in the monkey. *Brain Res* 631:175-179.
- Wilson M, Keys W, Johnston TD (1979) Middle temporal cortical visual area and visuospatial function in *Galago senegalensis*. *J Comp Physiol Psychol* 93:247-259.
- Wong P, Kaas JH (2009) Architectonic subdivisions of neocortex in the tree shrew (*Tupaia belangeri*). *Anat Rec (Hoboken)* 292:994-1027.
- Wu LG, Borst JG, Sakmann B (1998) R-type Ca<sup>2+</sup> currents evoke transmitter release at a rat central synapse. *Proc Natl Acad Sci U S A* 95:4720-4725.
- Zhan XJ, Cox CL, Rinzel J, Sherman SM (1999) Current clamp and modeling studies of low-threshold calcium spikes in cells of the cat's lateral geniculate nucleus. *J Neurophysiol* 81:2360-2373.

## CURRICULUM VITAE

Haiyang Wei

### Education and Training:

- 2010 Ph.D. Candidate, *Anatomical Sciences & Neurobiology*, University of Louisville, School of Medicine, Department of Anatomical Sciences & Neurobiology, Louisville, KY (anticipated defense date December 1st, 2010)
- 2007 Summer Course, Structure, Function & Development of the Visual System, Cold Spring Harbor Laboratory, Cold Spring Harbor, NY
- 2007 M.S., *Anatomical Sciences & Neurobiology*, University of Louisville, School of Medicine, Department of Anatomical Sciences & Neurobiology, Louisville, KY
- 2003 B.S., *Biophysics & Neurobiology*, University of Science and Technology of China, Department of Neurobiology & Biophysics, Hefei, China

### Awards, Honors:

- 2004-2010 University Scholarship & Fellowship, University of Louisville
- 2008 The Sigma Xi Grants-in-Aid of Research (GIAR) program, Sigma Xi
- 2003 “Challenge Cup” National College Student’s Tournament of Science and Technology award, China

### Research Experience:

- 2001-2004 Research Assistant, Vision Research Laboratory, University of Science and Technology of China, Department of Neurobiology & Biophysics
- Thesis Title:

1. "A New Method to Achieve Accurate Synchronized Trigger Signals on Computer Displays."
2. "Methods for Obtaining Stable in vivo Whole Cell Patch Clamp Recordings from Cortical and Subcortical Neurons."

Supervisor: Dr. Yifeng Zhou, Dr. Xiangrui Li

2004-2010 Graduate Research Assistant, University of Louisville, School of Medicine,  
Department of Anatomical Sciences & Neurobiology

Supervisor: Dr. Martha Bickford

Thesis Title:

"Signal Processing in the Tectothalamic Pathway"

**Teaching Experience:**

2007 Teaching assistant, Neuroanatomy, School of Medicine, University of Louisville.

**Peer reviewed Publications:**

1. Day-Brown, J. D., **Wei, H.**, Chomsung R.D., Petry, H. M., and Bickford, M. E. (2010). Pulvinar projections to the striatum and amygdala. *Front Neuroanat* 4:143.
2. Chomsung, R. D.\*, **Wei, H.\***, Day-Brown, J. D., Petry, H. M., and Bickford, M. E. (2010). Synaptic organization of connections between the temporal cortex and pulvinar nucleus of the tree shrew. *Cereb Cortex* 20, 997-1011. (\* Co-first author)
3. Whitaker, C. M., and **Wei, H.** (2009). An alternate cAMP pathway Epac promotes hippocampal long-term depression. *J Physiol* 587, 3067-3068.
4. Kralik, P. M., Long, Y., Song, Y., Yang, L., **Wei, H.**, Coventry, S., Zheng, S., and Epstein, P. N. (2009). Diabetic albuminuria is due to a small fraction of nephrons distinguished by albumin-stained tubules and glomerular adhesions. *Am J Pathol* 175, 500-509.

5. Bickford M.E., **Wei H.**, Eisenback M.A., Chomsung R.D., Slusarczyk A.S., Dankowski A.B. (2008) Synaptic organization of thalamocortical axon collaterals in the perigeniculate nucleus and dorsal lateral geniculate nucleus. *J Comp Neurol* 508:264-285.
6. Wang H., **Wei H.**, Chen B., Zhou Y. (2006) Chronic morphine exposure impairs short-term synaptic depression of geniculo-cortical visual pathway in vivo. *Neurosci Lett* 410:228-233.
7. Jia F., **Wei H.**, Li X., Xie X., Zhou Y. (2006) Short-term synaptic plasticity in the rat geniculo-cortical pathway during development in vivo. *Neurosci Lett* 398:73-77.

**Manuscripts in preparation:**

1. **Wei, H.**, Bonjean, M., Petry, H. M., Sejnowski, T. J. and Bickford, M. E. Thalamic Burst Firing Propensity: a Comparison of the Dorsal Lateral Geniculate and Pulvinar Nuclei in the Tree Shrew.
2. **Wei, H.**, Masterson, S. P., Petry, H. M., and Bickford, M. E. Two distinct types of tectopulvinar EPSPs and their contribution to short-term synaptic plasticity.
3. **Wei, H.**, Bickford, M. E. Cholinergic modulation of synaptic transmission and plasticity in the rat visual thalamus.

**Selected conference abstracts:**

1. Day-Brown, J. D., **Wei, H.**, Chomsung R.D., Petry, H. M., and Bickford, M. E. (2010). Pulvinar projections to the striatum and amygdala. Society for Neuroscience Abstracts, Program # 72.13.
2. **Wei, H.**, Petry, H. M., and Bickford, M. E. (2010) Thalamic Burst Firing Propensity: a Comparison of the Dorsal Lateral Geniculate and Pulvinar Nuclei in the Tree Shrew. Society for Neuroscience Abstracts, Program # 72.16.
3. Day-Brown, J. D., **Wei, H.**, Petry, H. M., Bickford, M. E. (2009) Characterization of claustrum-V1 connections. Society for Neuroscience Abstracts, Program # 848.11.

4. **Wei, H.**, Day-Brown, J. D., Chomsung, R. D., Petry, H. M., Bickford, M. E. (2009) The pulvinar nucleus and corticocortical communication. Society for Neuroscience Abstracts, Program # 848.19.
5. Chomsung, R., **Wei, H.**, Day-Brown, J. D II., Petry, H. M., Bickford, M. E. (2008) The projection from the pulvinar nucleus to the tree shrew striatum. Society for Neuroscience Abstracts, Program # 458.16.
6. **Wei, H.**, Masterson, S. P., Petry, H. M., Bickford, M. E. (2007) Development of low-threshold spikes in the tree shrew visual thalamus. Society for Neuroscience Abstracts, Program # 392.11.
7. Bickford, M. E., **Wei, H.**, Eisenback, M. A., Slusarczyk, A. S. (2007) Synaptic organization of subcortical geniculocortical axon collaterals. Society for Neuroscience Abstracts, Program # 392.8.
8. **Wei, H.**, Bickford, M. E. (2006) Cholinergic modulation of synaptic transmission in the rat visual thalamus. Society for Neuroscience Abstracts, Program # 241.5.
9. Chomsung, R. D., Masterson, S. P., **Wei, H.**, Bickford, M. E. (2005) Tectal terminals contact neurons in the lateral posterior nucleus that project to the visual cortex. Society for Neuroscience Abstracts, Program # 853.5.

**Professional Societies:**

2005-Present Member, Society for Neuroscience

2006-Present Associate member, Sigma Xi, The Scientific Research Society